

https://dspace.org/

The role of charge-transfer mechanisms in the oxidative and non-oxidative dissolution of Sphalerite.

Crundwell, Frank Kenneth

2015-01-15

http://hdl.handle.net/10539/16556

Downloaded from a DSpace repository. https://dspace.org/

THE ROLE OF CHARGE-TRANSFER MECHANISMS IN THE OXIDATIVE AND NON-OXIDATIVE DISSOLUTION OF SPHALERITE

Frank Kenneth Crundwell

A thesis submitted to the Faculty of Engineering, University of the Witwatersrand, Johannesburg, in fulfilment of the requirements for the degree of Doctor of Philosophy.

Johannesburg, 1988.

Declaration

I declare that this thesis is my own unaided work. It is being submitted for the degree of Doctor of Philosophy in the Faculty of Engineering at the University of the Witwatersrand, Johannesburg. It has not been submitted for any degree or examination in any other University.

F Cadwell

7 day of July 1988

ABSTRACT

A fundamental description of the mechanism of both the oxidative and non-oxidative dissolution reactions based on the transfer of charge across the phase boundary is given.

The rate of oxidative dissolution of iron-containing sphalerites in a ferric chloride solution is shown to be linear function of the concentration of the iron in the lattice. This is attributed to the formation of a narrow impurity band within the forbidden band gap of the sphalerite. The impurity band is of iron d-orbital origin. The transfer of electrons between this d-orbital band and the oxidant is energetically more favourable than that between the valence band and the oxidant. A fundamental model combining the electronic structure of the sphalerite and Gerischer's quantum theory of semiconductor electrochemistry is presented. An equation is derived that is consistent with the observed dissolution kinetics of iron-containing sphalerites, i.e., first order in the concentration of iron in the sphalerite and one-half order in the concentration of oxidant in the solution.

It was observed that the dissolution of the Gamsberg sphalerite in a ferric sulphate solution continued beyond 90 per cent conversion in two hours at 80°C. The rate of reaction is proportional to the sum of the concentrations of the $Fe^{3+}(aq)$ and the $FeHSO_4^{2+}$ complexes with a reaction order of one-half. The addition of Fe(II) to the solution had an indirect effect on the reaction rate, by decreasing the concentrations of the electroactive ions. Additions of $ZnSO_4$ did not affect the reaction rate. The kinetics of dissolution is successfully described by an electrochemical mechanism in which the charge transfer from the solid to the oxidant is rate-limiting.

The dissolution of the concentrates from Rosh Pinah and Black Mountain deposits failed to exceed a conversion of 90 per cent after 5 hours at 80°C with 0.5 M Fe(III) in an acidic ferric sulphate solution. X-ray diffraction analysis suggested the formation of an insoluble $PbSO_4$ or lead jarosite coating. Electron microprobe analysis was unable to

detect a continuous layer of material that covered the leached particles.

The kinetics of the non-oxidative dissolution of sphalerite are first order in $[H^+]$, and the reverse reaction is proportional to the square root of the concentration of zinc in solution and to the square root of the hydrogen sulphide partial pressure. The activation energies for the removal and deposition reactions are not sensitive to the iron impurity content in the solid. The rate of both the removal and the deposition reactions is described by a charge-transfer mechanism in which the movement of ions across the Helmholtz double-layer is the rate-controlling step.

The electrochemistry of other metal sulphides is reviewed with emphasis on the influence of the solid-state properties on the rate of dissolution. It is stressed that the electronic structure of the solid and of the solution must be taken into account in any fundamental description of the anodic behaviour of semiconducting minerals.

ACKNOWLEDGEMENTS

I would like to thank the following people and organizations:

Professor A.W. Bryson, my supervisor, for his help and advice during the course of this work and the preparation of this thesis.

The University of the Witwatersrand, for a Senior Bursary covering registration fees.

Dr R. Verbaan and Mr P. Soal, M.P. (PFP, Johannesburg North) for arranging that my service as a conscientious objector be done at MINTEK. They petitioned the Minister of Manpower on my behalf, and were it not for them I would have continued in the position of filing clerk in the Dept of Manpower for the full six years of this 'community' service.

Ms D. de Nooy and Mr S.J. Kruger for microscopic and electron microprobe analysis undertaken at the author's request,
Mr V. Pilley for the scanning electron-microscope analysis undertaken at the author's request.

CONTENTS

Declaration
Abstract
Acknowledgements
Contents

1. Introduction and literature review 1

1.1 Introduction 1
1.2 Research background and critical review of the literature 5
1.2.1 Dissolution reactions and products of dissolution 6
1.2.2 Investigations of the mechanism of oxidative dissolution 7
1.2.3 Investigations of the kinetics of non-oxidative dissolution 17
1.3 Aim, scope and contribution of this research 19

2. Solid-state properties of (Zn,Fe)S 21

3. The theory of charge transfer at the semiconductor-solution phase boundary 25

3.1 Semiconductor fundamentals 26
3.1.1 The vacuum and hydrogen energy scales 26
3.1.2 The band theory of semiconductors 26
3.2 The semiconductor-solution phase boundary 32
3.3 The kinetics of semiconductor-electrode processes 33
3.3.1 Charge-transfer reactions without a redox couple in solution 33
3.3.2 Charge-transfer reactions with a redox couple in solution 36
3.3.3 Fermi-level pinning model of semiconductor-solution junctions 43
3.3.4 The effect of illumination 45
3.4 Anodic corrosion of semiconductors 46

4. Experimental procedure and results 49

4.1 Sample preparation and characterization 50
4.2 Experimental apparatus 51
4.3 Experimental procedure 53
4.4 Microscopic and mineralogical investigation of the leached sphalerite samples 54
4.5 Experimental results 66
4.5.1 Effect of the iron impurity content in the sphalerite on the rate of dissolution 66
4.5.2 Effect of the solution concentration on the rate of leaching in ferric sulphate solutions 68
4.5.3 Refractory behaviour of the leaching of Black Mountain and Re. Pinah sphalerites in ferric sulphate solutions 71

5. Analysis of results and the application of the charge-transfer theory 79

5.1 Shrinking-particle model for the analysis of the experimental results 80
5.2 Effect of the solid-state properties of sphalerite on the rate of dissolution 82
5.2.1 Effect of iron content and UV radiation on the rate of leaching 82
5.2.2 Application of the fluctuating energy-level model to the dissolution of sphalerite 87
5.2.3 Summary 95
5.3 Mechanism of dissolution of sphalerite in iron (III) sulphate solutions 96
5.3.1 The effect of the solution composition on the rate of leaching of the Gamsberg sphalerite 96
5.3.2 Mechanism of dissolution of Gamsberg sphalerite in iron (III) sulphate solutions 98
5.3.3 The effect of complex formation on the leaching of sphalerite in ferric chloride solutions 110
5.3.4 Addition of Cu(II) to the leaching solutions 112
5.3.5 The effect of Fe(III) complex formation on the rate

potential of a chalcopyrite electrode 113
5.4 Application of the charge-transfer theory of the dissolution of ionic solids to the non-oxidative dissolution of sphalerite 118
5.4.1 Empirical correlation of the rate of non-oxidative dissolution of sphalerite 118
5.4.2 Application of the charge-transfer theory to the non-oxidative dissolution of sphalerite 125
5.4.3 Summary 134
5.5 Application of the fluctuating energy-level model to other systems - the influence of the electronic structure on the anodic electrochemistry of pyrite and chalcopyrite 135
5.5.1 The electrochemistry and dissolution of pyrite 136
5.5.2 Application of the energy-level model to the corrosion of chalcopyrite 138
5.5.3 Summary 142

6. Conclusions 143

References 147

Appendix A Mineralogical analysis of sphalerite samples 162

Appendix B Raw data 171

Appendix C Computer program for the calculation of the equilibrium species in solution 179

Appendix D The influence of the electronic structure of solids on the anodic electrochemistry of semiconducting sulphide minerals 182

NOTATION

a	Unit cell length	Å
A	Surface area	m^2
A_E	Electron affinity of an element	eV
C_{ox}	Concentration of oxidant	M
D(E)	Density of states	-
e^-	Electron in the conduction band	-
E	Energy level of an electron	eV
E_a	Activation energy	kJ mol^{-1}
E_A	Electron affinity of a compound	eV
E_F	Fermi energy level	eV
$_pE_{dec}$	Thermodynamic energy level for decomposition or dissolution	V
f(E)	Fermi function	-
f(0)	Function of concentration	-
F	Faraday constant	J(V mol)$^{-1}$
h^+	hole in the valence band	-
I_1	First ionization potential	eV
j	Current density	mA m^{-2}
k	Boltzmann constant	J K^{-1}
k	Rate constant (when subscripted, r, or superscripted, a,c)	
K	Equilibrium constant	-
K_D	Henry's law type constant	-
m	Amount of leachable material remaining in unreacted core	mol
m,n	Stoichiometric coefficients, equ. 3.49	-
N_d	Magnitude of Dirac function of density of states in the d-band	mol %
N_i	Carrier density of states of the insulator valence band	mol %
p	Concentration of holes	
$p(H_2S)$	Partial pressure of H_2S	kPa
q	Electronic charge	C
r	Rate of reaction	mol $m^2 min^{-1}$

r	Particle radius	m
R	Universal gas constant	J $K^{-1}mol^{-1}$
t	Time	min,s
s,t	Stoichiometric coefficient, defined by equs 5.42 and 5.43	-
T	Temperature	K, °C
V	Redox potential	V
V_l	Liquid volume	m^3
V_g	Gas volume	m^3
V^0	Standard reduction potential	V
$W(E)$	Probability that the energy level of an ion has fluctuated to E	-
x	Coefficient dependent on the cation and anion transfer coefficients	-
X	Conversion	-
z	Charge number	-
α	Charge-transfer coefficient	-
β,δ,γ	Coefficients describing the order of reaction	-
$\delta(E)$	Dirac function	-
λ	Reorganization energy	eV
ρ	Molar density	mol m^{-3}
η	Overpotential	V
ν	Transmission coefficient	s^{-1}
χ	Electronegativity	eV
ϕ	Potential	V
$\Delta\phi$	Potential difference	V

1 eV = 1.602 x 10^{-19} J = q J

Subscripts

b	Bulk
c	Conduction band
calc	Calculated

e	Equilibrium conditions
f	Freely dissolving
F	Fermi level
Fe	Relating to the iron couple in solution
g	Gas
gap	Band gap
H	Helmholtz layer
l	Liquid
lat	Lattice
meas	Measured
o	Initial conditions
ox	Oxidant
r	Reaction controlled
red	reductant
redox	Redox couple
s	Surface
sc	Space charge
v	Valence band
+,-	Cation, anion

Superscripts

a	Anodic
c	Cathodic

CHAPTER 1.

INTRODUCTION AND LITERATURE REVIEW

1.1 Introduction

Interest in the hydrometallurgical processing of base-metal sulphides has been maintained at a high level during the last fifteen years. The stringent environmental restrictions imposed on the sulphide smelters have led to the development of hydrometallurgical routes for the extraction of metals from sulphides that avoid the production of sulphur dioxide. These processes involve the aqueous oxidation of sulphide to elemental sulphur or to sulphate by an oxidant such as ferric ion or dissolved oxygen.

These alternative processes for the treatment of metal sulphides have other advantages over the conventional roast-leach process. Doyle *et al* (1978) compared these processes and estimated that at that time the capital requirements were up to 30% less for the leaching process. In addition, hydrometallurgical processes are in principle able to treat lower-grade ores. However, a major disadvantage is the need to heat large volumes of dilute solutions, and therefore the energy requirements may be prohibitive.

In particular, considerable attention has been focussed on the development of processes for the leaching of zinc sulphide concentrates in chloride and sulphate solutions using dissolved iron(III) as the oxidant.

Sherritt Gordon Mines, Ltd., have adapted their technology developed for the oxidation of nickel sulphide to the leaching of zinc sulphide (Veltman *et al*, 1978). The concentrates are leached directly in mill-house return acid with air or oxygen under pressure. The leach reactions are:

$$ZnS + Fe_2(SO_4)_3 \rightarrow ZnSO_4 + 2FeSO_4 + S \quad 1.1$$

$$2FeSO_4 + H_2SO_4 + HO_2 \rightarrow Fe_2(SO_4)_3 + H_2O \quad 1.2$$

$$ZnS + H_2SO_4 + HO_2 \rightarrow ZnSO_4 + S + H_2O \quad 1.3$$

The autoclave temperature is maintained above 160°C and surface-active agents are added to ensure complete conversion. This process, which is especially amenable to high iron and copper concentrates, has been installed at Cominco Ltd. (Trail, B.C., Canada) and at Kidd Creek Mines, Ltd., (Timmins, Ont., Canada).

The Sherritt-Gordon autoclave at Kidd Creek is a horizontal, four compartment unit, which is designed to treat 100 tons of concentrate per day. The zinc concentrate is fed to the autoclave as a slurry with a solids content of 70 per cent and a specific density of 2.1. The temperatures in the compartments range from 135°C in the first compartment to between 140 and 144°C in the other three. The total pressure is maintained at 1000 kPa. Oxygen-enriched air (85 to 90 per cent oxygen), drawn from the copper smelter, is fed to the autoclave at a rate about 50 per cent in excess of the stoichiometric requirement for sphalerite oxidation. The slurry is discharged from the autoclave through a stainless steel orifice, and regular blockage of the orifice by sticky elemental sulphur results in an autoclave downtime of about 30 per cent (Dry, 1987).

The pressure-leaching plant at Trail has been in operation since 1981. The four compartment autoclave has a working volume of 100 m^3, and the residence time at the design feed rate of 190 tons per day is about 100 minutes. The temperature is maintained at 150°C, and the total pressure is maintained at 1250 kPa. About 88 per cent utilization of the oxygen, which is 98 per cent pure, is achieved. Downtime in the pressure leaching plant is about 10 hours per month, significantly less than that at Kidd Creek (Dry, 1987).

Vielle-Montagne (Balen, Belgium) have commissioned a pilot plant in which the autoclaves, such as those used at Kidd Creek and Trail, are replaced with a pipe reactor. The reactor runs at a temperature of between 150°C and 160°C and at pressures of 4000 kPa. This high-pressure leaching process is presently being patented. The oxygen feed-rate to the leach reactor is controlled so that the final solution contains about 30 g l^{-1} of sulphuric acid and all the soluble iron is in the ferrous form. The formation of jarosite in the reactor is avoided. The residence time in the pipe reactor is about 10 minutes, a tenth of the residence time in the Sherritt-Gordon autoclaves. Extractions of between 95 and 98 per cent are obtained, and most of the sulphidic sulphur is converted to elemental sulphur. A surface-active agent, o-phenylene diamine, is added to the solution to prevent the agglomeration of the elemental sulphur that is produced, and it has been claimed that this speeds up the rate of reaction. An important advantage of this process is the high recovery of the associated silver and gold from the sphalerite ore. Ninety five per cent of the silver is recovered from the leach residue (Vegter, 1987).

MINTEK patented a process in which the zinc sulphide material is dissolved in a solution containing between 5 and 50 g l^{-1} iron and about 20 g l^{-1} sulphuric acid (Verbaan, 1981). The temperature is maintained below the melting point of sulphur, 119°C. The advantage of this process is that a milder temperature is used, and there is therefore a major saving on the energy required to heat the solution.

The dissolution of sphalerite in an acid solution in the absence of an oxidant produces hydrogen sulphide, which could be oxidized to pure elemental sulphur in a subsequent step. Attention has not been focussed on the non-oxidative dissolution of sulphides, presumably because the production of hydrogen sulphide would have its own environmental and production problems.

In the hydrometallurgical processing of sphalerite to obtain zinc

metal, the central operation is the leaching unit, which replaces the roast unit in the conventional plant. In the leaching process, the dissolution of the mineral is encouraged, and efforts are made to promote the dissolution rate. A fundamental understanding of the kinetics and mechanism of the dissolution of sphalerite would aid in the choice of flowsheet for the plant, and in the design and the operation of the plant.

The kinetics of the oxidative and non-oxidative dissolution reactions are reported in this thesis. The aim of the thesis is to present a fundamental description of the mechanism of both the oxidative and non-oxidative reactions based on the transfer of charge at the phase boundary. The electrochemical mechanisms proposed take into account the changes in the electrochemical potential of adsorbed ions, the transfer of electrons and ions across the Helmholtz layer, the effect of the distribution of charge within the solid and the effect of impurities within the solid.

This research is intended to present an original contribution to the kinetics of the dissolution of zinc sulphide concentrates by defining more clearly the mechanistic details and the electrochemistry of the system.

In the remaining section of this chapter the literature on the leaching of sphalerite is reviewed, and the aims and scope of this research are discussed in detail. In Chapter 2 the structure and solid-state properties of (Zn,Fe)S are reviewed, and the semiconductor nature of sphalerite is emphasized. In Chapter 3 the established theory of charge transfer at the semiconductor-solution phase boundary is discussed in detail, with particular reference to dissolution reactions. It is stressed that the electronic properties of the solid and the solution must be taken into account in any fundamental interpretation of the reaction kinetics and the anodic behaviour of semiconducting minerals, such as sphalerite. The experimental procedure and results are presented in Chapter 4, and these results are

discussed and analyzed in Chapter 5 in terms of the electrochemical theory presented in Chapter 3. It is shown that the mechanism proposed based on this theory is consistent with the dissolution kinetics. The conclusions of this work are presented in Chapter 6.

1.2 Research background and critical review of the literature

The dissolution of sulphides has received considerable attention from both hydrometallurgists and photoelectrochemists. Photoanodic corrosion at the surface of the sulphide anode is an ubiquitous problem in solar energy conversion, leading ultimately to the destruction of the photoelectric cell. Research work has been focussed on the search for redox couples that will suppress the corrosion by competing for surface holes, or for materials, such as MoS_2, that are resistant to corrosion. The electrochemistry of cadmium sulphide has received particular attention, and the kinetics of corrosion and photocorrosion have been interpreted in terms of the theory of semiconductor electrochemistry. Hydrometallurgists have investigated the kinetics of solution of the base-metal sulphides with the view to maximiz rate of dissolution. The kinetics of dissolution have been preted in terms of adsorption isotherms, and more recently in te. the electrochemical mixed-potential model developed to describe the mechanism of the corrosion of metals.

The electrochemistry of metal sulphides has been reviewed by Koch (1975) and Hiskey and Wadsworth (1981), while Wadsworth (1972) and Dutrizac and MacDonald (1974) reviewed the leaching studies of metal sulphides. Burkin (1969) has reported on solid-state transformations during leaching, emphasizing the formation of surface films that inhibit further dissolution, and Peters (1977) has discussed the experimental techniques used in sulphide electrochemistry.

1.2.1 *Dissolution reactions and products of dissolution*

Dissolution reactions can be classified on the basis of the overall reaction into non-oxidative dissolution, in which no change in the formal oxidation state of the constituent atoms of the solid occurs, and oxidative dissolution, in which such a change does occur (Diggle, 1973).

Forward and Warren (1960) reviewed the available literature for the extraction of metals from base metal sulphides by hydrometallurgical methods, and reported on the chemistry of the dissolution process. They concluded that the products of reaction are largely determined by the concentration of hydrogen ions, the presence or absence of an oxidizing agent, and the temperature in so far as it affects the formation of sulphates. In the absence of an oxidizing agent the non-oxidative reaction is:

$$ZnS + H_2SO_4 \rightarrow ZnSO_4 + H_2S \qquad 1.4$$

while in the presence of oxygen (or any other oxidant), the oxidative reaction is:

$$ZnS + H_2SO_4 + HO_2 \rightarrow ZnSO_4 + H_2O + S \qquad 1.5$$

Oxidation by oxygen can occur directly in solutions of higher pH values, as follows:

$$ZnS + 2O_2 \rightarrow ZnSO_4 \qquad 1.6$$

The dominant mechanism of dissolution would depend on the relative concentrations of oxidant and acid. In a solution with a high concentration of oxidant, oxidative dissolution would be expected to occur, while in a solution with a high concentration of acid, the non-oxidative process will dominate.

1.2.2 Investigations of the mechanism of oxidative dissolution

Effects of temperature, oxidant concentration and product formation on the rate of dissolution

Forward and Warren (1960) separated the factors that may control the rate of dissolution of sulphide minerals into three categories: (i) mass transfer of reactants and products in solution, (ii) coating of insoluble products on the surface of the mineral, or (iii) chemical reaction on the surface of the mineral. They reported that when oxidation occurs below 119°C, the film of elemental sulphur that is formed is porous, and does not inhibit oxidation. Between 119°C and 160°C, molten sulphur forms an impenetrable coating on the mineral surface and prevents further oxidation, while above 160°C the sulphur is oxidized to sulphate, and, therefore, it does not form a coating that inhibits the dissolution reaction.

Dutrizac and MacDonald (1974) reviewed the literature on the leaching of base-metal sulphides by ferric ion and reported that the leaching of sphalerite is controlled by the diffusion of ferric ions in solution (pH ≈ 2), with an activation energy of about 24 kJ mol^{-1}, which is consistent with diffusion control. It was also reported that the rate is directly proportional to the ferric ion concentration, and is not impeded by the formation of elemental sulphur.

Jan *et al* (1976) concluded that the rate-determining step was the reaction at the mineral surface, and not the diffusion of ferric ions to the surface, even though they observed an apparent activation energy of 24 kJ mol^{-1}, and a dependence of the rate on agitation. They attributed the linear kinetics that they obtained to the disk-like shape that the sphalerite particles appeared to have when examined under an electron microscope. They proposed that the reaction occurs by a mechanism in which the initial step is the non-oxidative

dissolution reaction, followed by the oxidation of the hydrogen sulphide by ferric ions. By leaching sphalerite in the presence of sulphuric acid and iodide, they demonstrated that the reaction

$$ZnS + H_2SO_4 \rightarrow ZnSO_4 + H_2S \qquad 1.7$$

is instantaneous, and that the oxidation of hydrogen sulphide by oxygen

$$H_2S + \tfrac{1}{2}O_2 \rightarrow H_2O + S \qquad 1.8$$

is slow and rate-determining. In the presence of ferric ion, they proposed that the role of the oxygen is to reoxidize the ferrous ion produced in the oxidation of the hydrogen sulphide. This scheme can be represented as follows

$$ZnS + H_2SO_4 \rightarrow ZnSO_4 + H_2S \qquad 1.9a$$

$$2FeSO_4 + H_2SO_4 + \tfrac{1}{2}O_2 \rightarrow Fe_2(SO_4)_3 + H_2O \qquad 1.9b$$

$$Fe_2(SO_4)_3 + H_2S \rightarrow 2FeSO_4 + H_2SO_4 + S \qquad 1.9c$$

and the overall reaction would then be

$$ZnS + H_2SO_4 + \tfrac{1}{2}O_2 \rightarrow ZnSO_4 + H_2O + S \qquad 1.9d$$

in which reaction 1.9b is the rate-controlling step.

Verbaan (1977) leached a number of sphalerites of different origin in the presence and absence of ferric ions in acid sulphate solutions. He showed that the amount of H_2S formed during reaction was dramatically decreased by the addition of ferric ion. He obtained conflicting evidence as to whether or not the elemental sulphur resulted in product-layer diffusion control. He attempted to explain the kinetics of the initial rate of reaction by a mechanism in which the

adsorption of ferric ions and hydrogen ions onto the surface is described by the Langmuir isotherm. This mechanism was relatively successful in the absence of ferric ions, i.e., it described the initial rate of the non-oxidative reaction. Van Sandwijk and Koopmans (1986) applied an adsorption model to the oxidative dissolution of sphalerite and evaluated the rate of dissolution in terms of the Langmuir isotherm. Their model is very similar to that proposed by Verbaan (1977).

It was common practice in hydrometallurgical studies to interpret the kinetics of dissolution in terms of adsorption isotherms. These isotherms make no provision for the effects of the electrical double-layer and for the changes in the electrochemical potentials of the adsorbed ions - effects that are incorporated in the charge-transfer theory.

Scott and Dyson (1968) noted the catalytic activity of several divalent metals on the pressure leaching of a chemically-prepared zinc sulphide by oxygen. This activity increased in the order Fe < Mo < Ru < Bi < Cu. The effect of the catalysts was attributed to the penetration of the metal ion into the lattice (substitution) which affects the electrical conductivity of the solid, and therefore enhances the electrochemical dissolution of the solid. The main parameters influencing the rate were reported to be the catalyst concentration, the temperature, the oxygen pressure, and the acid concentration. The sulphate that formed was attributed to the oxidation of hydrogen sulphide that formed as an intermediate product.

Scott and Nicol (1978) reported inconsistencies between the experimental observations for various different sphalerites and the predictions based on the assumption that the dissolution occurs by means of a initial non-oxidative reaction. They suggested that the mechanism of dissolution in acidic solutions of ferric sulphate may be direct oxidation, and concluded that the mechanism of dissolution is dependent on the origin of the sphalerite. Using a sphalerite-graphite

electrode, they indicated that the process directly responsible for the rate of dissolution occurs on the surface of the electrode, and that if direct oxidation does occur, one would expect the potential of the zinc sulphide surface to lie in the region anodic to 0.4 V with respect to the saturated calomel electrode (SCE). They experienced difficulties with this type of electrode due to the high resistivity of the sphalerite.

Pawlek (1969) described the kinetics of dissolution of sphalerite in terms of a model which incorporated an electrochemical step. This description involves anodic and cathodic reactions occurring on the surface of the mineral, with a current flowing between the separate localities where each reaction takes place. The anodic reaction releases electrons

$$ZnS \rightarrow Zn^{2+} + S + 2e^- \qquad 1.10$$

while the cathodic reaction consumes the electrons by

$$2e^- + 2H^+ + \tfrac{1}{2}O_2 \rightarrow H_2O \qquad 1.11$$

Although zinc sulphide is a semiconductor with a high resistivity, the electron exchange occurs over a limited locality, and the high resistivity of the mineral does not limit the electrochemical reaction. Pawlek did not describe the overall kinetics in terms of an electrochemical mechanism, but used a theory of boundary chemisorption, indicating that the rate-controlling process is not the electrochemical reaction. He found that initial dissolution resulted in the formation of hydrogen sulphide, which retards the rate of dissolution. Pawlek showed experimentally that the continous removal of hydrogen sulphide can increase the rate of dissolution by a factor of approximately four.

Verbaan (1980) concluded in a later examination that the rate-controlling step in the leaching of sphalerite is an electrochemical re-

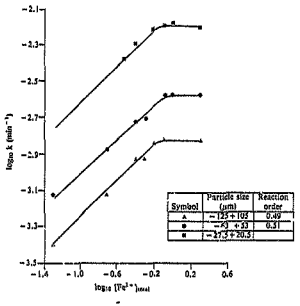

Figure 1.1 The order of reaction with respect to total ferric ion concentration for ferric chloride leaching of a natural ZnS concentrate (after Jin et al, 1985).

action. He reported that the rate is proportional to the ferric ion concentration to the power 0.4 and inversely proportional to the ferrous ion concentration to the power 0.25, and used this in an empirical correlation for his results in acidic ferric sulphate solutions. No attempt was made to apply electrochemical theory in the formulation of this correlation.

Jin and Warren (1985) proposed an adsorption-electrochemical model for the dissolution of sphalerite in ferric chloride solutions. They observed that the rate of reaction is proportional to $[Fe(III)]^{\frac{1}{2}}$ and that at higher concentrations of ferric chloride, the rate becomes independent of the ferric ion concentration. The change in Fe(III) dependence occurred at 0.8 M Fe(III) for particles of three size ranges. These results are illustrated in Figure 1.1. They attributed

this change to the onset of complete coverage of the surface by ferric ions. The ferric ions are assumed to be adsorbed at the inner Helmholtz plane (IHP) at anionic lattice sites. They described these results in terms of an adsorption isotherm in combination with the mixed-potential model. The rate of reaction was also dependent on the chloride ion concentration, the reaction order also being one-half. Competitive adsorption of H^+ onto the same sites as Fe^{3+} was not mentioned. In addition, it not clear how they would account for the effect of the addition of Fe(II) to the leaching solution in their model.

Crundwell (1985) and Verbaan and Crundwell (1986) derived a model in which the mixed potential (or corrosion potential) can be approximated by the redox potential, V, for the Fe^{2+}/Fe^{3+} couple. The rate of reaction, r, is given by

$$r = k_s \exp(0.5\ FV/RT) \qquad 1.12$$

where k_s is a rate constant, F is the Faraday constant, R is the gas constant, T is the temperature, 0.5 is the value of the charge-transfer coefficient, and the redox potential is given by

$$V = V^\circ + RT/F \ln ([Fe^{3+}]/[Fe^{2+}]) \qquad 1.13$$

where V° is the standard redox potential. (Although it is not standard practice to use the symbol V for the redox potential on the hydrogen scale, it will be used here because the symbol E will denote energy on the vacuum scale. It will be shown that the values V° and E°_{redox} are the same except that different energy scales are used.)

Equation 1.12 gives the same one-half order dependence on $[Fe^{3+}]$ at constant [Fe(II)] that was found by Jin and Warren (1985). The combination of this model with the shrinking-particle geometry and the calculation of the redox potential, gave an excellent reproduction of the results of batch leaching in which the ferrous ion concentration

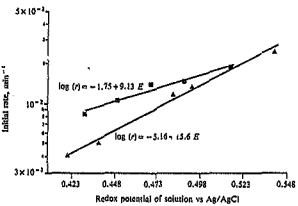

Figure 1.2 Correlation of the initial rate of reaction for the ferric sulphate leaching of sphalerite with the measured redox potential (vs Ag/AgCl) using Verbaan's (1980) data at 0.1 M H_2SO_4 and 65°C. Triangles: 0.025 M Fe(II), various Fe(III); Squares: 0.45 M Fe(III), various Fe(II).

was constant. Careful examination of this model indicates that the rate should be inversely proportional to $[Fe^{2+}]^4$. However, this is not consistent with the result obtained by Verbaan (1980) that the the rate is inversely proportional to $[Fe^{2+}]^{0.25}$.

The failure of this model is shown in Figure 1.2. At constant [Fe(II)] and varying [Fe(III)], equation 1.12 is satisfied, since the measured slope, 15.6 V^{-1}, is close to the expected slope of 17.2 V^{-1} (from equation 1.12) but at constant [Fe(III)] and varying [Fe(II)], equation 1.12 is not satisfied, since the measured slope, 9.1 V^{-1}, is far from the expected slope of 17.2 V^{-1}. The non-Nernstian response of the rate of dissolution with increasing [Fe(II)] at constant [Fe(III)] means that the model represented by equations 1.12 and 1.13 is incorrect.

In summary, recent studies of the oxidative dissolution of sphalerite in both ferric chloride and ferric sulphate solutions have emphasised an electrochemical reaction with a reaction order of 0.5 with respect to the ferric ion concentration. The mixed-potential model, developed to describe the mechanism of metallic corrosion, has gained acceptance in research on leaching and flotation and has been applied with modifications, such as adsorption isotherms, to the leaching of sphalerite with varying success. This model assumes that electron transfer is the rate-controlling step, and that the mechanism of dissolution is analogous to the corrosion of metals.

Effects of solid-state properties on the rate of dissolution

The application of the mixed-potential model to the leaching kinetics assumes that the potential across the solid side of the phase boundary (the space-charge region) remains constant, so that the applied potential appears across the Helmholtz layer. This is metal-like behaviour, and the dissolution reaction is predicted to have a charge-transfer coefficient of 0.5 for the ideal single electron-transfer reaction. However, many sulphide minerals are semiconductors. The semiconductor model assumes that most of the applied potential drop occurs across the space-charge region with a charge-transfer coefficient of 1 for the ideal case.

Solid-state properties have often been considered to influence the kinetics of dissolution and the flotation behaviour of semiconducting ore minerals. Simkovich and Wagner (1960) found that the dissolution of synthetically-grown stoichiometric, non-stoichiometric, and heavily-doped Ag- or Bi-doped lead sulphide varied with the concentration of point defects in the solid, and Sadington and Prosser (1969) reported a dependence of the oxidation rate on the degree of non-stoichiometry of the lead sulphide and, hence, on its electronic conduction type.

Richardson and O'Dell (1984) used a combination of electrochemical, interfacial-capacitance, and surface-photovoltage measurements in a study of oxygen reduction at, and xanthate adsorption onto, lead sulphide. They concluded that oxygen reduction is not dependent on the surface concentration of electrons, while xanthate adsorption is dependent on the Fermi level of the lead sulphide at the surface.

Exner *et al* (1969) and Pawlek (1969) proposed that the cathodic reduction of oxygen would vary with the number of charge carriers in the sphalerite, in support of which they found that the irradiation of sphalerite with UV light caused an appreciable increase in the rate of dissolution. This is illustrated in Figure 1.3. Photo-effects such as this are typical of n-type semiconductors in which the rate of charge transfer is limited by the supply of minority carriers (holes).

The rate at which iron-containing sphalerites, (Zn,Fe)S, are oxidatively dissolved is known to be higher than that of pure ZnS (Exner *et al*, 1969), and Piao and Tozawa (1985) reported that the rate of reaction is a linear function of the concentration of iron in the zinc sulphide lattice. Some data of Piao and Tozawa (1985) are reproduced in Figure 1.4. They studied the dissolution reaction at 150°C and used oxygen as the oxidant, i.e., conditions applicable to the Sherritt-Gordon process.

The results reported by Exner et *al* (1969), Pawlek (1969) and Piao and Tozawa (1985) indicate that the electronic structure is important in the dissolution of sphalerite, because of the influence of the iron content of the (Zn,Fe)S solid solution, and the influence of UV irradiation. Neither of these two influences has been explained in any satisfactory detail.

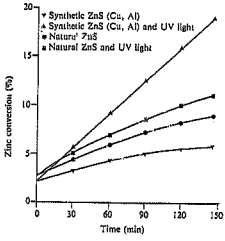

Figure 1.3 The effect of crystal doping and UV radiation on the dissolution of natural and synthetic ZnS (after Exner et al 1969)

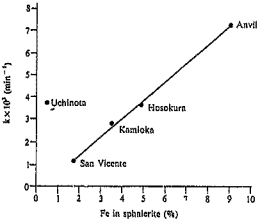

Figure 1.4 The effect of substitutional iron in sphalerite on the rate of dissolution using oxygen as an oxidant (after Piso and Tozawa 1985)

1.2.3 Investigations of the kinetics of the non-oxidative dissolution of sphalerite

Romankiw and DeBruyn (1965) and Locker and DeBruyn (1969) described the non-oxidative dissolution of ZnS, in the concentration range 0.25 M to 10 M H_2SO_4 and the temperature range 0.6 to 65°C by the relation

$$\frac{d[ZnS]}{dt} = A_o(k_1[H_2SO_4] - k_{-1}[ZnSO_4]^{0.5}p(H_2S)^{0.5}) \qquad 1.14$$

where A_o is the total initial area, k_1 and k_{-1} are rate constants, and the brackets indicate concentration. Locker and DeBruyn (1969) found that the kinetics of the non-oxidative dissolution of other group II-VI semiconductor compounds, such as ZnSe, CdS and $Zn_{0.85}Cd_{0.15}S$, are described by the same kinetic expression as that for ZnS (equation 1.14). The activation energies of the pure ZnS were 41.4 and 28.0 kJ mol^{-1} for the forward and reverse reactions respectively. Locker and DeBruyn (1969) reported that the iron content did not affect the activation energy; however, the rate of dissolution of the material containing 0.1 per cent Fe was 7 times higher than the high purity β-ZnS.

Locker and DeBruyn (1969) excluded diffusion control, and proposed that the initial rate was controlled by the adsorption of protons at sulphur sites. The ionic transfer or adsorption mechanism that was proposed is as follows. The initial rate of dissolution, r_o, is controlled by the adsorption of protons onto the surface,

$$r_o = k_r A_o [H^+]_s \exp(-E_a/RT) \qquad 1.15$$

where k_r and E_a are the rate constant and the activation energy for the forward reaction respectively, and $[H^+]_s$ is the surface concentration of adsorbed protons, which is related to the concentration of the bulk solution, $[H^+]_b$, by

$$[H^+]_s = [H^+]_b \exp(-\phi_\delta/RT) \qquad 1.16$$

where ϕ_δ is the potential of the ion at the distance of closest approach before adsorption onto the surface. This adsorption model involves only the transport of the adsorbed species across the electrical-potential barrier at the solid-solution phase boundary, and not across the electrochemical-potential barrier. They commented that when hydrochloric acid was used as the electrolyte, there was the possibility that specific adsorption of chloride ion would occur, which would change the surface charge and the distribution of active sites. However, they did not extend their model to include the effect of the chloride ion.

Verbaan (1977) investigated the non-oxidative dissolution of four zinc sulphide samples. He reported that the initial rate was proportional to the acid concentration, and interpreted his results in terms of the adsorption of H^+ and Zn^{2+} onto active sites at the surface. He did not analyse the final equilibrium or the reverse reaction, as was done by Romankiw and DeBruyn (1965).

Majima *et al* (1981) observed that not only was the rate of reaction first order in proton concentration, but the addition of NaCl to acidic chloride solutions also enhanced the rate of dissolution. They proposed an adsorption model similar to that of Locker and DeBruyn (1969) to account for their results, but failed to explain the effect of the chloride ion.

Although an empirical expression for the rate of dissolution of sphalerite has been established, the mechanism of dissolution has not been examined in any detail. The adsorption of protons at sulphur sites is the only mechanism that has been proposed, and the kinetics have been interpreted in terms of adsorption isotherms. These isotherms make no provision for the effects of the electrical double-layer that exists at the surface of a dissolving semiconductor. The transfer of a charged species at the phase boundary must be

expressed in terms of the electrochemical potentials of the adsorbed and solution species; the electrochemical potential differs from the chemical potential by a factor containing the electrical potential.

1.3 Aim, scope and contribution of this research

From the discussion of the literature it is apparent that, in spite of the number of studies, the kinetics of oxidative leaching are still partly shrouded in uncertainty. An acceptable explanation for the effect of the addition of ferrous ions to the ferric sulphate leaching solution (the results of Verbaan, 1980) has not been given, and more importantly, no attempt has been made to explain the effect of the iron impurity in the (Zn,Fe)S solid solution on the rate of oxidative dissolution.

In addition, the mechanism of the non-oxidative dissolution of sphalerite has not been examined in detail. Only the initial rate of dissolution has been discussed, and an adsorption model has been proposed to account for the first-order dependence of the rate on the hydrogen ion concentration. These adsorption mechanisms do not take into account the effects of the electrical double-layer that exist at the surface of a dissolving semiconductor, such as sphalerite.

The dissolution process is classified on the basis of the rate-determining step, for example, mass transfer, chemical reaction, or charge transfer. Charge-transfer reactions are those reactions in which charge carriers (ions or electrons) are transferred across the electrical potential barrier at a phase boundary (Vetter, 1967). The aim of this thesis is to argue that the rate-controlling step in both the oxidative and non-oxidative dissolution reactions is a charge-transfer reaction. Any such fundamental mechanism must be able to account for the effects of the electronic structure of both the solid (whether it is a semiconductor, or the effects of impurities) and the solution (whether some complexes are electroinactive), and the effects of the electrical double-layer at the solid-solution phase

boundary on the transfer of charge during dissolution. The theory of semiconductor electrochemistry, presented by Gerischer (1960) and others, will be used extensively in this analysis.

An electrochemical mechanism, such as the mixed-potential mechanism, would usually be verified by fundamental electrochemical techniques using a sphalerite electrode. Since sphalerite is unsuitable for use as an electrode in conventional electrochemical experiments because of its high resistivity, mixtures of sphalerite and graphite have been used as electrodes (Scott and Nicol, 1978; Gerlach and Kuzeci, 1984; and Guerrette and Ghali, 1985). The graphite serves to lower the resistivity of the electrode, so that the applied potential appears across the Helmholtz layer. However, Scott and Nicol (1978) reported that the presence of graphite in contact with the sphalerite altered the mechanism of dissolution, a fourfold to fivefold increase being obtained for a sphalerite-graphite electrode over that of a sphalerite-PTFE electrode. Guerrette and Ghali (1985) reported similar results, viz, the anodic behaviour of compacted sphalerite-graphite mixtures is different from that of uncompacted samples. For these reasons, the batch leaching test is the only method available to provide results for the formulation and confirmation of an electrochemical model.

The intention of this work is to restrict the investigation of the reaction kinetics to ferric sulphate or chloride solutions below the melting point of sulphur, 119°C. These conditions comply with the conditions of the MINTEK process discussed in section 1.1, so that the results would be directly applicable to that process.

CHAPTER 2.

SOLID-STATE PROPERTIES OF (Zn,Fe)S

Zinc sulphide exists as two polytypes: the hexagonal type (wurtzite) and the cubic type (sphalerite), which is the more abundant mineral. Sphalerite is widely distributed, and is normally associated with galena in zinc-lead ores or with chalcopyrite in zinc-copper-iron ores. It is present in hydrothermal deposits of all kinds.

The cubic structure of sphalerite is a fundamental crystal structure-type. The structure is a unit cube with zinc atoms at the corners and at the face centres. The four sulphur atoms within each unit cell are coordinated so that each sulphur atom lies at the centre of a regular tetrahedron of zinc atoms, and each zinc atom at the centre of a regular sulphur tetrahedron. This structure is shown in Figure 2.1.

Iron is the most common impurity in natural sphalerite, and iron atoms substitute for zinc atoms in the cubic lattice, i.e., FeS is in solid solution with ZnS as (Zn,Fe)S. The size of the unit cell, measured in Angstroms, increases with an increase in the iron content according to the equation (Vaughan and Craig, 1978):

$$a = 5.4093 + 0.0005637\ (\text{mole \% FeS}) \quad 0.000004107\ (\text{mole \% FeS})^2 \qquad 2.1$$

Both polytypes are semiconductors of intermediate ionicity, with a band gap - determined by optical measurement and quantum calculation - in the range 3.6 to 3.9 eV (Vaughan and Craig, 1978). Chemical bonding indicates that the bottom of the conduction band is derived from the zinc 4s-orbital, while the top of the valence band is derived primarily from the sulphur 3p-orbital (Shuey, 1975). The simplified molecular orbital diagram is shown in Figure 2.2. This chemical-bonding model is

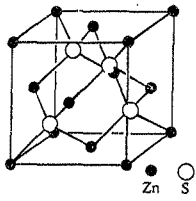

Figure 2.1 Cubic structure of the unit cell of sphalerite.

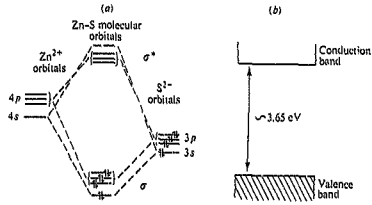

Figure 2.2 Simplistic molecular orbital and band model diagrams for sphalerite (or wurtzite) type phases: (a) schematic molecular orbital diagram for pure ZnS; (b) corresponding band diagram for ZnS.

in qualitative agreement with the ionic model, which associates the valence band with the anion, sulphur, and the conduction band with the cation, zinc (Mott and Gurney, 1948).

Zinc sulphide is such a poor electrical conductor that it is often classified as an insulator, and resistivities in the range 10^7 - 10^9 Ω·cm have been reported. The mechanism of intrinsic conduction in the zinc sulphide may be n- or p-type, depending on the stoichiometry. Tolkes (1950) obtained high, positive thermopowers, indicating p-type conduction for four samples of sphalerite. This, however, is probably due to the presence of iron as an impurity, giving rise to conduction in a d-orbital band by positive holes.

The substitution of transition metal impurities for zinc in zinc sulphide has a pronounced effect on the electronic properties. Measurements of the electrical conductivity of a natural sphalerite with an iron content of 12.4 atom per cent showed that this sphalerite exhibited typical semiconductor behaviour, with an activation energy for conduction of 0.49 eV, although its electrical resistivity was high at 8×10^7 Ω·cm (Keys *et al*, 1968). The absence of a measurable Hall effect and a positive thermoelectric power (Tolkes, 1950) suggest that the hopping of holes in a localized d-orbital band is the conduction mechanism (Vaughan and Craig, 1978; Keys *et al*, 1968). This model requires the holes to be generated as Fe^{3+} ions, i.e., the absence of one d-orbital is necessary, although only one in 800 iron atoms needs to be in the Fe^{3+} form in order to account for the conductivity (Keys *et al*, 1968).

The quantum calculation of the electronic structure of the FeS_4Zn_{12} cluster indicates that the $2e$ and $4t_2$ orbital levels due to the d-orbitals of the iron impurity in ZnS are about 0.56 eV and 1.44 eV above the valence band respectively (Majewski, 1981). These calculations give evidence for bond formation involving the iron impurity and the host ligands. The $2e$ and $4t_2$ orbitals can be represented as a localized band within the zinc sulphide band gap, and the removal of

electrons from either of these orbitals will create the holes required for the d-orbital conduction mechanism. The effect of the iron impurity is to create an impurity band within the band gap of the zinc sulphide. The two other elements that frequently substitute for zinc are cadmium and manganese, both of which have no effect on the electrical conductivity (Shuey, 1975)

CHAPTER 3

THE THEORY OF CHARGE TRANSFER AT THE SEMICONDUCTOR-SOLUTION PHASE BOUNDARY

Garrett and Brattain (1955) presented the first investigation of the semiconductor-solution phase boundary, which established the principles of semiconductor electrochemistry. Three models have been proposed for the semiconductor-solution phase boundary: the idealized model (Gerischer, 1970), the recombinative model (Frank and Bard, 1975; Peter *et al*, 1984) and the Fermi-level pinning model (Bard *et al*, 1980). Gerischer (1960a) and Green (1959) reviewed the semiconductor literature, and Morrison (1980) and Memming (1980) presented the approach of semiconductor electrochemistry in depth.

A description of the band structure of semiconductors, the semiconductor-solution phase boundary and charge-transfer reactions at this phase boundary is given in this chapter. Only the more important aspects of the idealized model and the Fermi-level pinning model will be summarized. The discussion of charge transfer at a semiconductor is divided formally into charge transfer in the presence of a redox couple in solution, i.e., electron transfer, and charge transfer in the absence of a redox couple in solution, i.e., ionic transfer. This division is also of assistance in the analysis of the dissolution reactions, since electron transfer occurs in oxidative dissolution, while ionic transfer occurs in non-oxidative dissolution.

3.1 Semiconductor fundamentals

3.1.1 *The vacuum and hydrogen energy scales*

Two zeros of energy are used in semiconductor electrochemistry. The zero of energy on the physical scale, often referred to as the vacuum scale, is the energy of an electron at infinity, while the zero of energy in electrochemistry is the standard hydrogen electrode (SHE), i.e., the energy of an electrochemical system is referred to the Fermi *level of the hydrogen reference electrode at standard conditions.* (The potential difference between two electrodes of a cell is the difference in their Fermi levels, and is measured in volts.) The conversion between these two scales is as follows.

$$E\left\{\begin{matrix}\text{measured on the}\\ \text{vacuum scale, eV}\end{matrix}\right\} = \text{const} + qV\left\{\begin{matrix}\text{measured on the electro-}\\ \text{chemical scale, V}\end{matrix}\right\}$$

where q is the electronic charge, and the constant is 4.44 ± 0.02 eV (Trasatti, 1986). The conversion between these two energy scales is shown in Figure 3.1.

3.1.2 *The band theory of semiconductors*

In a solid the coalescence of electronic energy levels associated with individual atoms results in a broadening of the levels into energy bands, which may or may not overlap. In metals, these bands do overlap, resulting in a delocalization of the valence electrons. In a semiconductor, these bands are separated by a forbidden band of width E_{gap}, the band gap. The band structure of a semiconductor is characterized by the forbidden band gap between the filled valence and empty conduction bands.

There are two types of charge carriers in a semiconductor: electrons

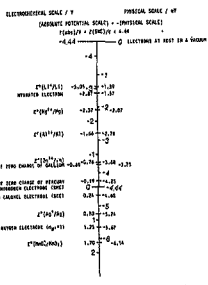

Figure 3.1 Conversion of electrode potentials into electronic energies for aqueous redox systems.

in the conduction band, and holes ('missing' electrons, representing a positive charge) in the valence band. The semiconductor is referred to as n-type if the mechanism of conduction is by electrons in the conduction band, and p-type if it is by holes in the valence band. The probability of any quantum state of the bands being occupied is governed by the Fermi-Dirac distribution law. The Fermi level is defined either as the energy level for which the probability of electron occupancy is one-half, or as the electrochemical potential of the electrons in the solid.

The band model for a semiconductor surface differs from that for a metal primarily because of the excess charge density in the surface of the solid, called the space-charge layer. A space-charge region in a

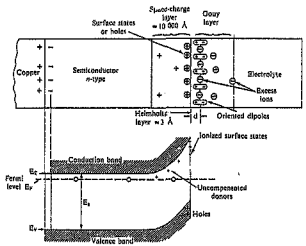

Figure 3.2 The charge distribution and energy level diagram at an n-type semiconductor-electrolyte interface (after Dewald, 1960)

solid exists only if the electron density is small, as in the case of semiconductors and insulators. In metals, the electron density is large, so that only the potential drop across the Helmholtz layer exists at the metal-solution phase boundary. In the case of a semiconductor, a potential drop also occurs across the space-charge region due to the low electron density. The excess charge density at the surface is a result of the termination of the lattice structure, forming Tamm or Shockley states (intrinsic states) at the surface. The excess density in the space-charge region results in a 'bending of the bands' at the interface. The bands in the bulk are lower than the bands at the surface if the applied potential difference is positive and *vice versa* if the applied potential difference is negative. The 'one-electron' band model for an n-type semiconductor (Dewald, 1960) is shown in Figure 3.2.

The concentration of charge carriers at the surface is an exponential function of the potential difference between the surface and the bulk semiconductor. The concentration of surface holes, p_s, is given by

$$p_s = p_b \exp[(\phi_b - \phi_s)q/kT] = p_b \exp(\Delta\phi_{sc} q/kT) \qquad 3.1$$

where p_b is the bulk concentration of holes, $\Delta\phi_{sc}$ is the potential drop across the space-charge region, q is the electronic charge, k is the Boltzmann constant and ϕ_s and ϕ_b are the surface and bulk potentials, respectively. The factor q/kT is the same as the factor F/RT found in the electrochemical literature. The value of the applied potential difference when the bands are flat is called the flatband potential.

The location of the bands of compound semiconductors at the flatband potential can be calculated using the method of Butler and Ginley (1978). The Sanderson electronegativity, χ, of a compound, defined as the geometric mean of the electronegativities of the constituent atoms, was assumed to be the mid-gap energy, $\frac{1}{2}(E^*_{vs} + E^*_{cs})$. Therefore, the electron affinity of a solid such as ZnS will be given by

$$EA = \tfrac{1}{2}(E^*_{vs} + E^*_{cs}) - \tfrac{1}{2}E_{gap} \qquad 3.2$$

$$= \chi(ZnS) - \tfrac{1}{2}E_{gap} \qquad 3.3$$

$$= [\chi(Zn)\chi(S)]^{\frac{1}{2}} - \tfrac{1}{2}E_{gap} \qquad 3.4$$

where E^*_{cs} and E^*_{vs} are the energies of the conduction- and valence-band edges at the surface at the flatband potential, respectively, and E_{gap} is the energy of the band gap between the valence and conduction bands. Butler and Ginley (1978) used the Mulliken definition of the electronegativity of an element,

$$\chi(M) = \tfrac{1}{2}(A_f + I_1) \qquad 3.5$$

where A_E is the electron affinity and I_1 is the first ionization potential. For ZnS these values are

$$\chi(Zn) = \tfrac{1}{2}(0 + 9.394) = 4.697 \text{ eV} \qquad 3.6$$

$$\chi(S) = \tfrac{1}{2}(200.4/96.486 + 10.36) = 6.218 \text{ eV} \qquad 3.7$$

$$\chi(ZnS) = 5.404 \text{ eV} \qquad 3.8$$

$$EA = 3.574 \text{ eV} = -E^{\circ}_{cs} \qquad 3.9$$

The electron affinity of the solid is the conduction band edge, as shown in Figure 3.3. This calculated value agrees reasonably well with the measurement of the electron affinity of zinc sulphide in a vacuum made by Swank (1967) of 3.9 eV. The calculated band edges for a number of sulphides are shown in Figure 3.4 as a means of comparison.

Adsorption of ions, particularly H^+ and OH^-, at the inner Helmholtz plane (IHP), i.e., contact adsorption, will alter the distribution of charge at the interface (Boddy and Brattain, 1963). Therefore, the conduction band edge is a function of pH,

$$E_{cs} = E^{\circ}_{cs} + \Delta\phi_H \qquad 3.10$$

where $\Delta\phi_H$ is the potential drop across the Helmholtz layer due to the specific adsorption of H^+ and OH^- ions. The band edges shift to lower energy levels by 0.059 V per pH unit for a decreasing solution pH. The point of zero zeta potential of ZnS occurs at a pH of about 4. The experiments in this work are done at a pH of 2, so this will mean a small correction of about 0.12 eV to the band edges calculated at the flatband potential.

Most sulphides occur as non-stoichiometric compounds, and this affects the electronic properties of the solid. A metal-excess compound, such

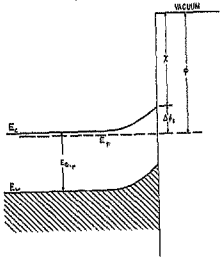

Figure 3.3 Energy diagram of the surface of an n-type semiconductor. E_c and E_v indicate the conduction- and valence-band edges, and E_F the Fermi level.

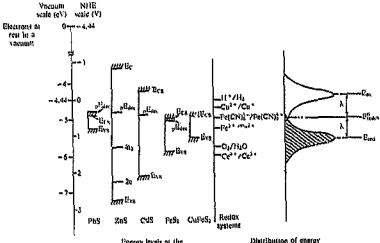

Figure 3.4 A comparison of the energy levels at the semiconductor surface for a number of mineral sulphides, and the energy levels of oxidants in aqueous solutions. The left-hand scale shows both the vacuum and hydrogen energy scales. E_{cs} and E_{vs} are the conduction and valence-band edges, respectively, and the $4t_2$ and $3e$ levels refer to the iron d-orbital levels in the end. pE_{abs} refers to the thermodynamic decomposition potential.

as chalcopyrite, will display n-type semiconduction, while an anion-rich compound will display p-type semiconduction.

3.2 The semiconductor-solution phase boundary

A difference in electrical potential usually forms at a boundary between two phases possessing sufficiently high electrical conductivities, such as the boundary between a metal and solution or a semiconductor and a solution. The formation of this potential difference arises because of the transfer of ions or electrons on breaking their bonds with the substance in one phase and reacting to form new bonds with the substance in the other phase.

The semiconductor-solution phase boundary consists of a double-layer structure in which the charge in the solid balances the charge in the solution. Three double layers are indicated in Figure 3.2. They include a space-charge layer, discussed in section 3.1, a Helmholtz double-layer between the solid and the outer Helmholtz plane which is at the distance of closest approach of non-adsorbed ions, about 0.3 nm, and the Gouy layer in the solution near the solid, in which an excess of ions of one sign exists. These charge contributions can be treated (to a good approximation) as capacitors in series.

A semiconductor and a solution are in equilibrium when the electrochemical potential of the electron in the solid is equal to the electrochemical potential of the electron in the solution, i.e., $E_F = E^{\circ}_{redox}$. Thus, the immersion of a solid in a redox solution redistributes any pre-existing charge in the interphasial region so that an excess of charge density in the solution is balanced by an equal density of charge in the solid (the space-charge layer) at equilibrium (Gerischer 1960a, 1970; Mehl and Hale, 1966). This redistribution of the charge results in a corresponding change in the flatband potential compared with its value in vacuo.

3.3 The kinetics of semiconductor electrode processes

Semiconductor processes that occur in the absence of a redox couple, such as anodic oxidation, O_2 evolution, and oxide formation, involve a strong interaction between the semiconductor and the solution. In processes that involve pure electron transfer between a redox couple and the semiconductor electrode, there is only a weak interaction between the semiconductor and the solution (stretching of the bonds in the solvation shell of the oxidant or reductant). The theory of charge transfer at semiconductors is divided along these lines: those processes that occur *in the presence and those* that occur in the absence of a redox couple in solution. This distinction is important for leaching, since oxidative dissolution requires an oxidant, while non-oxidative dissolution occurs in the absence of an oxidant. This distinction is the reason for the use of different aspects of the *charge-transfer* theory in the analysis of the results of oxidative and non-oxidative dissolution of sphalerite presented in Chapter 5.

3.3.1 *Charge-transfer reactions without a redox couple in solution*

The concepts of charge transfer were developed to describe the movement of an ion from a position in the metal surface to the solution across the Helmholtz double-layer. The *metal ion being transferred* is incorporated in the metal in an ionic state, since the bonding in metal lattices can be interpreted as being mainly due to the electrostatic interaction between the metal ions and the free electrons (conduction electrons). When the metal ion moves from the surface into the *solution*, the metallic bonding is reduced and the interaction with the polar solvent or with a complexing species in the solvent becomes stronger with increasing distance from the surface. This results in an activation barrier with a saddle point within the Helmholtz layer. The height of this barrier is influenced by the electrical field in the Helmholtz layer, and this results in an exponential relation between the rate of charge transfer and the

applied potential difference.

In a *semiconductor* the electrical field strength in the surface is normally much smaller than, and cannot be varied (by a change in the applied potential) as much as, that at the metal-solution interface. In addition, it cannot be assumed that all the atoms in the surface are like metallic ions in an electron gas, because of the directed covalent bonds in a semiconductor.

The simplest charge-transfer reaction for an elemental semiconductor, A, can be treated as a two-step process:

$$A_{lat} \rightleftharpoons A^{+}_{lat} + e^{-} \qquad 3.11a$$

or

$$A_{lat} + h^{+} \rightleftharpoons A^{+}_{lat} \qquad 3.11b$$

$$A^{+}_{lat} + \text{solvent} \rightleftharpoons A^{+}(\text{solvent}) \qquad 3.12$$

where reactions 3.11 a and b represent the probability that the semiconductor surface-atom will be found in the ionic state, h^{+} is a hole in the valence band at the surface, e^{-} is an electron in the conduction band at the surface and A_{lat} is an atom of the lattice at the surface. Reaction 3.12 is the charge-transfer reaction in which the ion is transferred across the potential-dependent activation barrier within the Helmholtz layer, and is described by the Butler-Volmer equation (Gerischer, 1960a). If charge transfer is the rate-controlling step, then the net anodic current due to dissolution is given by

$$j = k^{o}[A^{+}_{lat}]\exp(\alpha zF\Delta\phi_H/RT) - k^{o}[A^{+}]\exp(-(1-\alpha)zF\Delta\phi_H/RT) \qquad 3.13$$

where $[A^{+}_{lat}]$ and $[A^{+}]$ refer to the surface and solution con-

contrations of A, $\Delta\phi_H$ is the potential drop across the Helmholtz plane, α is the transfer coefficient and k^a and k^c are the rate constants for the anodic (removal) and cathodic (deposition) reactions of equation 3.12, respectively.

The potential drop between a *semiconductor* and the solution is the sum of the potential drops across the space-charge region and the Helmholtz double-layer (section 3.2), i.e.,

$$\Delta\phi = \Delta\phi_H + \Delta\phi_{sc} \qquad 3.14$$

where $\Delta\phi$ is the whole potential drop and $\Delta\phi_{sc}$ is the potential drop *across the space charge* region. If the Fermi level is pinned, then $\Delta\phi$ is equal to $\Delta\phi_H$. In addition, it can be seen that $[A^+_{sc}]$ is equivalent to the *surface concentration of holes*, p_s, as long as there is no surface degeneracy.

Therefore, equation 3.13 can be written as

$$j = k^a p_s \exp(\alpha z F \Delta\phi_H/RT) - k^c[A^+]\exp[-(1-\alpha)zF\Delta\phi_H/RT] \qquad 3.15$$

Substituting equation 3.1 into equation 3.15 gives

$$j = k^a p_b \exp(\Delta\phi_{sc}F/RT)\exp(\alpha z\Delta\phi_H F/RT) - k^c[A^+]\exp[-(1-\alpha)z\phi_H F/RT] \qquad 3.16$$

The changes in the potential occur primarily across the *space-charge* region for the ideal semiconductor-solution interphase. This means that $\Delta\phi_H$ is constant, and $\Delta\phi_{sc}$ is the independent variable, and that equation 3.16 can be rewritten as

$$j = k'^a \exp(\Delta\phi_{sc}F/RT) - k'^c \qquad 3.17$$

which implies a charge-transfer coefficient of 1 and a Tafel slope of 0.059 V decade^{-1}. For a p-type semiconductor, the anodic process will not be limited by the supply of holes; however, for an n-type semiconductor, the anodic process will be limited by the supply of holes, since the value of p_h in equation 3.16 is low, and the current will reach a saturation limit, analogous to the diffusion-limited supply of ions to the electrode in which the concentration of the electroactive ion is low.

Turner (1956), during the anodic dissolution of Ge, obtained saturation effects for n-Ge, but none for p-Ge. Boddy (1964) obtained Tafel slopes on n-Ge and p-Ge that were very similar, except that above 400 μA cm^{-2}, he observed a slight tendency towards saturation for n-Ge. The observed Tafel slope ranged between 0.07 and 0.082 V decade^{-1}, which is significantly higher than the expected 0.059 V. This was attributed to an appreciable change in potential of the Helmholtz double layer. Boddy (1964) confirmed this directly using measurements of the interfacial capacitance and the photovoltage response. Therefore, even for pure elemental semiconductors, a deviation from ideal behaviour is found.

3.3.2 Charge-transfer reactions with a redox couple in solution

The bonding between neighbouring atoms in a crystal is due the interactions in bonding orbitals of the neighbouring atomic nuclei. The bonding electron-states belong to the valence band of the solid, and the presence of a hole in this band means that one of the bonding electrons has been removed, and the bond weakened. Holes can be supplied to the surface from the electrode interior as a result of the application of a potential or, as in the case of leaching, they can be injected into the valence band at the surface by an oxidizing agent.

The oxidative dissolution of a compound semiconductor, $M^{\delta+}S^{\delta-}$, can occur in the following steps (Gerischer and Mindt, 1968):

$$(M^{\delta+}S^{\delta-})_s + X \rightarrow (MX)^+ + \cdot S_s + e^- \qquad 3.18a$$

$$(M^{\delta+}S^{\delta-})_s + X + h^+ \rightarrow (MX)^+ + \cdot S_s \qquad 3.18b$$

$$\cdot S_s + Y \rightarrow (SY)^+ + e^- \qquad 3.18c$$

$$\cdot S_s + Y + h^+ \rightarrow (SY)^+ \qquad 3.18d$$

$$\cdot S_s + \cdot S_s \rightarrow (S\text{-}S)_s \qquad 3.18e$$

$$S_n + \cdot S_s \rightarrow S_{n+1} \qquad 3.18f$$

where X and Y represent ionic species in solution. It can be predicted that the electropositive component, $M^{\delta+}$, i.e., the element associated with the conduction band, will go into solution while, in many cases, the more electronegative component will undergo a recombination reaction, which will result in the stable elemental state for this component.

In semiconductors with a band gap greater than 1 eV, anodic dissolution occurs almost entirely as a result of the hole injection into the valence band (Gerischer and Mindt, 1968). Table 3.1 summarizes the contribution of holes to the anodic decomposition reaction. Since dissolution involves the contribution of holes, one would expect that p-type semiconductors would leach at a greater rate than n-type. Endington and Fronser (1969) showed that p-type galena leached at a greater rate than n-type galena.

For oxidative dissolution to occur, electrons must transferred from the bonding orbitals of the semiconductor (the valence band, representing the occupied levels) to the oxidant in solution (the unoccupied levels) across the electrical potential barrier at the phase boundary. The rate of electron transfer depends on the number of

Table 3.1 Contribution of holes to the anodic dissolution of semiconductors (After Gerischer and Mindt, 1968)

	E_{gap} (eV)	Oxidative decomposition products	Contribution of holes (%)
Ge	0.66	Ge^{4+}	5* - 70
Si	1.09	Si^{2+} (Si^{4+})	ca 100
GaAs	[illegible]	Ga^{2+}, As^{3+}	ca 99.8
CdTe	[illegible]	Cd^{2+}, Te^{6+}	?
CdSe	[illegible]	Cd^{2+}, Se	ca 96
CuO	[illegible]	[illegible]$^{2+}$, HO_2	?
CdO	[illegible]	[illegible]$^{2+}$, HO_2	?
GaP	[illegible]	Ga[illegible], P or P^{3+}	ca 100
CdS	[illegible]	Cd^{2+}, S	ca 100
Zn	3.3	Zn^{2+}, HO_2	ca 100

[illegible]N levels available on either side of the interface, and on the occupancy of these levels. Since electrons are quantum particles, these occupancies are expressed in probabilities. The probability of an energy level in the semiconductor being occupied is given by the Fermi distribution, discussed in section 3.1. The probability of an energy level in the solution being occupied is described by the fluctuating energy-level model.

The fluctuating energy-level model of ions in solution

The representation of ions in solution as electronic energy levels is more complicated than the representation of energy levels found in or on solids. No distinction can be made between the energy levels of an occupied and an unoccupied state in a solid, but in the case of an ion in a polarizable and polar solvent, there is a Franck-Condon shift in the levels of the occupied and unoccupied states because of the strong interaction energies between the ion and the solvent. This shift in

levels is represented by the reorganization energy, λ, illustrated in Figure 3.4.

In addition, the energy levels of an ion in solution are distributed as a result of the thermal fluctuations of the dipoles in the solvation sheath surrounding the ion. Theories of electrostatic polarization (Marcus, 1964; Levich, 1970, indicate that the distribution of energy levels is a Gaussian distribution. Figure 3.4 illustrates this model for the ferricyanide and ferrocyanide ions.

The probability of electron transfer between an electrode and an ion in solution depends on the energy level of the ion at the instant of transfer, so these fluctuations are important (Marcus, 1964). The energy needed for an ion to reach the activated state is the difference in energy between the oxidizing agent, E_{ox}, and E^*, and the probability, W_{ox}, that the energy level of a species will be at E^* is given by

$$W_{ox}(E^*) = (4\pi\lambda kT)^{-\frac{1}{2}} \exp[-(E_{ox} - E^*)^2/4\lambda kT] \qquad 3.19$$

where λ is the reorganization energy, which includes the energy contributions from the stretching of bonds in the inner co-ordination sphere and the rotation of solvent molecules in the outer sphere (Gerischer, 1960; see also Bockris and Khan, 1985), k is the Boltzmann constant, and T is the temperature. These fluctuations in energy are not small, and the standard deviation, $(\lambda kT)^{\frac{1}{2}}$, can be several tenths of an electron volt (Morrison, 1978). Frese (1981) has determined λ for a number of oxidants and reductants.

The location of the energy levels of ions in solution can be obtained from the standard reduction potential of the redox couple. This can be shown as follows. An 'effective redox energy-level' in solution is defined as

$$E^*_{redox} = \tfrac{1}{2}(E_{ox} + E_{red}) \qquad 3.20$$

where E_{red} and E_{ox} are the energy levels of the occupied and unoccupied states, respectively. E°_{redox} can be interpreted as the chemical potential of the electron in the solution redox system.

Since the Fermi level of the electrode and E°_{redox} represent the chemical potential of the electron in the solid and the solution respectively, and the chemical potentials are equal at equilibrium, the Fermi level in an electrode at equilibrium at standard conditions is equal to E°_{redox}.

$$E_F = E^{\circ}_{redox} \qquad 3.21$$

The Fermi level of the solid is also related to the standard redox potentials tabulated in handbooks since the measured voltage is the difference in the Fermi levels of an electrode in equilibrium with the redox couple and the reference electrode in equilibrium with the hydrogen couple as a reference electrode. Therefore,

$$E_F = \text{const} - qV^{\circ} \qquad 3.22$$

where V° is the tabulated redox couple, and the constant is a factor to change between the physical energy scale (vacuum scale) and the electrochemical scale (normal hydrogen electrode) discussed earlier in this chapter. Equations 3.21 and 3.22 can be equated,

$$E^{\circ}_{redox} = \text{const} - qV^{\circ} \qquad 3.23$$

Therefore, the energy levels of simple ions, where solvent reorganization is the only transformation, can be related directly to reduction potentials on the electrochemical energy scale.

The value of the 'effective redox energy-level' is not the 'real' electronic energy-level, and it should be remembered that this is the average energy level of the occupied and unoccupied states, E_{red} and

E_{ox}, repectively. E°_{redox} is a type of thermodynamic energy-level, since equilibrium thermodynamics is used in its evaluation.

The levels of the ions on the vacuum energy scale and the hydrogen scale are shown in Figure 3.4.

Electron transfer between a semiconductor and the solution

Electron transfer can only occur between states of the same energy level (Gurney, 1931), i.e., without energy transfer with the surroundings and without radiation transfer. This means that, in terms of the fluctuating energy-level model, electron transfer can only occur with an ion whose energy level has a significant probability of fluctuating to the energy level of the semiconductor band with which electron transfer occurs.

The rate of electron transfer from the semiconductor to the solution is proportional to the number of occupied states in the semiconductor, $D_{sc}(E)f(E-E_{sc})$, and the number of unoccupied states in the redox solution, $D_{ox}(E)$, at the same energy E. $D_{sc}(E)$ is the density of states in the semiconductor, $f(E-E_{sc})$ is the Fermi function that describes how many of these states are occupied (the Fermi-Dirac distribution), and $D_{ox}(E)$ is the density of states in the oxidizing agent in the solution. The total current from the semiconductor to the solution is the integral of this probability over all possible energy levels (Gerischer, 1960 a, 1970).

$$j^{c} = qx \int_{-\infty}^{\infty} \nu(E) D_{sc}(E) f(E-E_{sc}) D_{ox}(E)\, dE \qquad 3.24$$

where $\nu(E)$ is the transmission coefficient, and $D_{ox}(E) = C_{ox}N_{ox}$, where C_{ox} is the concentration of oxidant in the solution.

For electron transfer to occur, the E°_{redox} of the electrolyte must

be sufficiently close to the conduction- or valence-band edges, and a comparison of the energy levels, i.e., a comparison of E_{vb} (the valence-band edge), E_{cb} (the conduction-band edge) and E°_{redox} will give a qualitative picture of whether electron transfer is possible or not (Morrison, 1978, 1980).

A redox couple may be able to exchange charge carriers with only one of the bands since the redox couple may have a significant probability of fluctuating to the energy of only one of the bands of the semiconductor. This has been determined for germanium by the transistor technique. Redox potentials with an $E^{\circ}_{redox} > 0.5$ V (NHE) are valence-band processes, while those with an $E^{\circ}_{redox} < 0$ V (NHE) are conduction-band processes (Gerischer, 1960 b).

Equation 3.24 has been integrated to give the current-potential behaviour of the ideal semiconductor-solution interface in the presence of a redox couple (Gerischer, 1970; Morrison, 1980). This current-potential behaviour is the same as that in the absence of a redox couple (equation 3.17) since the applied potential appears predominantly across the space-charge region, and it has often been described as a Schottky barrier (Morrison, 1980). The characteristic feature of a Schottky barrier is that, in the conduction band, only the cathodic process is influenced by the applied potential and in the valence band, only the anodic process depends on the applied potential. The anodic process in n-type semiconductors will thus be limited by the diffusion of minority carriers (holes) to the surface, and will display a saturation current (Morrison, 1980). Therefore, anodic dissolution of n-type minerals will be slower than that of p-type minerals.

3.3.3 *Fermi-level pinning model of semiconductor-solution junctions*

The ideal model of charge transfer at the semiconductor-solution phase boundary gives rise to the current-voltage behaviour of equation 3.17, often compared with the Schottky barrier formed at the semiconductor-metal interphase. The potential barrier is taken to be that due to the bending of the bands at the interface, and the potential drop within the semiconductor (the space-charge region) varies with the externally-applied potential, and the potential drop within the solution (Helmholtz layer) is independent of the applied potential.

Green (1959) questioned the applicability of ideal-model concepts to the semiconductor-solution phase boundary. Green pointed out that the behaviour of the interface as a Schottky barrier was dependent on the absence of a limiting number of surface states. If the surface states exceeded about 3 per cent of the total surface occupancy (i.e., about 10^{13} cm^{-2} since there are 3.5×10^{14} sites available for a molecular size of 0.3 nm in 1 cm^2 of the surface), the changes in potential would be predominantly in the Helmholtz region, and not in the space-charge region, and the pure Schottky-barrier model will fail. In this case, the Tafel slope will be close to a slope of 0.118 V $decade^{-1}$ with a charge-transfer coefficient of 0.5 for the single electron-transfer reaction, i.e., a Tafel slope similar to that expected for a metal electrode.

Bockris and Khan (1983) argued that ideal behaviour is exceptional, because of the specific adsorption of the anions and the solvent on the surface of the semiconductor. A large degree of specific adsorption on the semiconductor surface would indicate a high density of surface states, and the breakdown of the Schottky-barrier approximation. A degree of 'metallization' would occur.

The concept of Fermi-level pinning was initially formulated to account for the situation where the band bending in a semiconductor contacting

a metal is independent of the metal, even for a large variation in the work function of the metal. It has been noted that a similar situation sometimes results for a semiconductor contacting a solution containing redox potentials of different electrochemical potential (Bard *et al*, 1980). Fermi-level pinning is brought about by semiconductor surface-states, resulting in the situation where the potential drop across the semiconductor is fixed, and the change in the potential appears across the Helmholtz layer in solution. Therefore, if there is a high density of mono-energetic surface states, the Fermi level will be 'pinned' at the energy of the surface states, and the electrode behaviour of the semiconductor will be metal-like.

Iron-containing sphalerites have a relatively high density of mono-energetic states due to the contribution of the iron d-orbital band within the band gap of the ZnS (see Chapter 2). The d-band of [illegible] before 'pins' the Fermi level at the energy level of the [illegible].

The semiconductor will also display metal-like behaviour if the Fermi level in the semiconductor is in one of the energy bands. When this happens, the semiconductor is degenerate. The entire semiconductor may be degenerate, in which case the electrode simply acts like a metal, or degeneracy may be induced by the applied voltage, in which case the band bending forces the Fermi level into one of the bands, and the surface is degenerate. This applies especially to semiconductors with narrow band gaps. In semiconductors in which surface degeneracy occurs, a significant (or increasing) proportion of the applied potential appears across the Helmholtz layer, and the transfer coefficient of 1 for a non-degenerate semiconductor will move towards the 0.5 value, which is characteristic of a metal (Morrison, 1980).

3.3.4 *The effect of illumination*

The concentration of minority carriers can be changed by orders of magnitude from the equilibrium value by the illumination of the electrode by light of the energy of the band gap. The absorption of light by the semiconductor means that electrons are excited from the valence band to the conduction band (fundamental absorption), and the statistical distribution of electrons, described by the Fermi-Dirac equation, is disturbed. A hole is created in the valence band and an electron in the conduction band. These charge carriers have an appreciable life-time since the recombination of electrons and holes which would restore the equilibrium situation is slow (Gerischer, 1966).

The anodic current of an n-type semiconductor is limited by the supply of minority carriers (holes). This limiting current can be increased by the illumination of the electrode. Illumination creates minority carriers, which would react with the solution (or with the electrode at the surface), and majority carriers, which complete the external current. The limiting current is proportional to the light intensity (Williams, 1960).

Williams (1960) interpreted the effect of light on the anodic dissolution of n-type CdS as follows. Since the crystal becomes negatively charged during illumination, Cd^{2+} ions (associated with the conduction band), in equilibrium with the solution, leave an excess of S^{2-} ions (associated with the valence band) at the surface. (This is consistent with the solid-state considerations of sulphide minerals, in which the mobility of the metal ions is much greater than that of the larger sulphur ion, i.e., sulphur forms an immobile lattice.) The absorption of light excites the excess charge associated with the S^{2-} ions at the surface to the conduction band, the S^{2-} forms elemental sulphur, S, and the surface returns to its original uncharged position.

In the case of Fermi-level pinning by a deep surface-state within the band gap, response to light will still be obtained, but the output photovoltage will be independent of the solution potential. If the semiconductor, or the semiconductor surface, is degenerate, no response to illumination will be obtained.

3.4 Anodic corrosion of semiconductors

Hard and Wrighton (1977) and Gerischer (1977) have proposed a thermodynamic model for the anodic dissolution of semiconductors. They defined a redox potential for anodic dissolution, p^E_{dec}, for the dissolution reaction and this is compared with the level of the redox couple in solution, or with the Fermi level of the solid. The partial reactions for a decomposition mechanism in which holes are the major participating charge carriers are

$$MS + nh^+ + \text{solvent} \rightarrow M^{n+}(\text{solvent}) + S \qquad 3.25$$

$$nH^+(\text{solvent}) \rightleftharpoons n/2\ H_2 + nh^+ \qquad 3.26$$

The free energy difference, ΔG, for the combination of these reactions

$$MS + nH^+(\text{solvent}) \rightarrow M^{n+}(\text{solvent}) + n/2\ H_2 + S \qquad 3.27$$

gives the corresponding redox potential for decomposition

$$p^E_{dec} = \Delta G/nF \qquad 3.28$$

where F is the Faraday constant. For example

$$CdS + 2HCl \rightarrow CdCl_2 + S + H_2 \qquad 3.29$$

$$p^E_{dec} = \Delta G/2F = 0.4\ V\ (SHE) \qquad 3.30$$

and

$$ZnS + H_2SO_4 \rightarrow ZnSO_4 + S + H_2 \qquad 3.31$$

$$\Delta G = 68.7 \text{ kJ mol}^{-1} \qquad 3.32$$

$$pE_{dec} = 0.356 \text{ V} \qquad 3.33$$

Other calculated values of pE_{dec} are shown in Figure 3.4. The conditions for stability are

$pE_{dec} > E^{o}_{redox}$ or E_F stable

$pE_{dec} < E^{o}_{redox}$ or E_F unstable

pE_{dec} can be regarded as a thermodynamic energy-level for dissolution. The relative position of pE_{dec} to E_{cs} and E_{vs} for various sulphide semiconductors is shown in Figure 3.4. A mineral semiconductor will dissolve if the redox potential is greater than pE_{dec}, e.g., ZnS will oxidatively dissolve if the redox potential of the redox couple in solution is greater than 0.356 V.

The general requirement for steady-state corrosion is that the anodic and cathodic currents are equal: $j^a = j^c$. The electrical field at the surface of a metal has an opposite influence on these two processes, and it adjusts to fulfil the current equality condition. Corrosion can be described by the superposition of the anodic and cathodic partial currents. In semiconductors, the equality of these currents means that

$$j^a_c + j^a_v = j^c_c + j^c_v \qquad 3.34$$

where the subscripts 'c' and 'v' refer to the conduction band and valence band, respectively. The net currents in each band will have opposite signs

$$j_a - j_a^0 = j_v^0 - j_v^0 \qquad 3.35$$

In the corrosion of metals, the potential drop at the surface occurs across the Helmholtz plane. The superposition principle is used to obtain an expression for this potential drop, which is then substituted into the equation for the anodic dissolution current. This is the mixed-potential model of corrosion.

In order to understand the dissolution process, it is necessary to consider the crystal structure, the semiconduction type and the characteristics of the semiconductor-solution phase boundary.

CHAPTER 4

EXPERIMENTAL PROCEDURE AND RESULTS

Many of the results reported on in Chapter 1 were obtained with unsized concentrates containing substantial amounts of impurities. Dutrizac and MacDonald (1978) stated that the deduction of good kinetic data from such results is made difficult by the following factors.

(i) The use of crushed, unsized material makes it difficult to deduce the shape of the reaction curve.

(ii) The test conditions are frequently not held constant, and the acid and ferric ion concentrations may vary considerably during the course of a batch leaching experiment.

(iii) Often impure (poorly-liberated) material is used, and the impurities consume reagents, making it difficult to separate the effects due to the reaction that is under study and other reactions.

In studies of the dissolution of any concentrated mineral there is always the possibility that galvanic interactions between different minerals in contact with one another in the same particle may increase or decrease the rate of reaction. Therefore, well-liberated material must be chosen.

The experiments in this research were designed to avoid the problems cited above. Sized, well-liberated material was chosen. This material was characterized by mineralogical and chemical techniques.

The concentrations of acid and ferric ion in solution in the batch leaching experiments were monitored using a glass and a platinum electrode, respectively, and controlled by the addition of acid and

hydrogen peroxide. In this way only the kinetics of the dissolution reaction was measured.

4.1 Sample preparation and characterization

Samples of five sphalerites were used in the present study. All samples were wet-screened, and a sample in a narrow size range was selected. This fraction was first washed with sodium sulphide to remove flotation reagents (Jin and Warren, 1985) and with dilute sulphuric acid. The origin, chemical composition and mean particle size of each sample is given in Table 4.1. The Ward's sample is a natural pure sphalerite (museum grade), and is honey coloured. The other samples are impure flotation concentrates of South African and Namibian origin.

Polished sections of the samples were prepared, and mineralogical analyses were carried out. The mineralogical compositions of the samples are shown in Table 4.2. The degree of liberation was determined microscopically by a point count of 500 particles of each sample and the results for each sample are shown in Table 4.3.

The iron content of each sphalerite was determined by electron-microprobe analysis of about 100 particles. The arithmetic average iron content for each sample is given in Table 4.4. The distribution of iron in each sample is shown in Appendix A.

4.2 Experimental apparatus

The reactor consisted of a one litre cylindrical glass vessel with a flat perspex impeller driven by a variable-speed motor. A single Perspex baffle was installed. The apparatus is illustrated in Figure 4.1. The temperature was maintained to within 0.5°C of the set-point by a contact thermometer connected through one of the ports in the lid to a heating plate. A solution bridge connected a calomel reference electrode to the

Table 4.1 Chemical compositions of the sphalerite concentrates.
(All values in per cent)

	Origin of the sphalerite				
	Ward's	Zincor	Black Mountain	Rosh Pinah	Gamsberg
Zn	66.5	56.7	49.8	56.7	51.0
S	32.2	32.6	28.6	30.1	28.8
Fe	0.5	7.25	9.72	4.35	9.08
Cu	0.038	0.018	0.37	0.25	0.14
Pb	0.090	1.51	3.46	1.46	0.74
Cd	0.48	0.12	0.138	0.12	0.087
Mn	0.005	0.01	1.26	0.29	2.34

Table 4.2. Mineralogical compositions of the sphalerite concentrates
(All values in %)

	Origin of the sphalerite				
	Ward's	Zincor	Black Mountain	Rosh Pinah	Gamsberg
Sphalerite	100	88.9	97.4	92.2	96.8
Chalcopyrite + Covellite	trace	trace	trace	0.2	nd
Galena	trace	0.5	0.4	trace	nd
Pyrite + Pyrrhotite	trace	7.5	1.4	7.4	1.2
Silicate Gangue minerals	nd	3.1	0.8	0.2	nd

nd - not detected

Table 4.3 Degree of liberation of the sphalerite concentrates.

	Liberated (%)	Locked to sulphides (%)	Locked to gangue (%)
Ward's	≈ 100	nd	nd
Zincor	91.8	7.2	1.0
Black Mountain	90.2	9.6	0.2
Rosh Pinah	98.1	1.7	0.2
Gamsberg	99.4	0.6	nd

Table 4.4 Iron content in the (Zn,Fe)S mineral phase

Sphalerite	Fe in (Zn,Fe)S , in per cent
Ward's	0.55
Zinoer	2.56
Black Mountain	8.02
Rosh Pinah	1.79
Gamsberg	8.62

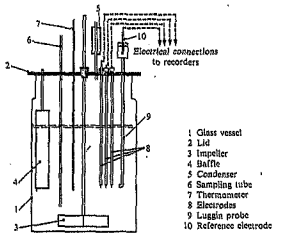

Figure 4.1 Diagram of the leaching apparatus

solution, and the redox potential was measured by use of a platinum electrode. All potentials reported here refer to the saturated calomel electrode (SCE) unless otherwise stated. The redox potential of the solution was maintained to within 2mV of the set-point by the addition of 3 per cent hydrogen peroxide, the amount of the addition being controlled by a Radiometer PHM84/TTT80 titrator system. The pH of the solution, which was measured with a glass-Ag/AgCl electrode, was maintained to with 0.1 units in the pH range 1 to 1.5 by the addition of 500 g l^{-1} of either sulphuric acid for ferric sulphate leaching, or hydrochloric acid for ferric chloride leaching. The pH was controlled by a similar system to that used for control of the redox potential. A Phillips 125 W UV lamp was used to irradiate the leaching vessel.

4.3 Experimental procedure

The standard conditions used in the investigation of the effect of the iron impurity on the rate of leaching were as follows. The leaching solution consisted of an aqueous solution of 0.2 M $FeCl_3$, 0.3 M HCl, 0.005 M $FeCl_2$, 2 M NaCl. The standard temperature was 65°C. A high concentration of chloride was chosen to prevent the formation of a film of insoluble lead sulphate on the surface of the concentrates with a high galena content (Crundwell, 1985). The standard conditions in the investigation of the effect of the concentrations of ferric and ferrous sulphate on the rate of dissolution were as follows. The leaching solution consisted of an aqueous solution of 0.1 M H_2SO_4, and 0.5 M $Fe_2(SO_4)_3$. The standard temperature was 78°C. Deionized water and analytical grade reagents were used in both sulphate and chloride solutions.

Once the initial conditions had stabilized, 1.5 g of concentrate was rapidly added to 0.75 dm^3 of solution in the experiments in which chloride solutions were used, and 3 g of concentrate was added to 1.5 dm^3 of leaching solution in the experiments in which sulphate

solutions were used. A low solid-to-liquid ratio was chosen so that the addition of hydrogen peroxide and acid during the reaction would not change the total volume of the solution to a significant extent.

Samples were taken during the reaction with a 15 ml syringe, and filtered immediately under pressure. The concentration of zinc in solution was determined by atomic-absorption spectrophotometry, and the addition of hydrogen peroxide was monitored as a check on the zinc concentration in solution. Direct oxidation of the sphalerite by hydrogen peroxide was assumed to be minimal due to the low solid-liquid ratio, and the rapid oxidation reaction with the Fe(II) in solution.

4.4 Microscopic and mineralogical investigation of leached sphalerite samples

Fresh and leached samples of sphalerite were investigated using scanning electron-microscope (SEM) and electron-microprobe techniques. Photographs 1 to 18 are photographs taken of the samples using the scanning electron-microscope and Photographs 19 to 21 are photographs taken of polished sections of the samples using a back-scatter electron image technique.

Photographs 1 to 4 are SEM photographs of the Ward's sample. The fresh sample (Photograph 1) is clean and angular. Photograph 2 shows the Ward's sample after it has been leached in the ferric chloride solution. The angular and crystalline deposit on the surface is the sulphur that is produced, and which has been physically removed in Photograph 3 by ultrasonic vibration. Photograph 4 is an enlargement of the uncleaned material of Photograph 2, indicating the angular sulphur deposit. The formation of hillocks on the surface of the sphalerite particle can be seen in Photographs 2 to 4; however, some of the faces do not display this hillock formation, suggesting that preferential dissolution takes place on some of the crystallographic

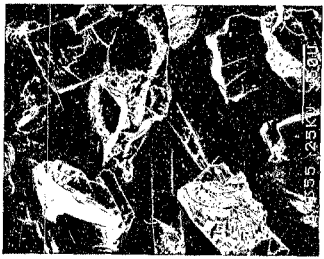

Photograph 1, Ward's sphalerite - fresh. The bar indicates the scale



Photograph 2, Ward's sphalerite - leached in ferric chloride solution

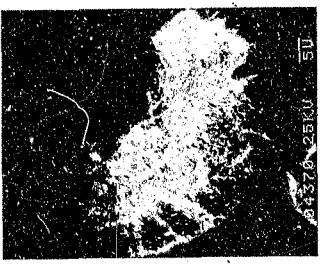

Photograph 3. Ward's sphalerite - leached in ferric chloride solution and ultrasonically cleaned.



Photograph 4. Ward's sphalerite - leached in ferric chloride solution

faces.

Photographs 5 to 8 are SEM photographs of the sample of Gamsberg sphalerite. Photograph 5 is a photograph of the fresh sample showing that there are numerous smaller particles, which are about 2 μm and less in size, that adhere to the surface of the larger particles, which are about 40 to 50 μm in size. The layer of sulphur on a well-leached particle is shown in Photograph 6. This layer of sulphur is porous and the leaching solution has access to the surface through numerous crevices in the layer. Photograph 7 shows the leached and cleaned Gamsberg sphalerite. The formation of hillocks is also present on the partially leached sphalerite particles. Photograph 8 indicates that the porous layer of sulphur that forms in ferric chloride leaching is similar to that which forms in ferric sulphate leaching (Photograph 6).

Photographs 9 and 10 are SEM photographs of the samples of Zinor sphalerite. Again, the photograph of the leached sample indicates evidence for the formation of sulphur product, i.e. the formation of hillocks on one face, and of preferential dissolution, in that one face has not been attacked.

Photographs 11 to 15 are SEM photographs of the samples of the Black Mountain sphalerite. The fresh sample is covered with small particles which adhere to the surface of the larger particles. Photographs 12 and 13 compare the products of ferric sulphate and ferric chloride leaching - the sample that was leached in a ferric sulphate solution has not leached well, since the surface is not covered by the characteristic layer of sulphur, while the sample that was leached in a ferric chloride solution is completely covered by a layer of sulphur. Photograph 14 is a photograph of a sample that has leached in a ferric chloride solution and the product layer has been been removed by ultrasonic vibration. This photograph shows the familiar formation of hillocks, and an adjacent surface that has not been attacked. Photograph 15 is a close-up of a cleaned (by ultrasonic vibration)

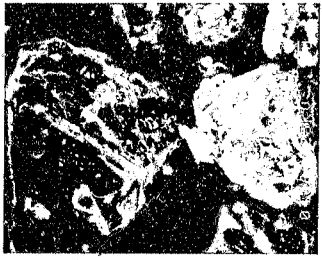

Photograph 5. Gamsberg sphalerite - fresh. The bar indicates the scale



Photograph 6. Gamsberg sphalerite - leached in ferric sulphate solution



Photograph 7. Gamsberg sphalerite + leached in ferric sulphate solution and ultrasonically cleaned.



Photograph 8. Gamsberg sphalerite + leached in ferric chloride solution



Photograph 9. Zincor sphalerite - fresh



Photograph 10. Zincor sphalerite - leached in ferric chloride solution



Photograph 11. Black Mountain sphalerite - fresh

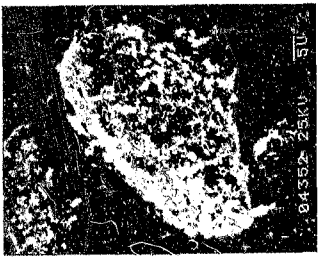

Photograph 12. Black Mountain sphalerite - leached in ferric sulphate solution

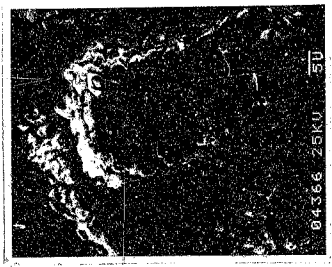

Photograph 13. Black Mountain sphalerite - ferric chloride leached

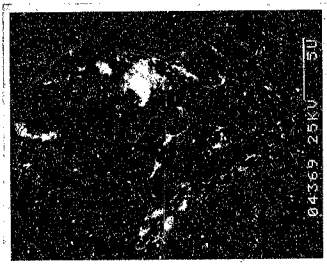

Photograph 14. Black Mountain sphalerite - ferric chloride leached and ultrasonically cleaned.



Photograph 15. Black Mountain sphalerite - ferric sulphate leached and ultrasonically cleaned

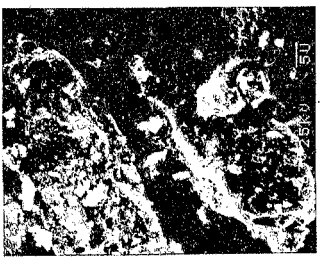

Photograph 16. Rosh Pinah sphalerite - fresh

sample of the Black Mountain sphalerite that has been leached in a ferric sulphate solution. The triangular hillocks are clearly visible.

Photographs 16 to 19 are SEM photographs of the Rosh Pinah sample. The fresh, unleached sample is covered with smaller particles which adhere to the surface of the larger particles. Photographs 17 and 18 compare the products of leaching in ferric sulphate and ferric chloride solutions, and as with the sample from Black Mountain, the sphalerite that has been subjected to a ferric sulphate solution is essentially unattacked, while that that has been subjected to a ferric chloride solution has reacted well, since it is covered by a layer of sulphur.

A number of photographs clearly show the formation of hillocks on one of the faces, indicative of dissolution on that face, and no hillocks on another face of the same particle. The dissolution of group III-V semiconductors has been studied, and the differences in the reactivities of the different crystallographic planes has been reported. Gatos (1960) reported that the (100) and (110) planes of a semiconductor with the zinc blende (sphalerite) structure are more reactive than the (111) face.

In the (111) direction, the planes are alternately occupied by atoms of group III or group V elements (for the III-V semiconductors). The atoms of one of the layers in the (111) direction are triply bonded to the lattice, while the atoms immediately below this are singly bonded to the lattice. The (111) surface must necessarily terminate with the atoms that are triply bonded to the surface. The outermost layer of the (100) surfaces are doubly bonded to the surface, and are therefore more easily dissolved than than the (111) surfaces. The (110) surfaces consist of atoms of both types, and are doubly bonded to the interior, singly bonded to another surface atom, and there is one dangling bond. For Ge, in which there is no difference between the constituent atoms, the reactivity increases in the order (111) < (110) < (100) (Gatos, 1960).



Photograph 17. Rosh Pinah sphalerite - leached in ferric sulphate solution

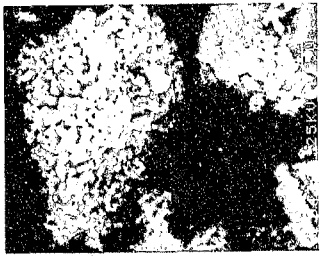

Photograph 18. Rosh Pinah sphalerite - leached in ferric chloride solution

It is quite possible that the (111) plane of sphalerite is much less reactive than the other surfaces and that small hillocks form on the surfaces of the other planes. It is more difficult to explain the shape of the hillocks, shown clearly in Photograph 15. In this photograph, one of the surfaces is covered with triangular hillocks, which are probably the results of the merging of pits, while the other surface is clearly being attacked in steps from the same direction as the surface covered in hillocks. This is clear evidence that one of the surfaces is less reactive than that of the others, and this is most likely to be the (111) surface.

4.5 Experimental results

4.5.1 *Effect of the iron impurity content of the sphalerite on the rate of leaching*

Previous study of the dissolution of the sphalerite concentrate from the Black Mountain showed that passivation occurred in ferric sulphate solutions, and that the concentrate would not dissolve beyond a conversion of about 50 per cent (Grundwell, 1985). Investigation of the *leaching characteristics of the sphalerite concentrates from* Black Mountain and Rosh Pinah in ferric sulphate solutions showed that both these materials displayed refractory behaviour, while they dissolved completely in ferric chloride solutions. The results of the investigation carried out to determine the cause of the passivation of these samples are reported in section 4.5.3 below. For this reason the effect of the iron content of the sphalerite on the rate of dissolution was investigated in a strong chloride solution.

Figures 4.2, 4.3, and 4.4 illustrate the effect of the iron content of the sphalerite on the rate of dissolution for three different temperatures. As expected, the Black Mountain and the Rosh Pinah sphalerites dissolve well in the ferric chloride solutions. Experi-

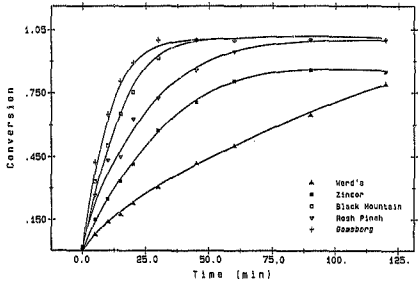

Figure 4.2 The dissolution of different sphalerite concentrates in ferric chloride solutions with 0.2 M $FeCl_3$, 0.3 M HCl, 0.005M $FeCl_2$, 2 M NaCl, 80°C.

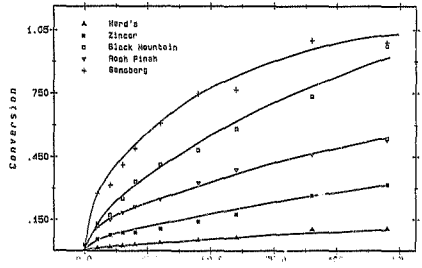

Figure 4.3 The dissolution of the different sphalerite concentrates in ferric chloride solutions with 0.2 M $FeCl_3$, 0.3 M HCl, 0.005M $FeCl_2$, 2 M NaCl, 45°C.

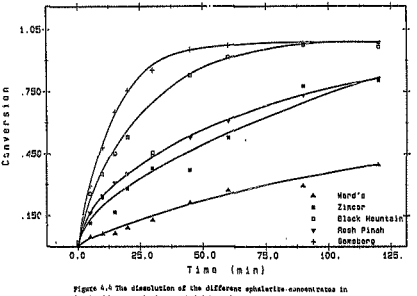

Figure 4.4 The dissolution of the different sphalerite concentrates in ferric chloride solutions with 0.2 M $FeCl_3$, 0.3 M HCl, 0.005M $FeCl_2$, 2 M NaCl, 65°C.

ments were conducted to determine the effects of UV radiation, and those results are discussed in Chapter 5. The raw data are given in Appendix B.

4.5.2 *Effect of the solution concentration on the leaching in ferric sulphate solutions*

The results reported in Table 4.3 indicate that the concentrate from Gamsberg is very well liberated, and is almost as mineralogically pure as the museum grade sphalerite from Ward's Scientific Establishment. It is also available in sufficient quantities, whereas the Ward's

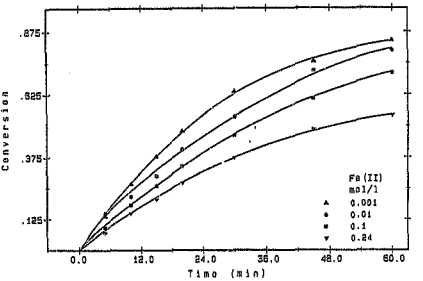

Figure 4.5 Dependence of the rate of reaction on the concentration of Fe(II) sulphate with 0.5M Fe(III) at 70°C

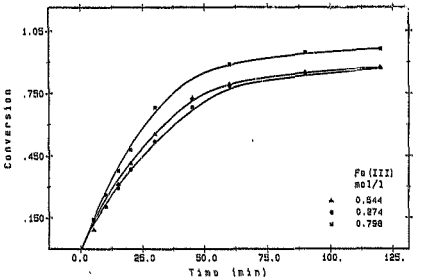

Figure 4.6 Dependence of the rate of reaction on the concentration of Fe(III) sulphate at a constant redox potential of 573 mV vs SCE at 70°C.

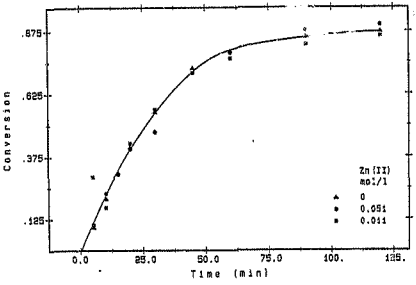

Figure 4.7 Effect of the addition of zinc to the leaching solution at 78°C, 0.5 M Fe(III) sulphate and 0.0048 M Fe(II) sulphate.

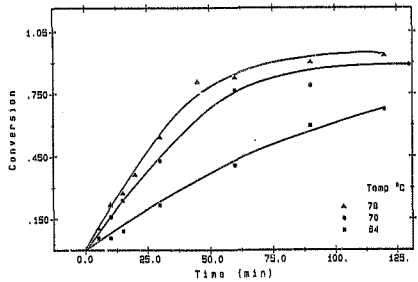

Figure 4.8 Effect of temperature of the dissolution of Gemaberg sphalerite in ferric sulphate solution with 0.25 M Fe(III) and 0.0048 M Fe(II).

sample was scarce. The high iron content of the Gamsberg sample means that it reacts a lot quicker than the Ward's sample, which considerably reduces the duration of the experiment. Thus, it was decided to use the Gamsberg sample in the investigation of the effect of the concentrations of oxidant and reductant on leaching of sphalerite.

Figures 4.5 to 4.8 illustrate the effect of an increases in the ferrous ion concentration, in the ferric ion concentration, in the zinc ion concentration and in the temperature on the leaching of Gamsberg sphalerite in ferric sulphate solutions. These results indicate that addition of ferrous ions to the leaching solution decreases the rate of dissolution, whereas addition of ferric ions to the leaching solution increases the rate of dissolution. The addition of zinc has little effect on the rate of reaction, and the dependence of the rate is that expected for a change in the solution temperature. These results are analysed in Chapter 5.3. The raw data are given in Appendix B.

4.5.3 The refractory behaviour of the leaching of Black Mountain and Rosh Pinah sphalerites in ferric sulphate solutions

Figure 4.9 illustrates the extent of reaction for a typical run on Rosh Pinah and Black Mountain sphalerites in a ferric sulphate leaching solution. In contrast to the leaching characteristics of the material from Gamsberg shown in Figures 4.5 to 4.8, both these sphalerites display passivation in that neither will dissolve completely. Previous investigation (Crundwell, 1983) has shown that an unscreened flotation concentrate from Black Mountain will not dissolve beyond 50 per cent conversion, and that the final extent of dissolution is proportional to the surface area, indicating that a surface phenomenon is responsible for the passivation behaviour. Increasing the temperature of reaction from 50°C to 90°C increased the initial rate of reaction, but the final extent of reaction only

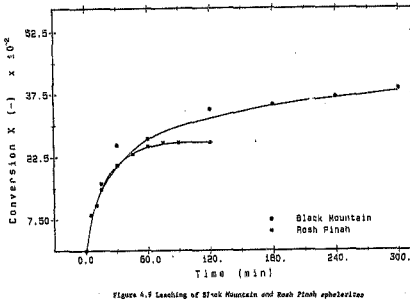

Figure 4.5 Leaching of *Black Mountain and Rosh Pinah sphalerites* showing passivation behaviour in sulphate solutions. Conditions: 0.5 M Fe(III), 0.1 M H_2SO_4, and 78°C.

increased from 24 per cent to 28 per cent for particles in the size range -74 +53 μm (Crundwell, 1985).

The main difference between the material from Gamsberg, which dissolved beyond a conversion of 90 per cent, and the material from Black Mountain is the increased lead content of the latter. The Gamsberg concentrate has 0.47 per cent lead, while the Black Mountain concentrate has 3.46 per cent lead. The mechanism for passivation could be due to the formation of an *insoluble coating of anglesite* ($PbSO_4$) or lead jarosite $[Pb_{0.5}(Fe,Zn)_3(SO_4)_2(OH)_6]$ on the surface of the particle. The subsequent removal of the sulphur product-layer and releaching did not result in futher dissolution (Crundwell, 1985), implying that the passivating coating is not the sulphur formed during the leach.

The concentrate from Rosh Pinah, which does not have as high a lead content as that from Black Mountain, also displays *passivation*.

Washing of the leached particles in CS_2 to remove the sulphur layer before they were returned to the leaching solution did not result in further dissolution for the Rosh Pinah sphalerite.

The mineralogical analysis of the three samples of sphalerite studied in ferric sulphate solutions is presented in Tables 4.5 and 4.6. It can be seen from these results that the concentrate from Gamsberg, which dissolved to beyond a conversion of 90 per cent, is more liberated than that from either Black Mountain or Rosh Pinah.

Kuzminkh and Yakoutova (1950) leached two natural sphalerites with different mineralogical compositions and reported that the sphalerites leached at similar initial rates under equivalent conditions. However, for similar conditions, an excess of 80 per cent conversion was achieved for one while only 33 per cent was achieved for the other. They proposed that the difference in the mineralogical composition was the principle reason for the difference in the final extents of reaction.

Both sphalerite concentrates studied by Kuzminkh and Yakoutova (1950) had high lead contents (about 6.8 per cent lead). They reported that the concentrate that dissolved well was well-liberated, while microscopic investigation of the concentrate that displayed passivation revealed that there was a close intergrowth of the sphalerite with other sulphide minerals. This supports the hypothesis that the deposition of a lead sulphate coating is the reason for the passivation.

The effect of a chloride solution rather than a sulphate solution as the leaching solution is shown in Figure 4.10 and 4.11 as a plot of $1-(1-X)^{1/3}$ against t. This should be a straight line if the shrinking-particle model is obeyed (Levenspiel, 1972). The deviation from linear behaviour for sulphate solutions is a result of the passivation illustrated in Figure 4.9. Figures 4.10 and 4.11 (and Figures 4.2, 4.3, and 4.4) clearly illustrate that neither the Black Mountain or the Rosh Pinah sphalerite passivate in chloride solutions.

Table 4.5 Mineralogical analysis of the *Gamsberg sphalerite* before and after leaching in ferric sulphate solutions. (All values in per cent).

	As Received	After Leached
Sphalerite - liberated	98.2	14.6
Sphalerite - locked to sulphides	0.6	0.3
Sphalerite - locked to gangue	-	-
Chalcopyrite	-	-
Galena	-	-
Pyrite and pyrrhotite	1.2	0.9
Gangue	-	1.0
Sphalerite and sulphur	-	63.6
Sulphur *products*	-	19.6

Table 4.6 Mineralogical compositions of the concentrates from Black Mountain and Rosh Pinah before and after leaching in ferric sulphate solutions. (all values in per cent).

	Black Mountain		Rosh Pinah	
	As Received	After Leached	As Received	After Leached
Sphalerite - liberated	88.6	88.2	90.4	88.8
Sphalerite - locked to sulphides	8.2	9.4	1.6	2.2
Sphalerite - locked to gangue	0.6	0.2	0.2	0
Chalcopyrite	Trace	0.2	0.2	0.4
Galena	0.4	0	Trace	0.2
Pyrite and pyrrohtite	1.4	1.2	7.4	8.4
Gangue	0.8	0.8	0.2	0

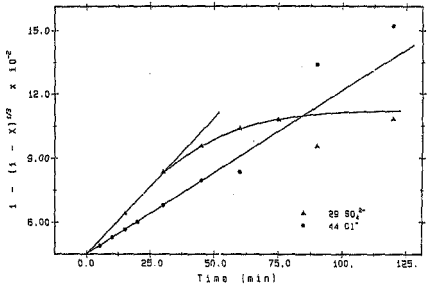

Figure 4.10 Leaching of Black Mountain sphalerite in sulphate and chloride solutions with 0.5M Fe(III) at 78°C.

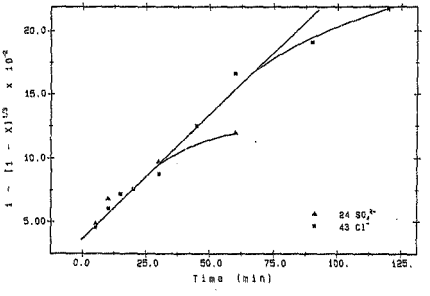

Figure 4.11 Leaching of Rosh Pinah sphalerite in sulphate and chloride solutions with 0.5M Fe(III) at 78°C.

X-ray diffraction showed minor peaks representing anglesite ($PbSO_4$) and jarosite [$K(Fe)_3(SO_4)_2(OH)_6$] for the leached Black Mountain and Rosh Pinah sphalerites. (These X-ray patterns are shown in Appendix A). Pb, Zn and trace amounts of Ag can be incorporated in the jarosite structure with the formula $Pb_{0.5}(Fe,Zn)_3(SO_4)_2(OH)_6$; Cu can be incorporated in a beaverite-plumbojarosite solid solution. These peaks were not observed for the leached material that displayed no passivation. Chemically-precipitated jarosites are often insufficiently crystalline for reliable identification by X-ray diffraction, and a degree of uncertainty is present. However, the formation of anglesite and jarosite would not occur in chloride solutions, and their presence is consistent with the passivation observed.

Analysis of the particles using electron microprobe and scanning electron-microscope with energy-dispersive (SEM-EDX) techniques did not reveal a layer of material that covered the leached particles. The surface of the Black Mountain sphalerite was covered with numerous small (< 2 μm) $PbSO_4$ particles, and sulphur product. Photographs 19 to 20 are electron back-scatter images of the particles of Black Mountain sphalerite, and show the extent of the formation of the $PbSO_4$ deposit. Photograph 19 shows that $PbSO_4$ particles are found around the entire circumference of the particle and not in a limited locality. Photograph 20 illustrates the formation of a $PbSO_4$ deposit at the surface of a galena inclusion, and Photograph 21 again shows the extent of the $PbSO_4$ formation. Although these particles of $PbSO_4$ were observed, a complete coating of $PbSO_4$ or any other lead salt was not detected. The layer of insoluble material that is needed to prevent dissolution is that needed to inhibit electron transfer, and is probably of the order of 1 nm (Diggle, 1973). A layer of this dimension is too small to be detected on the scale represented here.

The Rosh Pinah material was very similar to that of Black Mountain, except that it did not display as many $PbSO_4$ particles on the



Photograph 19. Back-scatter electron image of a Black Mountain sphalerite particle (dark grey). Note the distribution of anglesite (white grains) at the fragmented rim. Scale 10 μm



Photograph 20. Back-scatter electron image of a Black Mountain sphalerite particle showing the occurrence of anglesite (1) related to a galena inclusion (2) in the sphalerite.

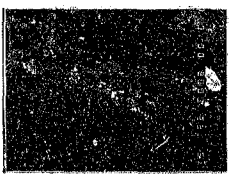

Photograph 21. Back-scatter electron image of a Black Mountain sphalerite particle showing the surface of the sphalerite (dark grey) and the distribution of anglesite. Scale 10 μm.

surface. Removal of $PbSO_4$ by washing the leached material in ammonium acetate before returning to the leaching solution did not result in additional dissolution, indicating that the formation of lead jarosite is probably responsible for the refractory behaviour. However, extensive investigation of the particles using electron-microprobe and SEM-EDX analysis did not detect such a coating.

CHAPTER 5

ANALYSIS OF RESULTS AND THE APPLICATION OF THE CHARGE-TRANSFER THEORY

In this chapter the experimental results for the oxidative and non-oxidative reactions are analyzed to determine the kinetic parameters, and a model for these two dissolution reactions is developed from the charge-transfer theory discussed in Chapter 3.

The experimental results for the oxidative reaction which were presented in Chapter 4 are analyzed in terms of the shrinking-particle model, from which a rate constant, k_r, is obtained. This rate constant is used to determine the activation energy, the order of reaction with respect to the concentration of iron in the zinc sulphide lattice, and the order of reaction with respect to the concentrations of reactants and products. A model based on the theory presented in section 3.3.2 is derived, and is shown to be consistent with the kinetics of oxidative dissolution of sphalerite.

The raw data of Verbaan (1977) is analyzed more thoroughly to determine the kinetic parameters of the non-oxidative reaction. A charge-transfer model, based on the theory presented in section 3.3.1, is derived, and is shown to be consistent with the kinetics of non-oxidative dissolution of sphalerite and other II-VI semiconductors.

The success of semiconductor electrochemistry theory in the formulation of a quantitative model to explain the effect of the concentration of iron in the zinc sulphide lattice on the rate of dissolution of sphalerite, suggests that the literature of other metal sulphides be examined in terms of this theory. This is done in the final section of this chapter, where it is stressed that the

electronic structure of mineral sulphides plays an important role in their dissolution behaviour.

5.1 Shrinking-particle model for the analysis of experimental results

The dissolution of sphalerite occurs by a surface-related phenomenon, i.e., an unreacted-core model applies. The dissolution of a particle for which this model applies, occurs in the following steps:

(i) diffusion of reactants and products through a liquid film surrounding the particle - called film-layer diffusion;
(ii) diffusion of reactants and products through the product layers, such as the sulphur layer on the particle surface - called product-layer diffusion;
(iii) reaction at the surface.

There is general agreement in the literature that the reaction at the surface controls the rate of dissolution in the initial stages of leaching. In this case, the rate of dissolution of sphalerite particles of the same size fraction is given by

$$\frac{dm_{ZnS}}{dt} = - k_s A f(C_{ox}) \qquad 5.1$$

where m_{ZnS} is the amount of leachable material remaining in the unreacted core, k_s is the rate constant, A is the surface area, and $f(C_{ox})$ is a function of the reactant concentration, C_{ox}. Assuming that the shape of the particles can be approximated by spherical geometry, then

$$\frac{dm_{ZnS}}{dt} = \rho_{ZnS}\, 4\pi r^2 \frac{dr}{dt} = - k_s\, 4\pi r^2\, f(C_{ox}) \qquad 5.2$$

where ρ_{ZnS} is the molar density of the sphalerite. Integration gives

$$t = \frac{\rho_{ZnS}}{k_s f(C_{ox})} (r_o - r) \qquad 5.3$$

where r_o is the initial particle size. Since the conversion, X, is given by

$$X = 1 - \left(\frac{r}{r_o}\right)^3 \qquad 5.4$$

the shrinking-particle model is given by

$$k_r t = 1 - (1 - X)^{1/3} \qquad 5.5$$

where

$$k_r = k_s f(C_{ox})/\rho_{ZnS} r_o \qquad 5.6$$

The solution of the shrinking-particle model for cubic and short-cylinder geometries gives the same equation as equation 5.5. The particles leached in this study are a random distribution of shapes whose size can be characterized by the geometric mean of the upper and lower screen sizes. It is reasonable to assume that the leaching reaction is described by the shrinking-particle model if chemical reaction is the rate-controlling step.

The shrinking-particle model has been shown to apply to the dissolution of sphalerite by several authors (Verbaan and Crundwell, 1986; Jin and Warren, 1985; Dutrizac and MacDonald, 1978), who demonstrated that the plot of $1-(1-X)^{1/3}$ against t was linear for their data. Figure 1.1 shows the values of k_r from these plots for different oxidant concentrations and different particle sizes. If the values of $k_r r_o$ had been plotted rather than k_r, the three

curves would fall on the same line.

5.2 Effect of the solid-state properties of sphalerite on the rate of dissolution

5.2.1 *Effect of the iron content and UV radiation on the rate of dissolution*

Typical results collected in this study and presented in Figures 5.1, 5.2, and 5.3 as plots of $1-(1-X)^{1/3}$ against t, illustrate the effect of the iron content of the different sphalerite concentrates on the rate of dissolution. The diagrams show that the reaction follows linear kinetics in the initial stage of reaction, while diffusion through the product layer is important in the latter stage. The value of k_r is obtained from the slope of the linear section of these diagrams. In order to eliminate the effect of the difference in the size of the particles, values of $k_r r_o$ are compared. These values are given in Table 5.1.

The effect of temperature on the rate of dissolution of the five sphalerite concentrates is shown in Figure 5.4 as an Arrhenius plot. The activation energies evaluated from this diagram are given in Table 5.2. No dependence of the activation energy on the iron content is apparent.

Figure 5.5 illustrates the effect of the iron content of the sphalerite concentrates on the rate of dissolution at three different temperatures. These results confirm the linear increase of the rate of dissolution with the increase in the iron content reported by Piao and Tozawa (1983), even though they used oxygen as the oxidant at 150°C. The use of a different oxidant does not affect the dependence of the rate on the iron content of the sphalerite.

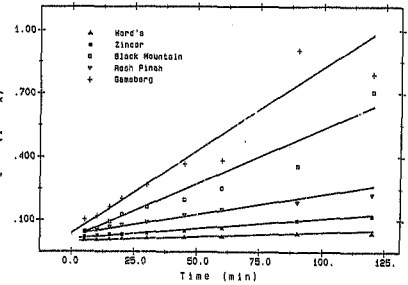

Figure 3.1 A plot confirming the shrinking particle model for the dissolution of sphalerite concentrates in ferric chloride solutions with 0.2 M $FeCl_3$, 0.3 M HCl, 0.003M $FeCl_2$, 2 M NaCl, 45°C.

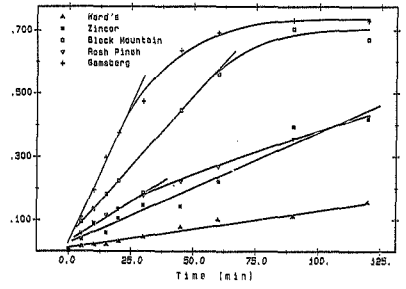

Figure 3.2 A plot confirming the shrinking particle model for the dissolution of sphalerite concentrates in ferric chloride solutions with 0.2 N $FeCl_3$, 0.3 N HCl, 0.003M $FeCl_2$, 2 N NaCl, 85°C.

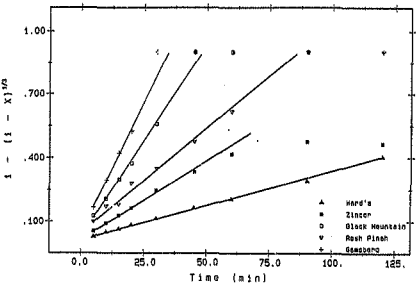

Figure 3.3 A plot confirming the shrinking particle model for the dissolution of sphalerite concentrates in ferric chloride solutions with 0.2 M $FeCl_3$, 0.3 M HCl, 0.005M $FeCl_2$, 2 M NaCl, 80°C.

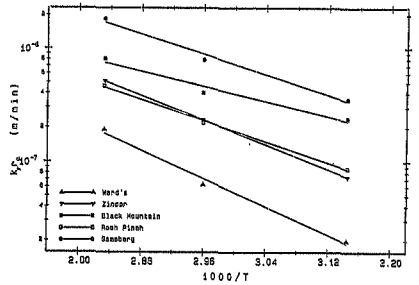

Figure 3.4 Arrhenius plot for the dissolution of the sphalerite concentrates with 0.2 M $FeCl_3$, 0.3 M HCl, 0.005 M $FeCl_2$, 2 M NaCl

Table 5.1 Values of the constants k_r from the shrinking-particle analysis of the leaching results.

Sample	r_o μm	Temp °C	k_r min^{-1}	$k_r r_o$ m min^{-1}
Wards	48.8	45	4.06×10^{-4}	1.98×10^{-8}
		65	1.28×10^{-3}	6.25×10^{-8}
		80	3.09×10^{-3}	1.9×10^{-7}
Zinoor	68.7	45	1.06×10^{-3}	7.29×10^{-8}
		65	3.38×10^{-3}	2.32×10^{-7}
		80	7.4×10^{-3}	5.08×10^{-7}
Black Mountain	44.8	45	5.31×10^{-3}	2.38×10^{-7}
		65	8.95×10^{-3}	4.01×10^{-7}
		80	1.80×10^{-2}	8.06×10^{-7}
Rosh Pinah	44.8	45	3.23×10^{-4}	8.68×10^{-8}
		65	4.90×10^{-3}	2.20×10^{-7}
		80	1.03×10^{-2}	4.60×10^{-7}
Gamsberg	44.8	45	7.88×10^{-3}	3.53×10^{-7}
		65	1.76×10^{-2}	7.88×10^{-7}
		80	4.10×10^{-2}	1.84×10^{-6}

Table 5.2 Activation energies for the leaching of sphalerites in ferric chloride solutions.

	E_a kJ mol^{-1}
Ward's	59.5
Zinoor	51.6
Black Mountain	31.7
Rosh Pinah	44.1
Gamsberg	43.3

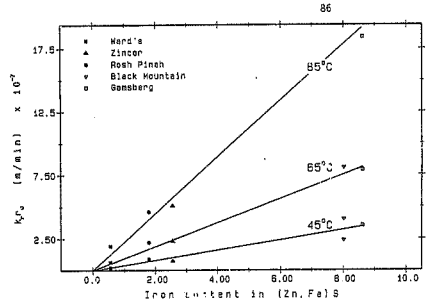

Figure 5.5 Effect of the iron content of (Zn,Fe)S on the rate of dissolution with 0.2 M $FeCl_3$, 0.3 M HCl, 0.005 M $FeCl_2$, 2M NaCl.

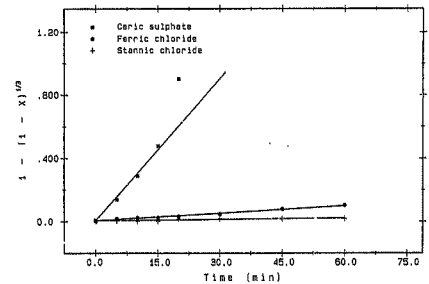

Figure 5.6 Effect of different oxidants on the rate of dissolution of the Ward's sphalerite.

The dissolution of the sphalerite from Black Mountain is consistently lower than that expected from the straight line variation in iron content, and this, together with its significantly lower activation energy, suggests that other sulphides present as inclusions in the sphalerite galvanically protect the sphalerite, or that a protective coating develops on the particle surface. This is most noticeable at higher temperatures.

The introduction of different oxidizing agents is illustrated in Figure 5.6 and the effect of UV irradiation is shown in Figures 5.7 and 5.8. The energy barrier between the d-band of the iron impurity or the valence band is smaller for ceric ion than for ferric ion (see Figure 3.4), and the rate of reaction is dramatically increased by the use of ceric ion as the oxidant. An oxidant with a V° lower than the iron couple may not be able to produce fluctuations in energy that have significant overlap with the valence band or the impurity band, and electron transfer will be slow, or will not take place at all. This is the case when stannic chloride is used as the oxidant, and virtually no dissolution occurs.

The radiation of a sample undergoing anodic dissolution results in enhanced rates of leaching, although this is not as pronounced as was reported by Exner *et al* (1969), shown in Figure 1.3. These results confirm the importance of semiconductor and other solid-state considerations in the dissolution of iron-containing sphalerites.

5.2.2 *Application of the fluctuating energy-level model to the dissolution of sphalerite*

In semiconductors with wide band gaps (E_{gap} > 1 eV), oxidation occurs as a result of the injection of holes into the valence band at the surface (Morrison, 1978); oxidation by surface holes will occur with 100 per cent corrosion efficiency. However, Figure 3.4 shows that the injection of holes into the narrow d-orbital band is

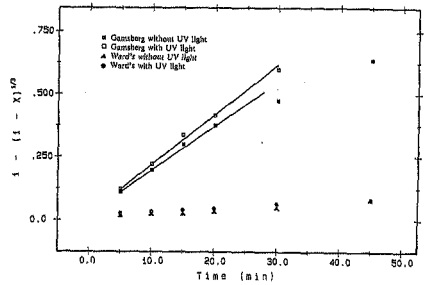

Figure 5.7 Effect of ultraviolet radiation on the rate of anodic dissolution for Ward's and Gamsberg sphalerites with 0.2 M $FeCl_3$, 0.3 M HCl, 0.005 M $FeCl_2$, 2 M NaCl at 45°C.

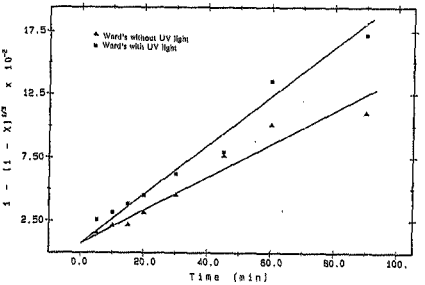

Figure 5.8 Effect of ultraviolet radiation on the rate of anodic dissolution for the Ward's sphalerite with 0.2 M $FeCl_3$, 0.3 M HCl, 0.025 M $FeCl_2$, 2 M NaCl at 85°C.

energetically more favourable than into the valence band of zinc sulphide. Large numbers of these holes can exist at the surface, resulting in a narrow space-charge region. If the space-charge region is sufficiently narrow (≈ 2 nm), quantum tunnelling can occur between the surface d-orbital and the valence band. The capture of two holes by the valence band at the surface will result in the oxidation of S^{2-} associated with the valence band to S and the concomitant release of zinc associated with the conduction band into solution as $Zn^{2+}(aq)$ (Williams, 1960; Koch, 1975). The electronic processes occurring during the dissolution of sphalerite are

$$ZnS + 2h^+ \rightarrow Zn^{2+} + S \qquad 5.7$$

$$ox \rightarrow red + h^+ \qquad 5.8$$

where h^+ represents a hole in the valence band, ox an oxidant in solution, and red a reduced species in solution.

The presence of an iron d-orbital within the band gap has two consequences for electron transfer between the solid and the electrolyte; it presents a narrow localized band with which the transfer of electrons is energetically more favourable than it is with the valence band, and it 'pins' the Fermi level at a level within the d-orbital band (Jellinek, 1972; Bard *et al*, 1980)

The rate of electron transfer from the semiconductor to the solution is given by equation 3.24:

$$j^c = qz \int_{-\infty}^{\infty} \nu(E) D_{sc}(E) f(E-E_{sc}) D_{ox}(E)\, dE \qquad 3.24$$

The first consequence of the iron impurity is that electron transfer occurs between a narrow d-orbital band within the semiconductor band gap and the solution. This means that the density of states for the carriers in the solid, $D_{sc}(E)f(E-E_{sc})$, resembles a Dirac-delta

function of density centred on the energy of the band with a magnitude of N_d (Mohl and Hale, 1966). The transmission coefficient $\nu(E)$ also has the form of a Dirac-delta function. D_{ox} is the density of states of the oxidant and is defined as $D_{ox}(E) = C_{ox}W_{ox}(E)$, where $W_{ox}(E)$ is the probability that the energy level of the oxidant in solution will be at E, as given by the fluctuating energy-level model (see section 3.3.2) and C_{ox} is the concentration of the oxidant in solution. Therefore, equation 3.24 becomes

$$j^c = qz \int_{-\infty}^{\infty} \delta(E-E^*)N_d\delta(E-E^*)C_{ox}W_{ox}(E)\,dE \qquad 5.9$$

$$= qzC_{ox}N_d \int_{-\infty}^{\infty} W_{ox}(E)\,dE \qquad 5.10$$

where E^* is the energy level of the d-band.

This integral can be evaluated if the approximation is made that $W_{ox}(E)$ is constant over the energy region of transfer (the assumption of Gerischer, 1960 a). It is normally argued that electron transfer will only occur with one of the bands, and, in most cases, overlapping of the states is limited to a rather small energy range, i.e., charge transfer will occur within 1 kT of the edge of the conduction band or valence band. If this is the case, it is reasonable to replace the integral by substituting $\Delta E = 1$ kT and $E = E_{cs}$ or E_{vs} for a conduction-band or valence-band mechanism. If E^* denotes the energy at which charge transfer occurs at the (Zn,Fe)S surface, i.e., the energy of the d-orbital band, then

$$j^c \approx qzC_{ox}N_dW_{ox}(E^*)kT \qquad 5.11$$

$W_{ox}(E^*)$ is given by equation 3.19, and substitution into equation 5.11 gives

$$j^c = qz(kT/4\pi\lambda)^{\frac{1}{2}}\, C_{ox}N_d\exp[-(E_{ox}-E^*)^2/4\lambda kT] \qquad 5.12$$

An equation of similar form has been derived by Mehl and Hale (1966) for the interaction of an insulator electrode, which has a narrow valence band, with an electrolyte. The Mehl and Hale (1966) formulation of the problem is as follows. Since the valence band of an insulator is narrow, the transmission coefficient and the densities of states can be treated as Dirac-delta functions; therefore,

$$j^c = q\nu N_I C_{ox}^* \qquad 5.13$$

where N_I is the carrier density of the valence band at the insulator surface when the current density is j^c A cm^{-2}, C_{ox}^* is the concentration of the acceptor molecules in the transition state, and ν is a constant containing the transmission coefficient (taken as unity), the Faraday constant, and the frequency of vibration of the activated complex. Assuming that C_{ox}^* is given by a Boltzmann-type expression,

$$C_{ox}^* = C_{ox} \exp(-\Delta G^*/kT) \qquad 5.14$$

where C_{ox} is the acceptor (oxidant) concentration in its equilibrium solvation configuration, and ΔG^* is the energy of activation of the solvation atmosphere. The activation energy ΔG^* is, according to theories of non-equilibrium electrostatic polarization of dielectrics (Marcus, 1964), a parabolic function of the excitation energy (Morrison, 1980, p36), and is given by

$$\Delta G^* = (E_{ox}-E^*)^2/4\lambda \qquad 5.15$$

where E_{ox} is the energy level of the acceptor (oxidant) state, and λ is the reorganization energy. Substituting equations 5.14 and 5.15 into 5.13 gives

$$j^c = q\nu N_I C_{ox} \exp[-(E_{ox}-E^*)^2/4\lambda kT] \qquad 5.16$$

which has the same form as equation 5.12.

The second consequence of the iron impurity is that the Fermi energy level, E_F, is pinned at the level of the d-orbital band. This means that the applied potential does not appear predominantly across the space-charge region as would be expected, but appears across the Helmholtz layer (see section 3.3.3). This is different from the case discussed by Mohl and Hale (1966) since the Fermi level of their insulator electrodes was not pinned, and the applied potential appeared across the space-charge region of the insulator. The energy at which electron transfer occurs is the energy of the Fermi-level which is pinned at the level of the d-band, i.e., $E^* = E_F$, and $E_F = E^\circ_{redox}$ at equilibrium since the electrochemical potentials of the electron in the solid and the solution are equal. $E_{ox} - E^\circ_{redox}$ varies directly with the applied potential, which appears across the Helmholtz layer as in the case of electron transfer at a metal electrode, i.e.,

$$E_{ox} - E^* = E_{ox} - E_F = E_{ox} - E^\circ_{redox} + \eta_H q \qquad 5.17$$

where η_H is the overpotential (which appears across the Helmholtz layer because the Fermi level is pinned). The overpotential is the difference between the measured potential and the equilibrium potential, i.e., $\eta = \Delta\phi - \Delta\phi_A$. Substitution of equation 5.17 into equation 5.12, gives the cathodic reduction of Fe^{3+} as

$$j^c = q\pi(kT/4\pi\lambda)^{\frac{1}{2}}C_{ox}N_d\exp[-(E_{ox}-E^\circ_{redox}+\eta_H q)^2/4\lambda kT] \qquad 5.18$$

Since

$$E_{ox} - E_{red} = 2\lambda$$

and

$$E^\circ_{redox} = \tfrac{1}{2}(E_{ox}+E_{red})+kT\ln(C_{red}/C_{ox})$$

(Gerischer, 1970) then

$$E_{ox} - E^{o}_{redox} = \lambda - kT \ln(C_{red}/C_{ox}) \qquad 5.19$$

and

$$j^{c} = qz(kT/4\pi\lambda)^{\frac{1}{2}}N_d C_{ox} \exp[-(\lambda - kT\ln(C_{red}/C_{ox}) + \eta_H q)^2/4\lambda kT] \qquad 5.20$$

The assumptions of Marcus (1964) and Levich (1970), i.e., $\lambda >> q\eta_H$ and $\lambda >> kT\ln(C_{red}/C_{ox})$, are applied, and the cross terms in $q\eta_H$ and $kT\ln(C_{red}/C_{ox})$ can be neglected. The resulting equation describes the reduction of Fe^{3+} at the sphalerite surface, i.e.,

$$j^{c} = k^{c} C_{ox} N_d \exp(-\eta_H q/2kT) \qquad 5.21$$

where k^c is a rate constant. The anodic current is also dependent on the number of point defects (Simkevich and Wagner, 1960). This is a result of the linear increase in the unit cell dimension with an increase in the iron content for the impurity ranges considered here (see equation 2.1). Locker and DeBruyn (1969) reported an enhanced rate of non-oxidative dissolution with an increase in the iron content, confirming that the anodic current is also dependent on the iron content. Therefore, for an electron-transfer reaction of the form of equation 3.18 b,

$$j^{a} = k^{a} N_d \exp(\eta_H q/2kT) \qquad 5.22$$

Since there is no net current, equation 3.34 applies, i.e., $j^c = j^a$, equations 5.21 and equations 5.22 can be equated, and an expression for η_H can be obtained. Then solving for j^a gives

$$j^{a} = (k^{c}/k^{a})^{\frac{1}{2}} N_d C_{ox}^{\frac{1}{2}} \qquad 5.23$$

This is first order in N_d, the number of occupied states in the d-band, i.e., the concentration of the iron in substitutional lattice sites, and half order in the concentration of the oxidant. This equation is capable of describing all the experimental results reported in the literature (Piao and Tozawa, 1985; Jin and Warren, 1985) and those results are confirmed by the results presented in Figure 5.5. For a particular sphalerite, the dependence of the rate on the oxidant concentration from equation 5.23 is the same as that described by the mixed-potential model. Indeed, the fact that the Fermi level is pinned justifies the use of the mixed-potential model for a semiconductor such as sphalerite.

From the energy-level model of semiconductor electrode-processes (Morrison, 1978), it is expected that the dissolution rate would be enhanced by the introduction of a stronger oxidizing agent, i.e., a higher E_{ox}, or by ultraviolet radiation (radiation of band-gap energy), which would create free electrons in the conduction band and holes in the valence band. That this does occur is shown in Figures 5.6, 5.7 and 5.8.

Exner *et al* (1969) investigated the effect of UV radiation on the dissolution rate of both natural and synthetic zinc sulphide crystals (Figure 1.3), and found that the rate of dissolution for synthetic doped crystals was dramatically increased, suggesting that n-type doping predominated. A smaller effect was reported for pure natural crystals. These results confirm the importance of the electronic structure of the solid.

The results of Jin and Warren (1985) show that there is a change in the reaction order, from half order to zero order at high oxidant concentration. Jin and Warren (1985) and Van Sandwijk and Koopmans (1986) proposed models for which they assumed that the oxidant is adsorbed onto the surface at anionic surface-sites (sulphur sites), and described this in terms of the Langmuir isotherm. These authors attributed the change in reaction order shown in Figure 1.1 to the

onset of complete coverage of the surface by the adsorbed oxidant.

The model presented in this thesis is in contrast to the adsorption models previously proposed. Metal ions in aqueous solution are solvated, the significance of which is that such ions are seldom adsorbed at the inner Helmholtz plane (IHP). Solvated ions, such as $Fe^{3+}(aq)$, are electrostatically adsorbed at the outer Helmholtz plane (and an outer-sphere electron-transfer reaction occurs). This is not identical to adsorption at a specific site, which is a requirement for the application of the Langmuir isotherm.

The change in reaction order that the above authors attempted to describe suggests that the anodic dissolution current (equation 5.22) reaches a limiting value because of a migration-limited supply of solid-phase charge carriers to the surface. The limiting current is constant for any change in the applied potential or in the oxidant concentration. Such limiting currents are a fundamental aspect of the anodic behaviour of n-type semiconductors, and this proposal is consistent with the characteristics of semiconductor electrochemistry and the model represented by the equations 5.21, 5.22 and 5.23.

5.2.3 Summary

It has been shown in this section that the solid-state properties of the sphalerite directly influence the rate of dissolution. The rate reaction has been shown to be a linear function of the concentration of iron in the zinc sulphide lattice. The rate of reaction is also increased by irradiating the leaching solution with UV light, and the rate is influenced by the use of different oxidants. The semiconductor model described in Chapter 3 has been applied to the situation in which the electron transfer occurs with a narrow band within the band gap of the sphalerite, and it has been shown that this model is consistent with the dissolution kinetics presented in this section, and with those presented in the literature.

This model justifies the use of the mixed-potential model that has previously been used to explain the kinetics of dissolution (Jin and Warren, 1985; Verbaan and Crundwell, 1986). In the next section of the chapter, this model is extended to account for the anodic oxidation of Fe(II) which could be in competition with the anodic dissolution reaction for the consumption of holes.

5.3 Mechanism of dissolution of sphalerite in iron(III) solutions

5.3.1 *The effect of the solution composition on the rate of leaching of the Gamsberg sphalerite*

Microscopic examination revealed that the Gamsberg material was surrounded by a rim of fractured material. This material dissolved rapidly, resulting in the initial conversion shown in Figures 5.9 and 5.10.

The value of k_r in equation 5.5 was determined by linear regression on the points up to 30 minutes. The deviation from reaction control is apparent at higher conversions, as a result of the sulphur that forms on the particle surface. As this layer increases in thickness, the supply of reactants and the removal of products through the layer becomes limiting, and shrinking-core kinetics are applicable in these regions. Unfortunately, attempts to model the entire reaction curve using mixed-reaction kinetics and fitting the reaction and diffusion parameters were unsuccessful. The incorporation of a pore-blockage mechanism, which is analogous to catalyst deactivation (Levenspiel, 1972), did not improve the model.

Figures 5.9 and 5.10 illustrate the effect of an increase in the ferrous and ferric concentrations, respectively.

If the model represented by equation 1.12 is correct, then all dis-

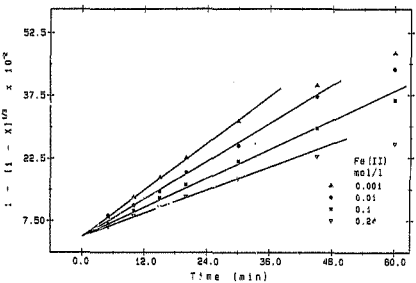

Figure 5.9 Dependence of the rate of reaction on the concentration of Fe(II) sulphate with 0.01M Fe(III) at 70°C

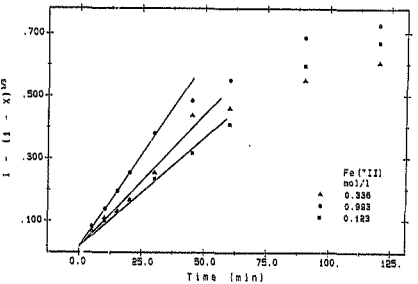

Figure 5.10 Dependence of the rate of reaction on the concentration of Fe(III) sulphate with 0.004M Fe(II) at 70°C.

solution at the same redox potential and temperature will have the same rate of reaction. Figure 5.11 illustrates three reactions at 575 mV and at different concentrations of Fe(II) and Fe(III), and shows clearly that this model does not adequately describe the mechanism of reaction. Figures 5.9 to 5.11 illustrate that, at high conversions, diffusion through the product layers becomes the rate-controlling step.

Figure 5.12 illustrates that there is no change in the initial rate of dissolution when zinc sulphate is added to the leaching solution.

Figure 5.13 illustrates the effect of temperature on the rate of dissolution. An Arrhenius plot of the reaction rate constant, k_r, is presented in Figure 5.14. An activation energy of 46 kJ mole^{-1} was obtained, which agrees favourably with that obtained by other researchers (Jin and Warren, 1985; Verbaan, 1980).

The effect of the addition of zinc sulphate to the leaching solution was investigated. The rate constant, k_r, was unaffected by zinc concentrations of 0.05 and 0.01 M. This result is consistent with previously published results (Dutrizac and MacDonald, 1974; Wadsworth, 1972).

5.3.2 *Mechanism of dissolution of Gamsberg sphalerite in iron(III) sulphate solutions*

The presence of dissolved iron in solution contributes to the kinetics by the redox couple

$$Fe^{3+} \rightleftharpoons Fe^{2+} + h^{+} \qquad 5.24$$

which exchanges holes with the iron-impurity band within the band gap (see section 5.2.2). That analysis was not concerned with the effect of the capture of holes from the d-orbital band, i.e., $Fe^{2+} + h^{+} \rightarrow Fe^{3+}$, which would be in competition with the anodic dissolution

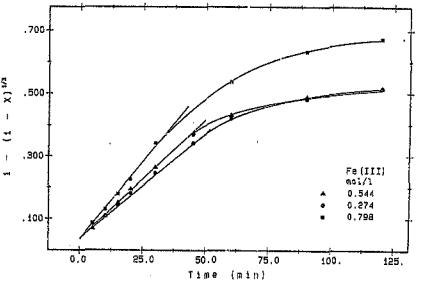

Figure 5.11 Dependence of the rate of reaction on the concentration of Fe(III) sulphate at a constant redox potential of 575 mV vs SCE at 75°C.

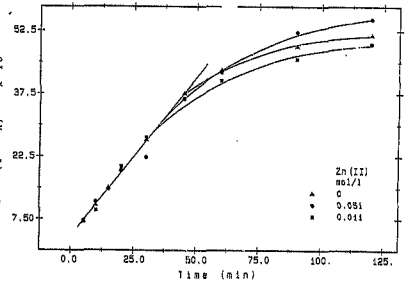

Figure 5.12 Effect of the addition of zinc to the leaching solution at 75°C, 0.5 M Fe(III) sulphate and 0.0048 M Fe(II) sulphate.

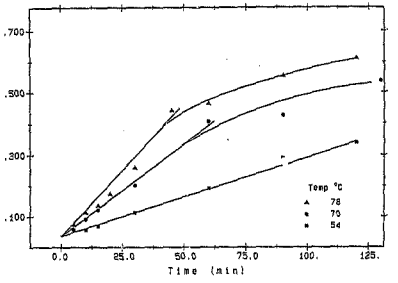

Figure 3.13 Effect of temperature on the dissolution of Gamsberg sphalerite in ferric sulphate solution with 0.28 M Fe(III) and 0.05M M Fe(II).

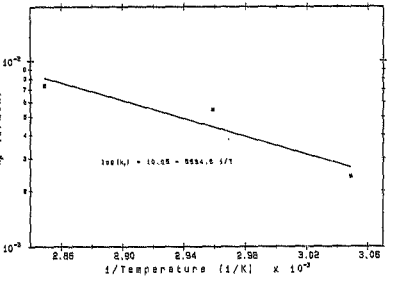

Figure 3.14 Arrhenius diagram for the dissolution of Gamsberg sphalerite in ferric sulphate solution.

reaction for the consumption of holes. The equations derived in that section from first principles gave a fixed value of 0.5 for the charge-transfer coefficient. In this chapter this analysis will be further extended to allow for a competitive reaction, and for a transfer coefficient that deviates from the expected value of 0.5.

The analysis of section 5.2.2 has clearly shown that, since the Fermi level is pinned, any changes of the potential at the surface would occur across the Helmholtz layer. Reactions that are limited by electron transfer across the Helmholtz layer are qualitatively described by equations of the same form as the Butler-Volmer equation, i.e., equation 3.13, which relates the current density, j, to the potential across the Helmholtz layer, $\Delta\phi_H$. In the anodic potential region, the anodic dissolution current given by equation 5.22

$$j^a = k^a N_d \exp(\eta_H q/2kT) \qquad 5.22$$

which can be expressed in the more familiar Butler-Volmer form as

$$j^a = k^a \exp(\alpha \Delta\phi_H F/RT) \qquad 5.25$$

where α is the charge-transfer coefficient which is expected to be close to the 0.5 value given by equation 5.22, F is Faraday's constant, and k^a is now the rate constant for a <u>particular</u> sphalerite, R is the universal gas constant, and T is the temperature. The factor F/R is equal to the factor q/k in equation 5.22.

The net anodic current density contributed by the ferrous-ferric couple is given by the Butler-Volmer expression

$$j_{Fe} = k^{\beta}_{Fe}[Fe^{2+}]\exp(\alpha_{Fe}\Delta\phi_H F/RT) \cdot \qquad 5.26$$

$$k^{\beta}_{Fe}[Fe^{3+}]\exp[-(1-\alpha_{Fe})\Delta\phi_H F/RT]$$

The concentration of oxidant and reductant in equation 5.26, and

therefore in the following equations 5.28 to 5.30 can represent any, or all of the ionic species present in solution. Since no net current flows during the dissolution of a particle, equation 3.34 applies ($j^a = j^c$), and the following expression is obtained:

$$0 = j^a + j_{Fe} \qquad 5.27$$

$$0 = k^a \exp(\alpha\Delta\phi_H F/RT) + k^c_{Fe}[Fe^{2+}]\exp(\alpha_{Fe}\Delta\phi_H F/RT)$$
$$- k^c_{Fe}[Fe^{3+}]\exp(-(1-\alpha_{Fe})\Delta\phi_H F/RT) \qquad 5.28$$

The role of the iron couple can be divided into three regions (Nicol *et al*, 1975), as follows.

Case (i): The partial anodic current due to the oxidation of Fe(II) is negligible.

$$j^a = (k^a)^\delta (k^c_{Fe}[Fe^{3+}])^\delta \qquad 5.29$$

$$\alpha = (1-\alpha_{Fe})/(1-\alpha_{Fe}+\alpha) \text{ and } \delta = \alpha/(1-\alpha_{Fe}+\alpha)$$

(Obviously case (i) is the same as equation 5.23 if $\alpha = \alpha_{Fe} = 0.5$ since in section 5.2.2 it was assumed that the partial anodic current due to the oxidation of Fe(II) is negligible.)

Case (ii): The partial anodic currents due to the oxidation of Fe(II) and ZnS are significant.

$$j^a = k^a (k^c_{Fe}[Fe^{3+}]/(k^a + k^c_{Fe}[Fe^{2+}]))^{\frac{1}{2}} \qquad 5.30$$

Case (ii) assumes that the α values are equal

Case (iii): The partial anodic current due to the oxidation of ZnS

is negligible compared to that due the oxidation of Fe(II).

$$j^a = k^a(k^a_{Fe}[Fe^{3+}]/k^a_{Fe}[Fe^{2+}])^\alpha \qquad 5.31$$

Case (iii) represents the reversible Fe^{2+}/Fe^{3+} couple used in the previous model, equation 1.12 (Verbaan and Crundwell, 1986). Figures 1.2 and 5.11 show that this model is inadequate as a description of the leaching characteristics in ferric sulphate solutions since the rates are not the same when the Fe^{3+}/Fe^{2+} ratio is the same (see Figure 5.11). However, the concentration of the oxidant in solution is dependent on the ionic equilibria, and the concentrations of the various species in solution were calculated to investigate whether effects of the solution equilibria are the cause of this 'non-Nernstian' behaviour.

Solution equilibria in ferric sulphate solutions

The redox potential, given by equation 1.13, is a measure of the activity ratio of the $Fe^{3+}(aq)$ and $Fe^{2+}(aq)$ ions (or any other redox couple formed by ferric and ferrous sulphate complexes) in a mixed electrolyte. Dry (1985) was able to calculate the Fe^{2+}/Fe^{3+} redox potential in the ionic strength range 0 to 4 and in the temperature range 22 to 90°C, by accounting for the following complexes in solution: $FeSO_4^+$, $FeHSO_4^{2+}$, $FeSO_4$, $FeHSO_4^+$, and HSO_4^-.
Dry used the Debye-Huckel equation, in which the real rather than the formal ionic strength was substituted, to estimate the individual activity coefficients of the ions in solution, and used Pitzer's correlations (Pitzer *et al*, 1977) to estimate the dissociation of HSO_4^- at the solution ionic strength. He selected values of the stability constants at zero ionic strength from within the range of values reported in the literature so as to minimize the difference between the measured and calculated redox potentials. The values of these

constants are given in Table 5.3. The use of the Debye-Huckel equation is justified in this calculation for ionic strengths up to 0.5 M (Pitzer, 1972).

The numerical procedure described by I and Koncallas (1972) was used in the present study in conjunction with Dry's stability constant data for the calculation of the concentrations of the iron sulphate species. The computer program used is given in Appendix C. Figure 5.15 is plot of the measured and calculated redox potentials using this numerical procedure. The measured potentials are taken from Dry (1985) and have been corrected by him for the junction potential. This figure indicates that this is an accurate calculation of the redox potential.

The root mean square deviation

$$S(V)=\sqrt{(1/(N-1)\Sigma((V_{cal}-V_{exp})/V_{exp})^2}$$

of the measured and calculated redox potentials is less than 1 percent for the initial conditions for all the experiments in this study. These values are shown in Table 5.4. It is concluded that since the redox potential is accurately calculated, this presents a reliable procedure for the calculation of the activities and concentrations of the complexes in solution.

$FeSO_4^+$ is the dominant species in solution (approximately 85%) at the leaching conditions, followed by $Fe(SO_4)_2^-$ (10 to 15 per cent). The concentration of the ferric aqua-ion is very low. The distribution of the ferric species in solution is shown in Figure 5.16.

Table 5.3 Iron stability constants at zero ionic strength.

Equation	Stability constant	Reference
$Fe^{3+} + SO_4^{2-} + H^+ \rightleftharpoons FeHSO_4^{2+}$	exp(33.334-7629.9/T)	Dry (1985)
$Fe^{3+} + SO_4^{2-} \rightleftharpoons FeSO_4^+$	exp(-900+39110.9/T+136.61log(T))	Dry(1985)
$Fe^{3+} + SO_4^{2-} \rightleftharpoons FeSO_4$	$10^{(3.339-337.37/T)}$	Dry(1985)
$Fe^{2+} + SO_4^{2-} + H^+ \rightleftharpoons FeHSO_4^+$	exp(30.69-7290.4/T)	Dry(1985)
$Zn^{2+} + SO_4^{2-} \rightleftharpoons ZnSO_4$	$10^{2.38}$exp(1.067-318.2/T)	Naumov(1980)
$H^+ + SO_4^{2-} \rightleftharpoons HSO_4^-$	exp(-14.0321+2835.2/T)	Pitzer (1977)
$Fe^{3+} + Cl^- \rightleftharpoons FeCl^{2+}$	$10^{1.009}$exp(6.85-2020.7/T)	Ashurst and Hancock(1978)
$Fe^{3+} + 2Cl^- \rightleftharpoons FeCl_2^+$	$10^{0.55}$exp(14.8-4366.1/T)	"
$Fe^{3+} + 3Cl^- \rightleftharpoons FeCl_3$	$10^{-0.67}$	"
$Fe^{2+} + Cl^- \rightleftharpoons FeCl^+$	$10^{0.32}$	"
$Fe^{2+} + 2Cl^- \rightleftharpoons FeCl_2$	$10^{0.35}$	"

Table 5.4 Values of the constant k_r from the shrinking-particle analysis of the Gamsberg leaching results at 78°C.

Run	k_r min^{-1}	V_{meas} mV vs SCE	V_{calc} mV vs SCE
3	0.00296	614	628
4	0.00738	547	558
5	0.00743	494	500
6	0.00607	472	479
7	0.00469	431	449
8	0.00753	595	606
9	0.00651	527	550
10	0.00442	472	480
11	0.00251	407	412
27	0.00658	527	547
28	0.00599	527	534
35	0.00753	575	582
36	0.00703	575	577
37	0.00979	575	576
38	0.00810	564	568
39	0.01117	591	590
40	0.00655	548	555
45	0.00750	588	584
46	0.00745	590	584

S(V) = 0.0209 = 2.09 %

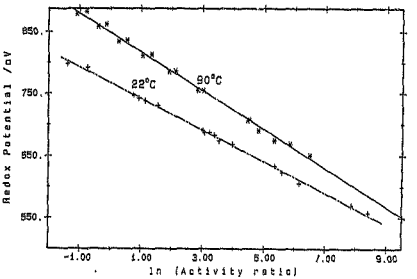

Figure 5.13 Plot of the measured and calculated redox potentials. The calculated potentials are represented by the straight lines and the measured values, taken from Doy (1983), are represented by the points.

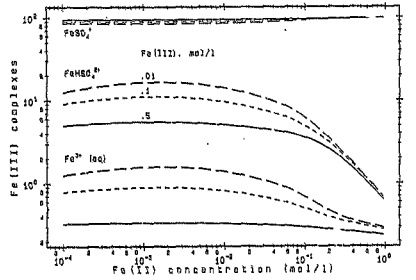

Figure 5.14 The distribution of the Fe(III) species in solution in 0.1 M H_2SO_4 at 70°C.

Application of solution equilibria to oxidative dissolution kinetics of Gamsberg sphalerite

An examination of Figure 1.2 suggests that the addition of ferrous sulphate does not directly affect the rate of leaching, i.e., the iron couple is not reversible at the sphalerite surface, and case (i) conditions apply. If this is so, then the reaction order with respect to the electroactive species should be $\alpha/(1-\alpha_{Fe}+\alpha)$, or close to 0.5 if $\alpha = \alpha_{Fe} = 0.3$, i.e., a plot of log k_r against log C_{ox}, where C_{ox} is the concentration of the electroactive species, should have a slope that is close to 0.5. Correlation of the rate with the $FeSO_4^+$ complex did not yield satisfactory results for this model.

However, Figure 5.17 shows the close correlation of rate of dissolution of sphalerite with the sum of the concentrations of $Fe^{3+}(aq)$ and $FeHSO_4^{2+}$ for the data of Verbaan (1980) from Figure 1.2. Figure 5.17 is a plot of the case (i) model assuming that the $FeSO_4^+$ complex is inactive at the sphalerite surface. The success of this assumption indicates that the $Fe^{3+}(aq)$ and $FeHSO_4^{2+}$ complexes are the electroactive species at the sphalerite surface. The slope of the best fit through these points is 0.45. This gives a Tafel slope of 0.122 V.decade^{-1}, significantly close to the expected value of 0.136 V.decade^{-1}.

Figure 5.18 is a similar diagram for all the experimental results obtained for the Gamsberg sphalerite at 78°C. Table 5.5 gives the calculated concentrations for the complexes for the initial conditions of the experiments. The slope of Figure 5.18 is 0.54, which gives a Tafel slope of 0.15 V.decade^{-1}. This is again close to the expected Tafel slope of 0.14 V.decade^{-1}. The close correlation of these results with the case (i) model demonstrates that the effect of the addition of Fe(II) to the solution is indirect, in that Fe(II) sulphate changes the concentrations of the electroactive species in the solution, and hence affects the rate of dissolution. The Fe^{2+}/Fe^{3+} couple is therefore irreversible at the Gamsberg sphalerite surface. Parker *et al* (1981) argued a similar case for the behaviour of a chalcopyrite electrode in iron sulphate solutions.

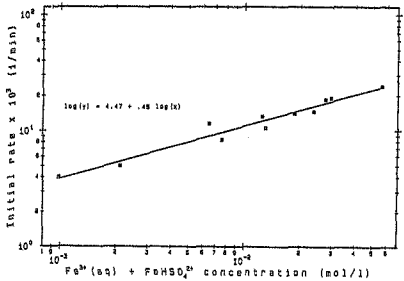

Figure 5.17 Case (1) model for data of Verhoeven (1980) presented in Figure 1.2 assuming that $FeSO_4^+$ is inactive.

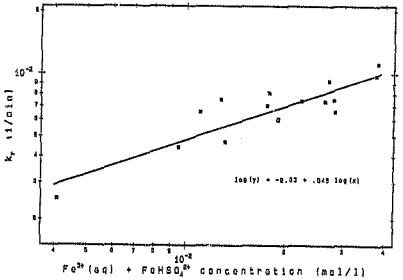

Figure 5.18 Case (1) model for the leaching of Gemsberg sphalerite assuming $FeSO_4^+$ is inactive for data from Figures 5.9-5.13

Table 5.3 Calculated concentrations of the ferric and ferrous sulphate species in solution for Gammarg leaching experiments

Species	3	4	5	6	7	8	9	10	11	27	28
Fe(III)	.511	.511	.511	.511	.511	.126	.126	.126	.126	.511	.266
Fe(II)	.1E-2	.1E-	.6E-1	.11	.24	.1E-2	.6E-2	.5E-1	.25	.15E-	.16E-1
H_2^+	.2	.2	.2	.2	.2	.21E	.21E	.21E	.21E	.21E	.21E
Fe^{3+}	.1645E-2	.1427E-2	.1545E-2	.1485E-2	.1362E-2	.9087E-3	.8668E-3	.7250E-3	.4553E-3	.1641E -	.1250E-2
Fe^{2+}	.1575E-3	.1590E-2	.1010E-1	.1960E-1	.4899E-1	.2062E-3	.1238E-2	.1043E-1	.5835E-1	.2209E-2	.2607E-2
H^+	.3029E-1	.2926E-1	.2426E-1	.2025E-1	.1316E-1	.6044E-1	.6598E-1	.4922E-1	.1772E-1	.3175E-1	.4016E-1
SO_4^{2-}	.2136E-0	.2186E-0	.2469E-0	.2739E-0	.3377E-0	.3609E-1	.3766E-1	.5418E-1	.1530E-0	.2163E-0	.1073E-0
$FeHSO_4^{2+}$	.2535E-1	.2437E-1	.2070E-1	.1732E-1	.1172E-1	.1180E-1	.1144E-1	.8741E-2	.3617E-2	.2638E-1	.1772E-1
$FeSO_4^+$	.4840E-0	.4846E-0	.4888E-0	.4920E-0	.4972E-0	.1133E-0	.1137E-0	.1165E-0	.1219E-0	.4820E-0	.2691E-0
HSO_4^-	.1437E-0	.1400E-0	.1203E-0	.1027E-0	.6922E-1	.1371E-0	.1365E-0	.1290E-0	.7785E-1	.1501E-0	.1498E-0
$FeHSO_4^+$	.2158E-2	.2258E-2	.1512E-1	.3056E-1	.8412E-1	.1142E-3	.7056E-3	.7346E-2	.7266E-1	.3182E-2	.2839E-2
$FeSO_4$	.6237E-3	.6171E-2	.3476E-1	.5955E-1	.1069E-0	.6796E-3	.4056E-2	.3202E-1	.1188E-0	.9529E-2	.1033E-1

Table 5.5 Continued

Species	33	34	37	38	39	40	45	46
Fe(III)	.344	.274	.798	.262	.8005	.123	.6129	.6129
Fe(II)	.47E-2	.36E-2	.76E-2	.46E-2	.48E-2	.48E-2	.48	.48E-2
H_2^+	.2	.2	.2	.2	.2	.2	.2	.2
Fe^{3+}	.1694E-2	.1309E-2	.2099E-2	.1220E-2	.2105E-2	.8537E-3	.1789E-2	.1605E-2
Fe^{2+}	.7312E-3	.6619E-3	.1071E-2	.8775E-3	.6735E-3	.1041E-2	.7126E-3	.7215E-3
H^+	.2924E-1	.3927E-1	.2389E-1	.3643E-1	.2611E-1	.6007E-1	.2021E-1	.2016E-1
SO_4^{2-}	.2329E-0	.9692E-1	.3603E-0	.1012E-0	.3681E-0	.3686E-1	.2849E-0	.2784E-0
$FeHSO_4^{2+}$	.2637E-1	.1633E-1	.3557E-1	.1635E-1	.3988E-1	.1019E-1	.2912E-1	.2893E-1
$FeSO_4^+$	.5160E-0	.2564E-0	.7603E-0	.2642E-0	.7624E-0	.1120E-0	.6820E-0	.6822E-0
HSO_4^-	.1616E-0	.1421E-0	.1339E-0	.1420E-0	.1349E-0	.1266E-0	.1397E-0	.1399E-0
$FeHSO_4^+$	.1034E-2	.6466E-3	.1853E-2	.8763E-3	.1163E-2	.6049E-3	.1103E-2	.1109E-2
$FeSO_4$	.2915E-2	.2291E-2	.4574E-2	.3046E-2	.2561E-2	.3154E-2	.2984E-2	.2973E-2

The dependence of the rate on the formation of particular complexes in solution is explicable in terms of the factors controlling the solution complexes. $FeSO_4^+$ is described by Ashurst and Hancock (1977) as an inner-sphere complex, whereas $FeSO_4$, $FeHSO_4^{2+}$, and $FeHSO_4$ are outer-sphere complexes (ion pairs). Charge transfer to $FeSO_4^+$ would require the breaking of the Fe^{3+} and SO_4^{2-} bond in the inner coordination sphere to form the $FeSO_4$ outer-sphere complex. Therefore, charge transfer to $FeSO_4^+$ is retarded due to the different bonding in the $FeSO_4^+$ and $FeSO_4$ complexes, and the outer-sphere couples $FeHSO_4^{2+}/FeHSO_4^+$ and $Fe^{3+}(aq)/Fe^{2+}(aq)$ are electroactive species.

5.3.3 *The effect of complex formation on the leaching of sphalerite in ferric chloride solutions*

Dutrizac and MacDonald (1978) reported that the addition of ferric ion to the ferric chloride leaching solution has a direct effect on the rate of dissolution of sphalerite. If this is the case, then the Fe^{2+}/Fe^{3+} couple can be regarded as being reversible at the sphalerite surface in chloride solutions, and the potential difference across the Helmholtz layer is dominated by this couple. A plot of the rate constant against the $FeCl_2$ concentration on a logarithmic scale for their data indicates that two distinct regions exist, corresponding to case (i) conditions (rate independent of $[FeCl_2]$) at low $FeCl_2$ concentrations (< 0.4 M) and case (iii) conditions at higher $FeCl_2$ concentrations (> 0.4 M). This aspect of the dissolution reaction is not examined in further detail in this work.

Dutrizac and MacDonald (1978) observed that the rate was proportional to $[Fe(III)]^{0.36}$. The concentrations of the ferric and ferrous species in solution were calculated from stability constants given by Ashurst and Hancock (1977) and Butler (1964) using the same numerical procedure as that for sulphate solutions. The stability constants

used are given in Table 5.4, and the numerical procedure used is given in Appendix C. The rate was proportional to $[FeCl^{2+}]^{0.42}$ and $[FeCl_2^+]^{0.31}$, which gives an overall reaction order of 0.36. Jin and Warren (1985) reported that the reaction rate is proportional to $[Fe(III)]^{0.5}$. The reaction order of the calculated concentrations of both the $FeCl^{2+}$ and $FeCl_2^+$ complexes was 0.5. Therefore, the charge transfer in chloride solutions is not dominated by a particular ionic species as it is in sulphate solutions.

The effect of the chloride ion is twofold: increasing the concentration of the chloride ion decreases the potential of the Fe^{2+}/Fe^{3+} redox potential, and contact adsorption at the inner Helmholtz plane is often observed for chloride ions. A dependence on Cl^- for non-oxidative dissolution of sphalerite has been observed, and this is explained in section 5.4 in terms of the formation of complexes of Zn^{2+} and Cl^-. The removal of zinc lattice ions, Zn_{lat}^{2+} across the Helmholtz double layer may be coupled with the complexing of chloride ions, according to

$$Zn_{lat}^{2+} + nCl^- \rightarrow ZnCl_n^{2-n} \qquad 5.32$$

for which equation 5.25 may be rewritten as

$$j^a = k^a[Cl^-]^n \exp(\alpha\Delta\phi_H F/RT) \qquad 5.33$$

If n is assumed to be one, and equation 5.33 is combined with the iron couple reactions, then a one-half order dependence is obtained for case (i) and a first-order dependence for case (iii). Case (ii) is given by

$$j^a = k^a[Cl^-](k^c_{Fe}[Fe^{3+}]/(k^a[Cl^-]+k^a_{Fe}[Fe^{2+}]))^{0.5} \qquad 5.34$$

which at constant and low concentrations of Fe(II), results in a one-half order [Cl^-] dependence. Since Cl^- is specifically adsorbed at the IHP, the change in reaction order with Cl[illegible]t was observed

by Jin and Warren (1985) is due to the onset of complete coverage. Hence Cl^- may be replaced by the term $[Cl^-]/(1+K[Cl^-])$, where K is the equilibrium constant for Cl^- contact adsorption.

5.3.4 *Addition of Cu(II) to the leaching solution*

Copper in the cupric form is a well-known activator in the flotation of sphalerite. Copper is exchanged with zinc lattice ions at the solid surface, and the flotation behaviour is that of CuS. Dutrizac and MacDonald (1978) reported that the addition of $CuCl_2$ to the Fe(III) chloride leaching solution increased the rate of reaction, and they accounted for this by proposing that either the CuS film resulted in enhanced galvanic corrosion, or that Cu(II) ions oxidize the sphalerite and the Fe(III) ions oxidize the resulting Cu(I) ions. The oxidation of chalcopyrite by $CuCl_2$ has also been proposed, whereas $CuSO_4$ is not an oxidant for chalcopyrite (Parker *et al*, 1981).

The dissolution of the sphalerite concentrate used in this study in the presence of $Fe_2(SO_4)_3$ and $CuSO_4$ resulted in diminished rates of reaction. This is illustrated in Figure 5.19. The dissolution kinetics are described by the shrinking-particle model, and the reaction rate constant, k_r, decreased by a factor of 3.3 on the addition of 0.01 M cupric ion to the 0.5 M Fe(III) leaching solution.

In chloride solutions, Cu(II) can act as an oxidant, e.g., in the case of chalcopyrite leaching, since the Cu(I) species is soluble in high chloride solutions; however, in sulphate solutions the Cu(II) does not act as an oxidant because the Cu(I) species is insoluble. The decrease in the rate of dissolution on the addition of Cu(II) sulphate to the ferric sulphate leaching solution may be due to the formation of a surface state when Cu(II) is exchanged with zinc lattice ions at the surface inhibiting the rate of electron transfer between the d-orbital band and the oxidant in solution.

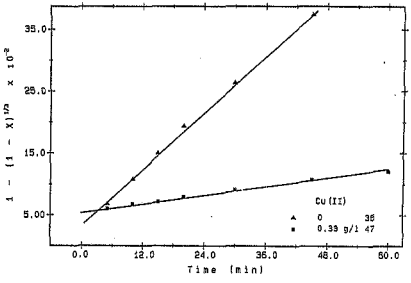

Figure 5.19 The effect of copper addition to the ferric sulphate leaching solution in 0.5 M Fe(III) and 0.0046 Fe(II) at 78°C

5.3.5 The effect of complex formation on the mixed potential of a chalcopyrite electrode

The leaching of chalcopyrite in sulphate and chloride solutions using dissolved iron(III) has been extensively examined, and the electrochemistry of chalcopyrite has been well documented. Many researchers have proposed that the oxidation products that form around the core are resistive. Sulphur, p- and n-type semiconductors, such as the p-type CuS, and metal-deficient polysulphides have been proposed as hindering the transfer of ions or electrons at the interface.

Parker *et al* (1981) conducted extensive tests to characterize the electrochemistry of chalcopyrite. They performed their tests in the temperature and potential ranges applicable to leaching They inves-

tigated the effect of using different redox couples, and reported anodic saturation currents, which are typical for n-type semiconductors, for the oxidation of Fe^{2+} in solution. They also reported that the chalcopyrite electrode displayed irreversible behaviour in ferric sulphate solutions.

Jones and Peters (1976) investigated the steady-state response of the chalcopyrite electrode to the Fe^{2+}/Fe^{3+} redox couple in both sulphate and chloride solutions. They reported that the measured mixed potential showed a Nernstian response to the increase in Fe(III) concentration in sulphate solutions, the slope being 62 mV.decade^{-1}, which is close to the expected 72 mV.decade^{-1} expected from the Nernst equation at 90°C. Their results are shown in Figure 5.20. However, they reported a non-Nernstian response of the electrode to increases in the Fe(II) concentration in sulphate solutions. This is shown in Figure 5.21.

If equation 5.28 is solved for the mixed potential, $\Delta\phi_H$, assuming case (i) conditions apply, the following expression is obtained:

$$\Delta\phi_H = 6RT/F \ln(k\beta_{Fe}[Fe^{3+}]/k^2) \qquad 5.35$$

where

$$\delta = 1/(1 - \alpha_{Fe} + \alpha)$$

and α is the transfer coefficient for the anodic dissolution of chalcopyrite. The slope of the plot of the mixed potential against $\log[Fe^{3+}]$ for case (i) conditions should be $2.3RT/F$ or 72mV.decade^{-1}. Figure 5.22 shows the close correlation between the mixed potential and the sum of the concentrations of the $Fe^{3+}(aq)$ and $FeHSO_4^{2+}$ complexes for the data of Jones and Peters (1976). The measured slope of 82 mV.decade^{-1} is close to the expected slope of 72 mV.decade^{-1}, and these results confirm and add emphasis to the leaching results for Gamsberg sphalerite.

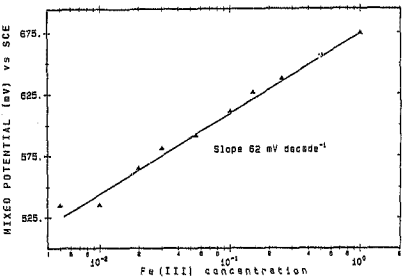

Figure 5.10 The effect of ferric sulphate additions to the 0.2 M H_2SO_4 solution on the mixed potential of a chalcopyrite electrode at 90°C (after Jones and Peters, 1976).

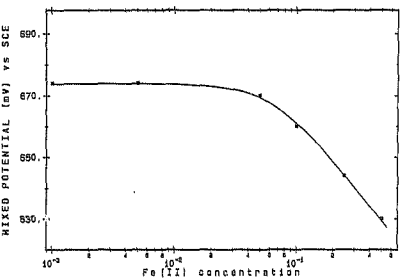

Figure 5.11 The effect of ferrous sulphate additions to the 0.2 M H_2SO_4 solution on the mixed potential of a chalcopyrite electrode at 90°C (after Jones and Peters, 1976).

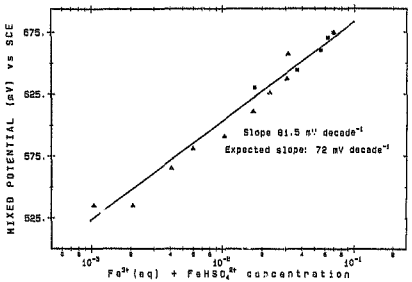

Figure 5.22 Case (i) model for data of Jones and Peters (1976) presented in Figures 5.20 and 5.21 assuming that $FeSO_4^+$ is inactive. The triangles are the data from Figure 5.20 and the squares the data from Figure 5.21.

The response of the mixed potential of the chalcopyrite electrode to changes in the concentrations of Fe(III) and Fe(II) in chloride solutions is shown in Figures 5.23 and 5.24, and confirms that case (i) conditions apply. Figure 5.23 illustrates that for an increase in the concentration of Fe(III), the measured slope of 75 mV.decade^{-1} is close to the expected slope of 72 mV.decade^{-1}, while for an increase in the concentration of Fe(II), there is very little change in the mixed potential. Figure 5.24 also confirms that complexing of the iron species in chloride solutions does not affect the mixed potential significantly, since behaviour such as that shown in Figure 5.21 is not observed.

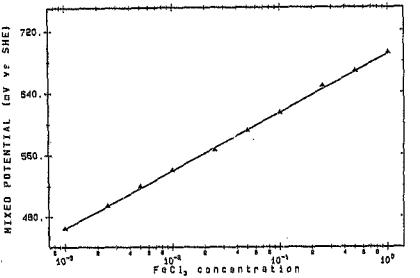

Figure 3.33 The effect of the addition of ferric chloride to the 0.2 M HCl solution on the mixed potential of the chalcopyrite electrode at 90°C (after Jones and Peters, 1976)

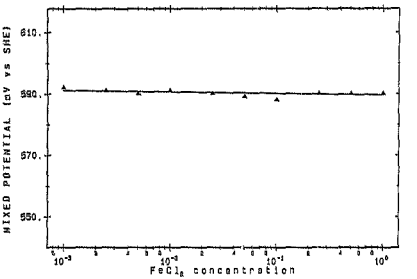

Figure 3.34 The effect of the addition of ferrous chloride to the 0.2 M HCl solution on the mixed potential of the chalcopyrite electrode at 90°C (after Jones and Peters, 1976).

5.3.6 Summary

It has been shown in this section that one of the ionic species in ferric sulphate solutions is inactive while leaching sphalerite. The electroactive complexes in ferric sulphate solutions are $Fe^{3+}(aq)$ and $FeHSO_4^{2+}$, while $FeSO_4^+$ is inactive. The reaction rate was shown to be one-half order with respect to the sum of the concentrations of the electroactive complexes. No complexes were found to be inactive during the leaching of sphalerite in ferric chloride solutions for the data reported in the literature. The same ferric sulphate complex was found to be inactive at the chalcopyrite electrode, a result that tends to confirm the results obtained with sphalerite. The electrochemical model derived in section 5.2 has been extended in this section to give the more familiar mixed-potential model, and this has been combined with the solution equilibria to give a more complete view of the oxidative dissolution process.

5.4 Application of the charge-transfer theory of the dissolution of ionic solids to the non-oxidative dissolution of sphalerite

5.4.1 Empirical correlation of the rate of non-oxidative dissolution of sphalerite

The experimental results used in this analysis were obtained by Verbaan (1977). As was mentioned in section 1.2.3, Verbaan (1977) reported extensive data on the non-oxidative dissolution of sphalerite in sulphuric acid solutions. However, he only analyzed the initial rate of reaction, and did not analyze the kinetics of the reverse reaction or the establishment of equilibrium. This will be done here in order to show that the kinetic parameters are the same as those reported by Romankiw and DeBruyn (1965) and Locker and DeBruyn (1969).

The theory presented in Chapter 3 will be used to derive an equation based on the electrochemical model that is consistent with the kinetics of dissolution.

The experimental equipment and procedure was described by Verbaan (1977) and summarized more recently by Crundwell and Verbaan (1987). Verbaan (1977) leached four samples of sphalerites: a natural pure sample, obtained from Ward's Scientific Establishment, a synthetic product (B.D.H.) and two natural impure sphalerite concentrates of South African origin, which are designated ZCR (Zincor) and PR (Prieska) respectively. (The designations are those of Verbaan's; they are used in this study to facilitate reference with that work.) Size reduction was effected by ball or vibratory milling, and the natural sphalerites were pretreated in a dilute sulphuric acid solution to remove any possible oxide layers or flotation reagents.

The initial rate of reaction at a stirrer speed of 400 rev.min^{-1} was 0.047 mmol m^{-2}min^{-1} (298 K, 1 M H_2SO_4) for the B.D.H. sphalerite and the initial rate at stirrer speeds of 700 and 1000 rev.min^{-1} was 0.062 mmol m^{-2}min^{-1}. The initial rates for the natural samples had a similar dependence on the stirrer speed. On the basis of this observation Verbaan used a stirrer speed of 1000 rev.min^{-1} in all subsequent experiments so as to avoid the region in which film-layer diffusion is the controlling mechanism.

Typical results collected by Verbaan (1977) are presented in Figure 5.25, which illustrates that an increase in temperature has a large effect on the rate of dissolution. All figures illustrating the increase of pressure with reaction time represent the continuous chart recorder output, and the points on these figures represent times at which solution samples were taken.

If it is assumed that the dissolution is controlled by a surface reaction in which the acid is the reactant, then, following Romankiw and DeBruyn (1965), the rate of dissolution, r, is given empirically

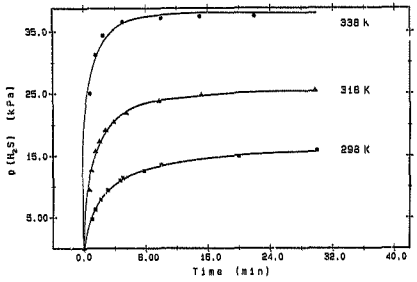

Figure 3.23 The effect of temperature on the dissolution of Ward's sphalerite in 1 M H_2SO_4.

by

$$r = \frac{1}{A}\frac{dn}{dt} = k_1[H^+]^{\delta} + k_{-1}[Zn^{2+}]^{\beta}p(H_2S)^{\gamma} \qquad 3.36$$

where A is the surface area, n is the number of moles of H_2S or Zn^{2+} produced, and δ, β and γ are empirical rate coefficients.

Analysis of the initial rate of reaction

The number of moles of solid dissolved was calculated from the measured H_2S partial pressure from

$$n = p(H_2S)\, V_1[1/K_D + V_g/RTV_1] \qquad 5.37$$

where $K_D = p(H_2S)/[H_2S]_{aq}$. V_g is the gas volume and V_1 is the liquid volume and T is the temperature. The derivation of equation 5.37, presented elsewhere (Romankiw and DeBruyn, 1965) assumes that the $[H_2S]_{aq}$ is in equilibrium with the $p(H_2S)$ (Henry's law) and that H_2S behaves like an ideal gas (low pressure, 298-343 K). The initial rate was determined by

$$r_o = \frac{1}{A}\left[\frac{dn}{dt}\right]_o = \frac{V_1}{A}\left[\frac{dp(H_2S)}{dt}\right]_o [1/K_D + V_g/RTV_1] \qquad 5.38$$

The derivative term $(dp(H_2S)/dt)_o$ was determined graphically from the chart-recorder traces of the H_2S pressure and by a non-linear regression technique using numerous points from the H_2S pressure data by Verbaan (1977). The non-linear regression technique was similar to that used by Romankiw and DeBruyn (1965). The initial rate was then calculated using equation 5.38. The dissolution of Fe and Cu components in the PR and ZCR samples would lead to evolution of H_2S not attributable to ZnS, and therefore a minor deviation from equation 5.38.

The effect of the acid concentration was determined from a plot of the initial rate of reaction as a function of the H_2SO_4 concentration. This graph for th Ward's and B.D.H. sphalerites is shown in Figure 5.26, from which it is concluded that the rate is first order with respect to the H_2SO_4 concentration. This was also found to be true for the ZCR and PR sphalerites.

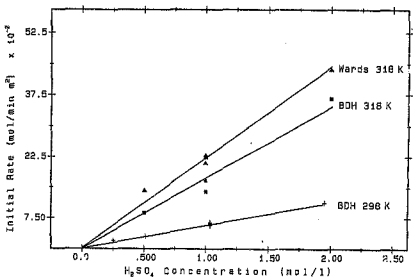

Figure 5.26 The effect of the H_2SO_4 concentration on the dissolution of Ward's and BDH samples.

The activation energy for the forward reaction was determined by plotting the logarithm of the initial rate, log r_o, against 1/T, as shown in Figure 5.27. The values of r_o, taken from Warhsan (1977), are given in Table 5.6. From Figure 5.27 it is concluded that the level of impurity does not significantly affect the activation energy.

Analysis of the rate of the reverse reaction

Figures 5.28 and 5.29 show the effect of $p(H_2S)_o$ and $[Zn^{2+}]_o$ on the rate of dissolution, where $\Delta p(H_2S)$ is the increase in the H_2S pressure above $p(H_2S)_o$. At equilibrium, the rate of the removal reaction is equal to the rate of the deposition reaction; therefore, since the order of dependence on $[H^+]$ is unity, $\delta = 1$ and

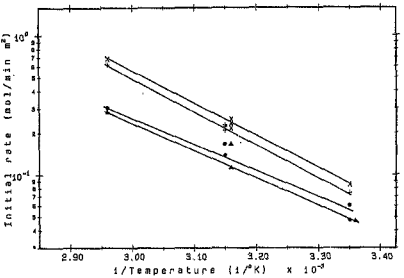

Figure 5.27 Arrhenius diagram for the initial rate of reaction for the various aphelerites. ▼ Ward's ● B.D.H. X BCR ▲ PR

Table 5.6 Effect of temperature on the initial rate of non-oxidative dissolution.

Sample	Run	Temp K	r_i' mmol $m^{-2}min^{-1}$	r_R mmol $m^{-2}min^{-1}$
Ward's	I2	318	7.46	0.228
	I3	318	13.7	0.209
	I4	298	4.86	0.074
	I5	338	40.44	0.618
BDH	"37	318	12.0	0.167
	I38	298	3.42	0.0475
	I39	338	21.8	0.303
	I36	318	3.97	0.138
	I49	298	1.74	0.604
BCR	I18	318	13.6	0.251
	I19	318	12.6	0.233
	I20	298	4.61	0.0851
	I21	338	36.9	0.681
	I16	318	3.19	0.236
	I17	318	3.83	0.216
PR	I27	318	2.95	0.112
	I29	298	2.45	0.0466
	I30	338	14.8	0.282

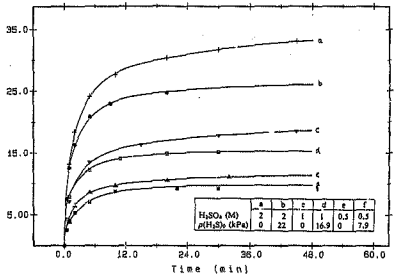

Figure 5.28 The effect of $p(H_2S)$ on Ward's sphalerite in different concentrations of H_2SO_4 at 45°C.

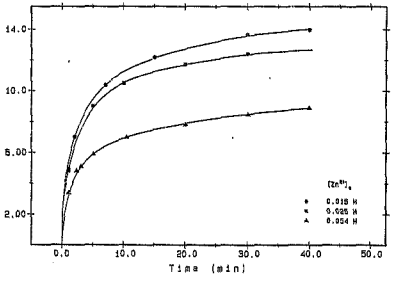

Figure 5.29 The effect of $[Zn^{2+}]_0$ on Ward's sphalerite in 1 M H_2SO_4 at 45°C.

$$k_{-1} = \frac{k_1 [H^+]_e}{[Zn^{2+}]_e^{\beta} p(H_2S)_e^{\gamma}} \qquad 5.39$$

where the subscript e denotes the value at equilibrium, and k_1 is determined from the slope of plots like Figure 5.26. The coefficients β and γ are determined from the logarithm of equation 5.39 and the use of a multilinear regression technique. The equilibrium values taken from Verbaan (1977) and used for this calculation are given in Table 5.7, and the values for the calculation of the activation energy for the reverse reaction are given in Table 5.8.

For the Ward's, B.D.H., ZCR and FR sphalerites, values close to 0.5, which are consistent with previous results (Locker and DeBruyn,1969) were determined for both these coefficients. The activation energies for the removal and deposition reactions are presented in Table 5.9. This table also gives the calculated values of the β and γ coefficients.

The effect of small additions of Fe(III) to the leaching solution on the rate of the two pure sphalerites is shown in Figure 5.30 and 5.31 This decrease in initial rate was also observed for various acid concentrations in the range 0.5 to 2 M. This effect was not observed under similar conditions for the ZCR and FR sphalerites. The initial rates of reaction for ZCR and FR sphalerites increased with increasing Fe(III) concentration.

5.4.2 Application of the charge-tranfer model to the non-oxidative dissolution of sphalerite

For a dissolving semiconductor, such as sphalerite, a significant portion of the potential drop may occur over the the space-charge region within the solid. Locker and DeBruyn (1969) proposed that the

Table 5.7 Determination of β and γ coefficients

	$[H_2SO_4]_o$	$[H_2SO_4]_e$	$[Zn^{2+}]_e$	$p(H_2S)_e$
BDH 298K	1.0	0.9912	0.00872	12.03
	1.0	0.9867	0.0133	18.48
	1.0	0.988	0.0119	17.59
	0.5	0.492	0.00791	11.05
	2.0	1.977	0.0229	33.04
	1.0	0.990	0.0252	13.96
	1.0	0.991	0.0345	12.39
	1.0	0.994	0.0603	8.87
	0.5	0.493	0.00685	17.09
	1.0	0.988	0.0116	32.07
	2.0	1.983	0.0174	46.71
	$\log [H^+] = -0.08 + 0.41 \log[Zn^{2+}] + 0.60 \log p(H_2S)$			
BDH 318K	1.0	0.9886	0.0114	26.31
	1.0	0.9821	0.0179	25.9
	0.5	0.4911	0.0089	10.27
	2.02	1.9919	0.0285	45.75
	1.0	0.9894	0.0246	18.25
	1.0	0.9830	0.017	38.7
	$\log[H^+] = 0.14 + 0.46 \log[Zn^{2+}] + 0.48 \log p(H_2S)$			
ZCR 318K	1.0	0.9879	0.0121	17.04
	1.0	0.9835	0.0165	20.24
	1.0	0.9832	0.0168	21.71
	1.0	0.9845	0.0155	20.35
	0.5	0.4913	0.00872	13.15
	2.0	0.1973	0.0275	40.53
	1.0	0.990	0.0243	17.67
	1.0	0.9884	0.0116	28.52
	$\log[H^+] = -0.11 + 0.44 \log[Zn^{2+}] + 0.67 \log p(H_2S)$			
PR 318K	1.0	0.9885	0.0115	16.08
	1.0	0.9805	0.0195	25.25
	1.0	0.9817	0.0183	20.3
	1.0	0.9818	0.0182	20.15
	0.5	0.4925	0.00754	8.41
	2.0	1.9766	0.0234	34.22
	1.0	0.9920	0.0222	12.18
	1.0	0.9886	0.0114	26.31
	$\log[H^+] = 0.11 + 0.4 \log[Zn^{2+}] + 0.48 \log p(H_2S)$			

Table 5.8 Determination of the activation energy for the reverse reaction of the non-oxidative dissolution of sphalerite

Sample	r_o nmolm^{-2}min^{-1}	Temp K	$\ln(r_o/[Zn^{2+}]p(H_2S))$
Ward's	0.209	318	-8.1079
	0.074	298	-8.6034
	0.618	338	-7.2786
BDH	0.1667	318	-8.4885
	0.0475	298	-9.4111
	0.303	338	-8.1029
	0.1378	318	-8.5046
	0.0604	298	-9.0795
ZCR	0.251	318	-7.7857
	0.233	318	-7.7827
	0.0851	290	-8.7058
	0.681	338	-7.2847
PR	0.166	318	-8.2084
	0.0466	298	-8.9033
	0.282	338	-7.8981

Table 5.9 Activation energies for the removal and deposition reactions (Equation 5.36) and the coefficients β and γ

Sample	Activation Energy (kJ mol^{-1}) Removal	Deposition	β	γ
Ward's	43.9	31.6	0.41	0.60
B.D.H.	37.9	25.4	0.46	0.48
PR	37.4	21.1	0.44	0.67
ZCR	44.3	30.4	0.40	0.48

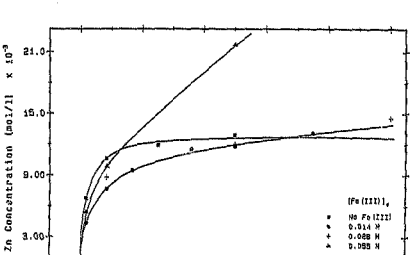

Figure 5.30 The effect of $[Fe(III)]_o$ on Ward's sphalerite in 1 M H_2O_2 at 45°C.

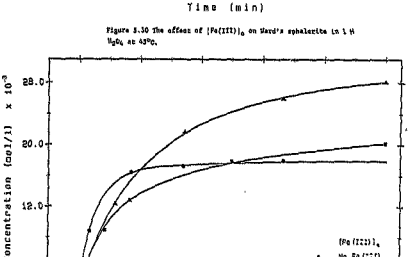

Figure 5.31 The effect of $[Fe(III)]_o$ on B.D.H. sphalerite in 1 M H_2O_2 at 45°C.

rate of non-oxidative dissolution of ZnS is controlled by the adsorption of hydrogen ions onto the surface rather than by charge carriers in the solid. Their proposal that changes in the potential appear across the Helmholtz layer is confirmed by the theoretical work of section 5.2.2, in which it is shown that the Fermi level of the sphalerite is pinned by the iron impurity of the sphalerite.

The activation energies for the removal and deposition reactions, given in Table 5.9, are between 30 and 50 kJ mol^{-1}, and are higher than those expected for diffusion-controlled processes (12 - 24 kJ mol^{-1}). It is therefore more likely that the chemical reaction is the rate-controlling step.

Vermilyea (1956) and Engell (1956) derived a charge-transfer model for the dissolution of ionic solids. They proposed that the transfer of ionic species across the electrochemical potential barrier at the solid-solution phase boundary controls the rate of dissolution. The main features of that theory are as follows: (i) The rates of transfer of anions and cations are exponentially dependent on the potential difference between the mineral surface and the outer Helmholtz plane, (ii) the transfer of cations and anions can be treated as independent processes, (iii) at steady state, the rates of transfer of cations and and anions are equal, and (iv) the rate equation for each process at the 'freely-dissolving' potential can be combined in a way that is analogous to the mixed-potential model for corrosion.

Diggle (1973) discussed the application of this model to the non-oxidative dissolution of metal oxides, and Nicol (1983) applied it to the leaching of metal sulphides, chiefly FeS. Scott *et al* (1977) interpreted the results of the kinetics of dissolution of uranium trioxide in terms of this theory.

According to Vetter (1967), Engell (1956) and Vermilyea (1966), the the dissolution reaction may be governed by the movement of zinc lattice ions across the Helmholtz plane.

$$Zn^{2+}_{lat} \rightleftharpoons Zn^{2+}(aq) \qquad 3.40$$

and the net rate of removal is given by the Butler-Volmer expression (Vetter, 1967; Engell, 1956; Vermilyea, 1966). The removal of cations is given by equation 3.13 and the net rate of removal can be rewritten as

$$r_+ = k^0_+(Zn^{2+}_{lat})\exp(\alpha_+ z_+ F\Delta\phi_H/RT) - k^0_+[Zn^{2+}]\exp(-(1-\alpha_+)z_+F\Delta\phi_H/RT) \qquad 3.41$$

where $\Delta\phi_H$ is the potential drop across the Helmholtz plane, α_+ is the cation transfer coefficient, k represents a rate constant, and the other symbols have their usual significance. The subscripts '+' and later '-' refer to the cation and the anion. This is the same equation as equation 3.13, and the theory of Vermilyea (1966) effectively assumes that the Fermi level of the solid is pinned, so that the applied potential only appears across the Helmholtz double-layer. For purposes of this analysis, it is assumed that the transfer of ions across the Helmholtz layer is the rate determining step (i.e. equation 3.12) and then equation 3.13 is applicable.

The removal of sulphur lattice ions may be followed by the complexing of protons, according to

$$S^{2-}_{lat} + (a-t)H^+ \rightarrow SH^{-2+a-t}_{a-t} \qquad 3.42$$

$$SH^{-2+a-t}_{a-t} + tH^+ \rightleftharpoons SH^{a-2}_a \qquad 3.43$$

for which the Butler Volmer expression (Vetter, 1966) is

$$r_- = k^0_-[S^{2-}_{lat}][H^+]^{a-t}\exp(\alpha_- zF\Delta\phi_H/RT) - k^0_-[SH^{a-2}_a][H^+]^{-t}\exp(-(1-\alpha_-)Fz\Delta\phi_H/RT) \qquad 3.44$$

where s and t are stoichiometric coefficients. The freely dissolving crystal has a double-layer potential, $\Delta\phi_E$, at which the net rate of removal of the cation, r_+, is equal to the net rate of removal of the anion, r_-. The initial rate is obtained by ignoring the deposition reactions, and equating the rates. This yields

$$r_o = k_+^o[Zn^{2+}_{lat}]\left(\frac{k_-^o[S^{2-}_{lat}][H^+]^{s-t}}{k_+^o[Zn^{2+}_{lat}]}\right)^x \qquad 5.45$$

where $x = \alpha_+ z_+/(\alpha_+ z_+ - \alpha_- z_-)$. The linear dependence of the initial rate on the acid concentration is obtained by assuming that each sulphide lattice ion reacts with two protons to form H_2S, i.e., $s = 2$, $t = 0$, and $x = 0.5$, which yields $\alpha_+ = \alpha_- = 0.5$.

The rate of the reverse reaction, i.e., the deposition reaction, is proportional to $[Zn^{2+}]^{0.5}$ and to $p(H_2S)^{0.5}$ (equation 5.36 and Table 5.12). The reverse reaction has a characteristic double-layer potential, $\Delta\phi_E$, at which the rate of the deposition of the cation is equal to the rate of deposition of the anion. The electrochemical expression for the deposition reaction is obtained by ignoring the dissolution terms in equations 5.41 and 5.44, and equating the rates for the cation and anion deposition. This yields

$$r_{dep} = k_+^o[Zn^{2+}]\left(\frac{k_-^o[SH_2^{2-s}][H^+]^{-t}}{k_+^o[Zn^{2+}]}\right)^x \qquad 5.46$$

where $x = (1-\alpha_+)z_+/\{(1-\alpha_+)z_+ - (1-\alpha_-)z_-\}$, which gives the correct half order dependence on $[Zn^{2+}]$ and $p(H_2S)$ if $\alpha_+ = \alpha_- = 0.5$, and $s = 2$ and $t = 0$, which are the same requirements for the forward reaction.

The situation at equilibrium is described as that when the rate of removal is equal to the rate of deposition for both the cation and

the anion. By setting r_+ and r_- equal to zero in equation 5.41 and 5.44, the following expression is obtained:

$$\exp(z_- F\Delta\phi_a/RT) = \frac{k_-^c[SH_s^{s-2}][H^+]^{s-c}}{k_+^c[S_{lat}^{2-}][H^+]^{s-c}} = \frac{k_-^a[Zn_{lat}^{2+}]}{k_+^a[Zn^{2+}]} \qquad 5.47$$

The equilibrium constant, K, is given by

$$K = \frac{k_+^a k_-^a}{k_+^c k_-^c} = \frac{[SH_s^{2-s}][Zn^{2+}]}{[H^+]^s} \qquad 5.48$$

From a comparison of equation 5.48 with the equilibrium constant for the overall reaction (equation 1.4) and from the arguments for the initial rate dependence on $[H^+]$, it is concluded that $s = 2$. The values of the parameters required to predict the correct reaction orders are the same for the forward and reverse reaction and for the equilibrium constant. The charge-transfer theory presented above is therefore a consistent model for the non-oxidative dissolution of sphalerite.

Therefore, equations 5.41 and 5.44 are the component equations for the rate equation 1.14 and equation 5.36. Equations 5.41 and 5.44 describe the initial rate and the establishment of equilibrium, that is, they are the definitive equations for the dissolution curves obtained in this study.

The addition of zinc ions to the solution in large concentrations has the effect of decreasing the initial rate, because equilibrium is established between the ions in solution and those at the surface (Figure 5.29). This is verified by the calculation of the equilibrium constant, i.e., $K_{sp} = 0.0001 < [Zn^{2+}][H_2S]$ at 1 M H_2SO_4 as calculated from the values given by Sillen (1965).

Small additions of ferric ions have the effect of increasing the double-layer potential in an anodic direction, which decreases the rate. A similar effect, in which additions of Fe(III) to the solution decreased the rate, was reported by Scott and Nicol (1978). Kuniada *et al* (1973) observed that the rate of non-oxidative dissolution of synthetic ZnS was decreased in the presence of dissolved oxygen. Nicol (1983) described results in which the dissolution of FeS, MiS, and PbS rotating-disc electrodes displayed a maximum in the curve of rate versus applied electrode potential. Figures 5.30 and 5.31 indicate that the Fe(III) also oxidizes the H_2S product (also observed in the curves of $p(H_2S)$ versus time), allowing the reaction to proceed beyond the non-oxidative equilibrium level. It was found that the presence of activated charcoal increased the level of dissolution for a similar reason.

It was assumed in the derivation of equation 5.43 that the supporting anion did not participate in the reaction. However, Majima *et al* (1961) have observed a first-order dependence of the rate on chloride ion at higher concentrations, and a rate that is independent of the chloride concentration at low concentrations. Equation 5.41 is therefore obeyed at lower concentrations and at higher concentrations equation 5.41 can be rewritten in a form analogous to equation 5.44 to include the effect of the complexing of the cation by the anion. Solving for the initial rate yields:

$$r_o = \vec{k}_s [Zn^{2+}_{lat}] [Cl^-]^{n-m} \left(\frac{\vec{k}_- [S^{2-}_{lat}] [H^+]^{a-t}}{\vec{k}_s [Zn^{2+}_{lat}] [Cl^-]^{n-m}} \right)^x \qquad 5.49$$

To obtain first-order dependence on Cl^- and H^+, one assumes that two chloride ions react with a zinc ion to form the $ZnCl_2$ complex (n-m = 2, a-t = 2, and x = 0.5).

5.4.3 Summary

This section has shown that the non-oxidative dissolution of sphalerite is more adequately described by the charge-transfer mechanism than by the previously proposed adsorption models. This mechanism is described by a Butler-Volmer expression for the removal of cations and anions from the solid lattice, and successfully describes the order of dependence of the initial rate on the proton concentration and the supporting anion, and the order of dependence of the final rate on the zinc ion concentration and the partial pressure of hydrogen sulphide. This model is derived from the model of charge transfer at a semiconductor-solution phase boundary in the absence of a redox couple, given by equation 3.13.

Locker and DeBruyn (1969) found the same kinetics for ZnS, CdS, ZnSe and $Zn_{0.85}Cd_{0.15}S$ as those found in this study, indicating that this model is applicable to the non-oxidative dissolution of other group II-VI semiconducting compounds.

In the next section, the model of electron transfer at the semiconductor-solution phase boundary will be applied to the dissolution behaviour and electrochemistry of pyrite and chalcopyrite.

5.5 The application of the fluctuating energy-level model to other systems - the influence of the electronic structure of solids on anodic electrochemistry of semiconducting sulphide minerals

Attempts have been made to correlate the rates of dissolution with the solid-state properties of minerals. Pawlek (1969) presented a table that listed the electrical resistivity, the atomic structure and the rate of dissolution of a series of minerals. He admitted that no correlation could be found, and added that little was known of the atomic bonding structure of the minerals. Daiger and Gerlach (1982) proposed that, since the oxidation of the sulphide occurs as a result of the consumption of two holes, fast dissolution rates can be expected when the concentration of holes is high, viz, in p-type semiconducting minerals. Copper sulphides, as well as NiS, FeS and $CuFe_2S_3$ belong to this group, whereas sphalerite and chalcopyrite, which dissolve slowly, are n-type (Daiger and Gerlach, 1982).

Springer (1970) studied the anodic and cathodic polarization curves of n- and p-type pyrite, n-type galena, and n-type chalcopyrite, and found no evidence to suggest a rate-determining involvement of electronic charge carriers. He concluded that the conduction properties of minerals do not normally play a significant role in the dissolution reactions.

Despite the lack of unanimity in the literature, a deeper understanding of anodic-dissolution reactions can be gained from a consideration of the structure of the solid and the theory of semiconductor electrochemistry (Gerischer, 1970).

This section of the thesis applies the energy-level model of semiconductor electrochemistry summarized in Chapter 3 to the dissolution kinetics of ore minerals. A more detailed discussion of the dissolution of these and other sulphides and the application of the fluctuating energy-level model is given in Appendix D. The aim of

this section is only to demonstrate that a model which accounts for the electronic structure of the solid gives a more thorough understanding of the mechanism of dissolution.

5.5.1 The influence of the electronic structure of pyrite on its dissolution kinetics

Pyrite is generally regarded as displaying noble electrochemistry. It has a high open-circuit potential and is galvanically protected from corrosion when in contact with other minerals. Parker *et al* (1981) presented current-voltage curves that were very similar to those of platinum.

Peters (1984) proposed that the differences in behaviour between sulphides can be accounted for by changes in the molar volume of the solids when the metal dissolves and solid sulphur forms. For example, pyrrhotite dissolves rapidly, while pyrite has a slow rate of dissolution. Peters proposed that, since the molar volume of pyrite is 12 $cm^3\ mol^{-1}$ of contained sulphur and the molar volume of sulphur is 16 $cm^3\ mol^{-1}$, there will be an increase in volume when the pyrite is oxidized, and the sulphur layer will protect the pyrite from further dissolution. Peters did not consider the differences in the structure and bonding of the minerals in the formulation of his proposal.

An important difference between transition metal disulphides, such as pyrite and molybdenite, and other polar semiconductors, such as CdS, ZnO, and GaP, is that the valence band is narrow and of non-bonding character. The 'one-electron' energy band diagram is shown in Figure 5.32. Electron transfer with this band (hole injection) will therefore have no effect on the structure or bonding of the solid, and corrosion will not occur. This feature was exploited by Tributsch and co-workers (Tributsch, 1977; Tributsch and Bennat, 1977; Jaegermann and Tributsch, 1983; Ennaoui *et al*, 1986) in their search for a

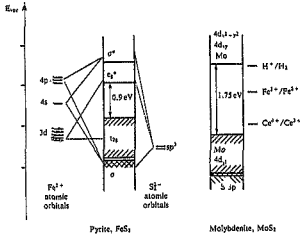

Figure 5.22 The band diagram for pyrite and molybdenite. The pyrite diagram shows a simplified molecular orbital diagram indicating the origin of the non-bonding valence band, the t_{2g} band. The crystal-field splitting of the Mo 4d orbitals in MoS_2 is also shown. The $4d_{z^2}$ band of MoS_2 is a non-bonding valence band.

suitable material for the conversion of solar energy.

There seems little doubt that the non-bonding character of the valence band is the reason for the slow dissolution behaviour and the reversible current-voltage behaviour of pyrite (and, for that matter, molybdenite which also has non-bonding valence band).

The formation of a hypothetical sulphur layer that is capable of preventing further oxidation is not consistent with the observed Tafel slope of 0.093 V.decade^{-1} (Biegler and Swift, ,1979) and Peters' (1984) proposal that dense sulphur layers are the reason for the slow rates of oxidation of pyrite must be rejected in favour of an explanation based on the band structure of pyrite.

5.5.2 Application of the energy-level model to the corrosion of chalcopyrite

Parker *et al* (1981) conducted extensive studies of the electrochemistry of chalcopyrite in chloride solutions in the temperature range 70 to 90 °C and the potential range 0.2 to 0.6 V (SCE), which is appropriate for chalcopyrite leaching. They reported that the rates of reduction of oxidants were in the order

$$Br_2,\ CuCl_2,\ I_3^- > Fe(CN)_6^{3-} > FeCl_3 > Fe_2(SO_4)_3,\ Cl_2$$

The location of the bands at the flatband potential and the redox potentials of these oxidants is shown in Figure 5.33. In order for electron capture or hole injection to occur, the energy level of the oxidant must overlap the conduction-band edge or the valence-band edge, respectively. It is apparent from the diagram that the rate of reduction of $CuCl_2$ and I_3^- is high because the energy levels of these ions overlap the conduction-band edge, and the rate of reduction of Br_2 is high because the bromine energy level overlaps the valence-band edge. In contrast, the iron chloride and iron sulphate energy levels are well within the band gap, and the rate of reduction is low. $Fe(CN)_6^{3-}$ is reported by Parker *et al* (1981) as having a lower rate of reduction than I_3^-, which has a higher E^o_{redox}, but this is because they compared these rates at different temperatures. The rate of reduction of $Fe(CN)_6^{3-}$ was determined at 25°C, while the others were all determined at 80°C. The level of Cl_2 is well below the valence-band edge.

Parker *et al* (1981) also reported anodic saturation currents, which are typical for n-type semiconductors where the supply of holes is migration-limited, for the oxidation of Fe^{2+} in solution. Similarly,

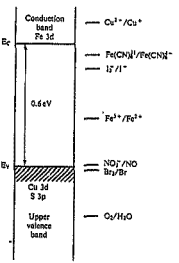

Figure 5.33 The energy level diagram for $CuFeS_2$, indicating the Cu 3d contribution to the valence band, and the Fe 3d contribution to the conduction band.

Beckstead *et al* (1976) presented results showing that the rate of dissolution increased with Fe^{3+} and then reached a steady value, indicative of saturation currents. Saturation currents were not found for I^- or $CuCl_2^-$ by Parker *et al* (1981), however, since the energy levels of these ions overlap the conduction band edge. From these arguments, it may be concluded that the interaction of

I_3^-/I^-,

$CuCl_2/CuCl_2^-$ and

$Fe(CN)_6^{3-}/Fe(CN)_6^{4-}$ are conduction band processes,

while Fe^{3+}/Fe^{2+} and

Br_2/Br^- are valence band processes.

Table 5.10 Comparison of the corrosion currents of chalcopyrite. (after Parker *et al*, 1981)

Ox	Red	V_{corr} (V vs SCE)	j_{corr} (mA cm^{-2})	Source
Fe^{3+}	Fe^{2+}	0.39	5500	Ward's
Fe^{3+}/Cu^{2+}	Fe^{2+}	0.48	11000	Ward's
Cu^{2+}	Cu^{+}	0.28	250	Ward's

Mechanism of dissolution of chalcopyrite

An interesting observation of Parker *et al* (1981) and others (Jones and Peters, 1976) is that the addition of $CuCl_2$ to a $FeCl_3$ solution results in enhanced current densities at a chalcopyrite electrode.

Table 5.10 presents a selection of data from Parker *et al* (1981), which indicates that the anodic dissolution of chalcopyrite occurs with a contribution of holes in the valence band and electrons in the conduction band. This is the case for many semiconductors, such as Ge, with a band gap of less than 1 eV (Gerischer and Mindt, 1966). Since the dissolution current for the contribution of holes from oxidant Fe^{3+} is greater than for the contribution of electrons to Cu^{2+} in solution, it is assumed that the initial step in the dissolution of chalcopyrite is the consumption of a hole. Chalcopyritic Fe^{3+} is associated with the conduction band and chalcopyritic Cu^{+} with the valence band; the electropositive Fe^{3+} will therefore be released into solution, and the Cu^{+} will remain after the initial step. The initial hole transfer is followed by electron transfer, according to

$$CuFeS_2 + 3h^{+} \rightarrow Fe^{3+} + {}^{\cdot}CuS_2 \qquad 5.50$$

followed by hole transfer

$$\cdot CuS_2 + 2h^+ \rightarrow Cu^{2+} + 2S \qquad 5.51$$

or electron transfer

$$\cdot CuS_2 \rightarrow Cu^{2+} + 2S + 2e^- \qquad 5.52$$

The first step illustrates the breaking of the Fe-S bond and the second the breaking of the Cu-S bond. $\cdot CuS_2$ is an unstable radical intermediate. This mechanism implies that copper remains in the lattice because it is associated with the valence band, which is consistent with the observation that the Fe/Cu ratio in solution is greater than 1 in the initial stages of leaching.

The radical intermediate, $\cdot CuS_2$, may decompose to form a stable CuS intermediate according to

$$\cdot CuS_2 \rightarrow CuS + S \qquad 5.53$$

Biegler and Swift (1979 b) presented cyclic voltammogramms for pure natural chalcopyrite. A large anodic response occurs at potentials greater than 1.0 V. Prior to this response, a smaller 'prewave' response occurs at 0.8 V, which they interpreted as the formation of a copper sulphide film.

The mechanism presented here accounts for the increased leaching rates obtained when $CuCl_2$ is added to the $FeCl_3$ leaching solution. However, more thorough investigation of this proposal is required.

5.5.3 Summary

In the case of pyrite, crystal field splitting results in a valence band that is of non-bonding character, and holes in this band can not result in bond breaking. Thus, pyrite resists dissolution. This proposal is in contrast to the work of Peters (1984) who proposed that a dense sulphur layer is the cause the slow dissolution. The proposal must be rejected in favour of an explanation based on the electronic structure of pyrite.

The kinetics of the dissolution of chalcopyrite is complicated by the formation of a surface film, probably copper sulphide. It is argued in this section that the Cu^{2+}/Cu^{+}, $Fe(CN)_6^{3-}/Fe(CN)_6^{4-}$ and I_3^-/I^- couples are conduction band processes, while the Fe^{3+}/Fe^{2+} and Br_2/Br^- couples are valence band processes. Since the addition of $CuCl_2$ to a $FeCl_3$ leaching solution enhances the rate of dissolution, it is proposed that the dissolution mechanism involves both electrons and holes. This mechanism is similar to that proposed for the dissolution of Cu.

CHAPTER 6

CONCLUSIONS

A review of the literature suggested that the previously proposed mechanisms of the oxidative dissolution reaction did not include the effects of the solid-state properties of sphalerite, particularly the effect of the iron impurity in sphalerite. In addition, a satisfactory mechanism of the non-oxidative dissolution reaction had not been given.

In order to understand the dissolution process it is necessary to consider the electronic structure of the solid and the transfer of charge at the solid-solution phase boundary. Sphalerite is a semiconductor with a band gap of 3.65 eV. The major impurity in sphalerite is iron, which displaces zinc in the lattice to form a (Zn,Fe)S solid-solution. The d-orbitals of the iron contribute to a narrow band within the band gap of the sphalerite. A fundamental description of the mechanism of the dissolution of sphalerite based on the transfer of charge at the sphalerite-solution phase boundary has been given. This charge-transfer theory accounts for the oxidative and non-oxidative reactions.

6.1 The oxidative dissolution of sphalerite

Experimental results obtained for the leaching of iron-containing sphalerites in Fe(III) chloride solutions are presented that confirm the results of a previous experimental investigation (Pine and Tozawa, 1986). An equation has been derived that describes the known features of the dissolution of sphalerite, i.e, first-order dependence on the concentration of iron in the zinc sulphide lattice and half-order dependence on the concentration of oxidant in solution. This equation assumes that the transfer of electrons takes place between the

iron-impurity band in the band gap of the sphalerite and the oxidant in solution, and that the Fermi level of the sphalerite is pinned by the iron impurity. Since sphalerite is a semiconductor, the enhanced rates of reaction obtained by irradiation of the leaching solution with UV light is simply the result of photocorrosion. Such photo-effects are still expected despite the fact that the Fermi level is pinned. The dissolution of sphalerite has therefore been described by a fundamental model that combines the considerations of the electronic structure of (Zn,Fe)S and of the transfer of charge at the phase boundary.

It was also found that some ionic complexes are inactive during the leaching of Gamsberg sphalerite in ferric sulphate solutions. The electroactive species in Fe(III) sulphate solutions are $Fe^{3+}(aq)$ and $FeHSO_4^{2+}$, while $FeSO_4^+$ is inactive. Results reported for the mixed potential of a corroding chalcopyrite electrode indicate that the $FeSO_4^+$ complex is also inactive during charge transfer at the chalcopyrite surface. This was attributed to the fact that $FeSO_4^+$ is an inner sphere complex, while $FeSO_4$ is an outer sphere complex, and charge transfer to $FeSO_4^+$ would require the breaking of the Fe^{3+} - SO_4^{2-} bond in the inner coordination sphere to form the outer sphere complex.

Therefore, the outer sphere $FeHSO_4^{2+}$ and the $Fe^{3+}(aq)$ aquo-ion species are more easily reduced than the $FeSO_4^+$ complex. The fact that the Fermi level level is pinned means that the mixed-potential model can be applied to the dissolution of sphalerite. The mixed-potential model has been combined in this study with a knowledge of the solution equilibria to give a more complete view of the dissolution process in Fe(III) sulphate solutions. This electrochemical mechanism was applied to the results reported in the literature for the leaching of zinc sulphide concentrates in Fe(III) chloride solutions, and successfully yields the order of dependance of the rate on the concentrations of Fe(III), Fe(II) and Cl^-. No complexes were found to be inactive in Fe(III) chloride solutions.

The formation of an insoluble surface film passivates the leaching of two high lead content (about 2 % Pb) sphalerite concentrates in ferric sulphate solutions. Such passivation is not observed in ferric chloride solutions. This surface coating may consist of $PbSO_4$ or lead jarosite, both of which are insoluble in sulphate solutions. This finding means that the Mintek process (Verbaan, 1981), in which the sphalerite concentrate is leached in a ferric sulphate solution, is not suitable for the treatment of these concentrates.

6.2 The non-oxidative dissolution of sphalerite

This thesis has shown that the non-oxidative dissolution of sphalerite is more adequately described by a charge-transfer mechanism than by the previously proposed adsorption models. This mechanism is described by a Butler-Volmer expression for the removal of cations and anions from the solid lattice, and describes the order of dependence of the proton concentration and the supporting anion. The reverse reaction in which the cation and the anion are deposited on the surface is also described by the transfer of charge at the phase boundary.

Locker and DeBruyn (1969) found the same kinetics for ZnS, CdS, $Zn_{0.85}Cd_{0.15}S$ and ZnSe as those found in this study, indicating that this model is applicable to the non-oxidative dissolution of other group II-VI semiconductor compounds.

6.3 Application of the fluctuating energy-level model to the anodic electrochemistry of metal sulphides

The bonding structure of the solid is particularly important with transition metal sulphides. In sphalerite, the substitutional iron content provides a substantial d-band within the band gap with which it is preferable to transfer charge; in pyrite, crystal-field

splitting results in a valence band that has non-bonding character, and is therefore less easily oxidized.

The kinetics of chalcopyrite dissolution is complicated by the formation of a surface film, probably a film of copper sulphide. The influence of redox couples is in accordance with the semiconductor model, and a dissolution mechanism involving both electrons and hole is proposed.

Ore sulphides contain larger concentrations of impurities than synthetic sulphides, and this makes the direct application of semiconductor principles to the leaching and flotation more difficult. However, any fundamental or mechanistic study of the electrochemistry of leaching and flotation must take into account the influence of the electronic structure of the mineral.

6.4 Recommendations for further work

The model proposed here includes the effects of the electronic structure both of the solid and of the solution. This has not been the approach of previous studies; emphasis was placed either on the electronic structure of the solid, e.g. the work of Springer (1970), or on the solution, e.g., the work of Warren *et al* (1986).

This approach must be extended to the modelling of the kinetics of dissolution of other sulphides. An interpretation of the kinetics of dissolution of a number of sulphides reported in the literature has been given in Appendix D, but this interpretation must be verified, and the model must be extended.

The leaching of sphalerite in Fe(III) sulphate solutions suggests that one of the complexes in solution is electroinactive; it should be established to what extent this affects the rate of dissolution of other sulphides, particularly chalcopyrite

REFERENCES

Ashurst, K.G. and Hancock, R.D. (1977) National Institute for Metallurgy, Report nos. 1820 and 1914, Randburg, South Africa

Bailey, L.K. and Peters, E. (1976) Decomposition of pyrite by pressure leaching and anodization: the case for an electrochemical mechanism *Can Metall Quart* 15 333

Bard, A.J., Bocarsly, A B., Fan, F-R, Walton, E.G., Wrighton, M.S. (1980) The concept of Fermi level pinning at *semiconductor/liquid* junctions *J Am Chem Soc* 102 3671

Bard, A.J. and Wrighton, M.S. (1977) Thermodynamic potential for the anodic dissolution of n-type semiconductors *J Electrochem Soc* 124 1706

Beckstead, L.W., Munoz, P.B., Sepulveda, J.L., Herbst, J.A., Miller, J.D., Olson, F.A., Wadsworth, M.E. (1976) Acidic ferric sulphate leaching of attritor ground chalcopyrite concentrates In J.C. Yannopoulos and J.C. Agarwal (editors) *Extractive Metallurgy of Copper*, Vol 2, AIME, New York.

Biegler, T. (1975) Oxygen reduction on sulphide minerals *J Electroanal Chem* 70 265

Biegler, T. and Horne, M.D. (1984) The electrochemistry of chalcopyrite In P.E. Richardson *et al* (editors) *Proc Int Symp Electrochem Mineral Metal Process* The Electrochem Soc, Pennington.

Biegler, T. and Swift, D.A. (1977) Dissolution of copper sulphide anodes *Hydromet* 2 335

Biegler, T. and Swift, D.A. (1979 a) Anodic behaviour of pyrite in acid solutions *Electrochimica Acta* 24 415

Biegler, T. and Swift, D.A. (1979 b) Anodic electrochemistry of

chalcopyrite *J Appl Electrochem* 9 545

Bither, T.A., Bouchard, R.J., Cloud, W.H., Donohue, P.L., Siemens, W.J. (1968) Transition metal pyrite dichalcogenides. High pressure synthesis and correlation of properties *Inorg Chem* 7 2208

Bockris, J.O'M. and Khan, S.U. (1985) On the evolution of concepts concerning events at the semiconductor/solution interface *J Electrochem Soc* 132 2648

Boddy, P.J. (1964) The structure of the semiconductor-electrolyte interface *J Electrochem Soc* 111 1136

Boddy, P.J. and Brattain, W.H. (1963) The distribution potential at the germanium aqueous electrolyte interface *J Electrochem Soc* 110 570

Brodie, J.B. (1968) MSc. Thesis, University of British Columbia.

Burkin, A.R. (1969) Solid-state transformations during leaching *Mineral Sci Engng* 1(1) 4

Butler, J.N. (1964) *Ionic equilibrium - a mathematical approach*, Addison Wesley, Reading, Massachusetts

Butler, M.A. and Ginley, D.S. (1978) Prediction of the flat band potentials at semiconductor interfaces from atomic electronegativities *J Electrochem Soc* 125 228

Crundwell, F.K. (1985) MSc Thesis, University of the Witwatersrand, Johannesburg

Crundwell, F.K. and Verbaan, B. (1987) Kinetics and mechanism of the non-oxidative dissolution of sphalerite *Hydromet* 17 369

Daiger, K. and Gerlach, J. (1982) The kinetics of the direct leaching of sulphide ores *Erzmetall* 35 609

Dewald, J.F. (1960) In H. Gatos (editor), *Surface Chemistry of Metals and Semiconductors*. John Wiley and Sons, New York.

Diggle, J.W. (1973) Dissolution of oxide phases In: J.W. Diggle (editor) 'Oxides and oxide films', Marcell Dekker Inc., New York, vol 2, 281.

Doyle, D.N., Mastes, I.M., and Webster, I.C. (1978) Acid pressure leaching of zinc concentrates with elemental sulphur as a by-product In Jones M.J. (ed) *Eleventh Commonwealth Min Metall Congress*, Inst. Min. Metall., London, 645

Dry, M.J. (1985) PhD Thesis, University of the Witwatersrand, Johannesburg

Dry, M.J. (1987) Plant visit to Trail and Kidd Creek, Personal communication

Dutrizac, J.E. (1981) The dissolution of chalcopyrite in ferric sulphate and ferric chloride media *Metall Trans B* 12B 371

Dutrizac, J.E. and MacDonald, R.J.C. (1974) Ferric ion as a leaching medium *Mineral Sci Engng* 6(2) 59

Dutrizac, J.E. and Mac Donald R.J.C. (1974) The kinetics of the dissolution of covellite in acidified ferric sulphate solutions *Can Metall Quart* 13 423

Dutrizac, J.E. and MacDonald, R.J.C. (1978) The dissolution of sphalerite in ferric chloride solutions *Metall Trans B* 9B 543

Eadington, P. and Prosser, A.P. (1969) Oxidation of lead sulphide in aqueous suspensions *Trans Inst Min Metall* 78 c74

Eadington, P. (1973) The leaching of illuminated lead sulphide with nitric acid as a function of the solid-state electronic properties

Trans Inst Min Met 82 C158

Engell, H.J. (1956) Dissolution of oxides in dilute acid. A contribution to the electrochemistry of ionic solids *Z Physik Chem NF*, 7 158.

Ennaoui, A. *et al* (1986) Photoelectrochemistry of highly quantum efficient single crystalline n-FeS_2 (pyrite) *J Electrochem Soc* 133 97

Ettienne, A. and Peters, E. (1972) Thermodynamic measurements in the Cu-S system in the temperature range 40 - 80°C *Trans Inst Min Met* 81 C176

Exner F., Gerlach, J. and Pawlek, F. (1969) Pressure leaching of zinc sulphide *Erzmetall* 22 219

Forward, F.A. and Warren, I.H. (1960) Extraction of metals from sulphide ores by wet methods *Met Reviews* 5 (18) 137

Frank, S.N. and Bard, A.J. (1975) Semiconductor electrodes II - Electrochemistry at n-TiO_2 electrodes in acetonitrile solutions *J Am Chem Soc* 97 7427

Frese, K.W. (1981) A study of the rearrangement energies of redox systems *J Phys Chem* 85 3911

Garrett, C.G.B. and Brattain, W.H. (1955) Physical theory of semiconductor surfaces *Phys Rev* 99 376

Gatos, H. (1960) In H. Gatos (editor) *Surface Chemistry of Metals and Semiconductors*, John Wiley and Sons, New York.

Gerischer, H. (1960 a) Semiconductor electrode reactions In C.W. Tobias and P.Delahay (editors) *Advances in Electrochem and Electrochem Engng*, vol 1, Interscience.

Gerischer, H. (1960 b) In H. Gatos (editor) *Surface Chemistry of Metals and Semiconductors*, John Wiley and Sons, New York.

Gerischer, H. (1966) Electrochemical behaviour of semiconductors under illumination *J Electrochem Soc* 116 1174

Gerischer, H. (1970) Semiconductor electrochemistry In H.Eyring *et al* (editors), *Physical Chemistry - an advanced treatise*, Academic Press, New York, vol 9A.

Gerischer, H. (1977) On the stability of semiconductor electrodes against photodecomposition *J Electroanal Chem* 82 133

Gerischer, H. and Meyer, E. (1971) On the mechanism of electron transfer and corrosion on a cadmium sulphide electrode in the I_3^-/I^- redox system *Z Physik Chem NF* 74 302

Gerischer, H. and Mindt, W. (1968) The mechanism of the decomposition of semiconductors by electrochemical oxidation and reduction *Electrochimica Acta* 13 1329

Gerlach, J. and Kuzeci, E. (1984) Electrochemical behaviour of zinc sulphide in graphite paste *Erzmetall* 37 261

Ghali, E., Dandapani, B., and Lawenstam, A. (1982) Electrodissolution of synthetic covellite in hydrochloric acid *J Appl Electrochem* 12 369

Ginley, D.S. and Butler, M.A. (1978) Flatband potential of CdS photoanodes and its dependence on surface ion effects *J Electrochem Soc* 125 1968

Goodenough, J.B. (1972) Energy bands in TX_2 compounds with pyrite, marcasite and arsenopyrite structures *J Solid State Chem* 5 144

Green, M. (1959) Electrochemistry of the semiconductor electrolyte interface In J. O'M. Bockris (editor), *Modern aspects of*

electrochemistry, vol 2, Butterworths, London.

Guerretta, C. and Ghali, E. (1985) The anodic dissolution of ZnS-graphite mixture in a dilute hydrochloric acid solution In K. Tozawa (editor) *Proc. of Internat. Sym. on extractive metall. of Zinc* Min. and Metall. Inst. of Jpn., Tokyo.

Gurney, R.W. (1931) Quantum mechanics of electrolysis *Proc. Roy. Soc. London* A134 137, A136 378

Hillrichs, E. and Bertram, R. (1983a) The anodic decomposition of $Cu_{2-x}S$ *Hydrometall* 11 181

Hillrichs, E. and Bertram, R. (1983b) The anodic decomposition of CuS *Hydrometall* 11 195

Hillrichs, E. *et al* (1982) Investigations of the electrochemical dissolution of copper sulphide ores in sulphuric acid solutions In K. Osseo-Assare and J.D. Miller (editors) *Hydrometallurgy. Research Development and Plant Practice*, TME-AIME, Warrendale, Pennsylvania.

Hiskey, J.B. and Schlitt, W.J. (1981) Aqueous oxidation of pyrite In *Proc 2nd SME-SPE Int Solution Mining Symp*, Denver, AIME, p.55

Hiskey, J.B. and Wadsworth, M.E. (1981) Electrochemical processes in the leaching of metal sulphides and oxides In H. Kuhn (editor) *Process and fundamental considerations in selected hydrometallurgical systems*, SME-AIME, New York, p.303

Holberg, H. and Schneider, F.U. (1975) Investigations into the improvement of floatability of minerals by means of radiation *Proc of 11th Int Min Process Cong*, Cagliari

I, T-P, and Nancollas, G.H. (1972) EQUIL - A general computational method for the calculatin of solution equilibria, *Anal Chem* 44 1940

Jaegerman, W. and Tributsch, H. (1983) Photoelectrochemical reactions of FeS_2 (pyrite) with H_2O and reducing agents *J Appl Electrochem* 13 743

Jaffe, J.E. and Zunger, A. (1983) Electronic structure of ternary chalcopyrite semiconductors *Phys Rev B* 28 5822

Jan R.J., Hopworth, M.T. and Fox, V.G. (1976) A kinetic study of the pressure leaching of sphalerite *Met Trans B* 7B 353

Jellinek, F. (1972) In D.W.A. Sharpe (editor) *International Review of Science, Transition Metals* Part 1, Inorganc Chemistry Series 1, Vol 5, Butterworth, London.

Jin, Z-M. and Warren, G.W. (1985) Reaction kinetics and electrochemical model for the ferric chloride leaching of sphalerite In K. Tozawa (editor), *Proc Int Symp Ext Metall of zinc*, Min. and Metall. Inst. of Jpn., Tokyo

Jones, D.L. and Peters, E. (1976) The leaching of chalcopyrite with *ferric sulphate and ferric chloride* In J.C. Yannopoulos and J.C. Agarwal (editors) *Extractive Metallurgy of Copper*, vol 2, p 633, AIME, New York.

Keys, J.D., Horwood, J.L., Balashta, T.M., Gabri, L.J., Harris, D.C. (1968) Iron-iron interaction in iron-containing zinc sulphide *Can Mineral* 9 453

Khan, S.U. (1983) Some fundamental aspects of electrode processes In R. White *et al Aspects of Modern Electrochemistry*, vol 13, Plenum Press, New York.

Koch, D.F.A. (1975) Electrochemistry of sulphide minerals In J.O'M Bockris and B.E. Conway (editors) *Modern Aspects of Electrochemistry*, vol 10, Plenum Press, New York.

Koch, D.F.A. and McIntyre, R.J. (1976) The application of reflectance spectroscopy to a study of anodic oxidation of cuprous sulphide *J Electroanal Chem* 71 285

Krishnaswamy, P. and Fuerstenau, D.W. (1982) Electrochemical mechanisms for the aqueous dissolution of molybdenite In K. Osseo-Assare and J.D. Miller (editors) *Hydrometallurgy, Research, Development and Plant Practice* TMS-AIME, Warrendale, Pennsylvania

Kunioda,Y, Sameshoto,H, and Oki,T. (1973) Effects of dissolved oxygen on th the dissolution of ZnS in sulphuric acid solution *J Japan Inst Metals* 37 803

Kuzminkh, I.N. and Yakautova, E.L. (1950) Actions of ferric sulphate on zinc sulphide, *J Appl Chem USSR* 23 1197

Levich, V.G. (1970) In H. Syring *et al* (editors) *Physical Chemistry - An Advanced Treatise*, vol 9A Academic Press, New York

Linge, H.G. (1976) A study of chalcopyrite dissolution in acidic ferric nitrate by potentiometric titration *Hydromet* 2 51

Levenspiel, O. (1972) *Chemical Reaction Engineering*, 2nd Ed, John Wiley and Sons, New York

Lockor, L.D. and DeBruyn, P.L. (1969) The kinetics of the dissolution of II-VI semiconductor compounds in non-oxidizing acids *J Electrochem Soc* 116 12 1659.

Majima, H. (1969) How an oxidant affects selective flotation of complex sulphide ores *Can Metall Quart* 8 269

Majima, H., Awakura, Y., and Miskaki, N. (1981) A kinetic study on non-oxidative dissolution of sphalerite in aqueous hydrochloric solutions *Metall Trans B* 12B 846

Majewski, J.A. (1981) Electronic structure of transition metal

Impurities in zinc sulphide Phys Stat sol B 102 663

Marcus, R.A. (1964) On the theory of electron-transfer reactions *Ann Rev Phys Chem* 15 155

McMillan, R.S., MacKinnon, D.J. and Dutrizac, J.E. (1982) Anodic dissolution of n- and p-type chalcopyrite *J Appl Electrochem* 12 743

Mehl, W. and Hale, J.M. (1966) Insulator electrode reactions In C.W. Tobias and P. Delahay (editors), *Advances in Electrochem. and Electrochem. Engng.*, vol. 6, Interscience.

Memming, R.J. (1969) Mechanism of the electrochemical reduction of persulphates and hydrogen peroxide *J Electrochem Soc* 116 785

Memming, R. (1980) Processes at semiconductor electrodes In B.E. Conway *et al* (editors) *Comprehensive Treatise on Electrochemistry*, vol 7, Plenum, New York.

Mercantonio, P. (1976) PhD Thesis, University of Utah.

Meyer, R.E. (1979) Electrochemistry of FeS_2 *J Electroanal Chem* 101 59

Morrison, S.R. (1977) *The Chemical Physics of Surfaces* Plenum, New York.

Morrison, S.R. (1978) Study of semiconductors using electrochemical techniques *J Vac Sci Technol* 15 1417

Morrison, S.R. (1980) *Electrochemistry at semiconductor and oxidised metal electrodes*, Plenum Press, New York.

Mott, N.F. and Gurney, R.W. (1948) *Electronic processes in Ionic Crystals* 2nd Edition, Oxford University Press, New York.

Muldar, E.J. (1972) *Optical properties of crystals of cuprous sulphides Phys Status Solidi A* 13 79

Munoz, P.B., Miller, J.D. and Wadsworth, M.E. (1979) Reaction mechanism of the acid ferric sulphate leaching of chalcopyrite *Metall Trans* 10B 149

Naumov, G.B., Rhyzhenko, B.N., Khadakovsky, I.L.(1974) *Handbook of Thermodynamic data*, National Technical Information Service, US Geological Survey, Menlo Park, California

Nicol, M.J., Needles, C.R.S., Finkelstein, N.P. (1975) Electrochemical model for the leaching of uranium dioxide in Burkin, A.R. (ed) *Leaching and reduction in hydrometallurgy*, I.M.M., London.

Nicol, M.J. (1983) The non-oxidative leaching of oxides and sulphides - an electrochemical approach In K. Osseo-Asare and J.D Miller (ed.) Proc. 3rd *Int. Symp. Hydrometallurgy*, 177.

Parker, A.J., Paul, R.L. and Power, G.P.(1981) Electrochemistry of the oxidative leaching of copper from chalcopyrite *J Electroanal Chem* 118 305 and *Aust J Chem* 34 13

Paul, R.L., Nicol, M.J., Diggle, J.W. and Saunders, A.P (1978) The electrochemical behaviour of galena *Electrochimica Acta* 23 625

Pawlek, F. (1969) Research in pressure leaching *J S Afr Inst Min Metall* 69 632

Peter, L.M., Li, J. and Peat, R. (1984) Surface recombination at semiconductor electrodes *J Electroanal Chem* 165 29

Peters, E. (1977) The electrochemistry of sulphide minerals In J. O'M. Bockris *et al* (editors) *Trends in Electrochemistry*, Plenum, New York.

Peters, E. (1984) Electrochemical mechanisms for decomposing sulphide

minerals In P.E Richardson et a. (editors) *Proc. Internat. Sym. on Electrochem. in Mineral and metal processing*, The Electrochem Soc, Pennington.

Piao, S.Y. and Tozawa, K. (1985) Effect of iron content in zinc sulphide concentrates on zinc extraction *J Min Metall Inst Jpn* 101 795

Pitzer, K.S. (1972) Activity coefficients of divalent metal sulphates *Faraday Trans II*, 68 101

Pitzer, K.S., Roy, R.N., Sylvester, L.F. (1977) Thermodynamics of electrolyes 7 Sulphuric acid *J Am Chem Soc* 99 4930

Potter, R.W. (1977) An electrochemical investigation on the system copper-sulphur *Econ Geol* 72 1524

Price, D.C. (1981) Application of chronopotentiometric analysis to the anodic treatment of copper sulphides *Metall Trans B* 12B 231

Richardson, P.E. and O'Dell, C.S. (1984) Semiconducting characteristics of galena electrodes In P.E. Richardson *et al* (editors) Proc of *Int Symp Electrochem Mineral and Metal Process*, The Electrochem Soc., Pennington.

Romankiw, L.T. and DeBruyn, P.L. (1965) The kinetics of dissolution of zinc sulphide in aqueous sulphuric acid In M. Wadsworth (editor) 'Unit operations in Hydrometallurgy' Gordon and Breach.

Scott, T.R. and Dyson, N.F. (1968) The catalysed oxidation of zinc sulphide under acid pressure leaching conditions *Trans Met Soc A.I.M.E.* 242 1813

Scott, P.D., Glasser, D. and Nicol, M.J. (1977) Kinetics of dissolution of β-uranium trioxide in acid and carbonate solutions *J Chem Soc, Dalton Trans* 1939-1943

minerals In P.E Richardson *et al* (editors) *Proc. Internat. Sym. on Electrochem. in Mineral and metal processing*, The Electrochem Soc, Pennington.

Piao, S.Y. and Tozawa, K. (1985) Effect of iron content in zinc sulphide concentrates on zinc extraction *J Min Metall Inst Jpn* 101 795

Pitzer, K.S. (1972) Activity coefficients of divalent metal sulphates *Faraday Trans II*, 68 101

Pitzer, K.S., Roy, [illegible], Silvester, L.F. (1977) Thermodynamics of electrolyes [illegible] *J Am Chem Soc* 99 4930

[illegible]er, R.W [illegible] electrochemical investigation on the system [illegible] *Soc* 72 1524

Pri[illegible] (1971) Application of chronopotentiometric analysis to the [illegible] of copper sulphides *Metall Trans B* 12B 231

Richardson, P.E. and O'Dell, C.S. (1984) Semiconducting characteristics of galena electrodes In P.E. Richardson *et al* (editors), *Proc of Int Symp Electrochem Mineral and Metal Process*, The Electrochem Soc., Pennington.

Romankiw, L.T. and DeBruyn, P.L. (1965) The kinetics of dissolution of zinc sulphide in aqueous sulphuric acid In M. Wadsworth (editor) 'Unit operations in Hydrometallurgy' Gordon and Breach.

Scott, T.R. and Dyson, N.F. (1968) The catalysed oxidation of zinc sulphide under acid pressure leaching conditions *Trans Met Soc A.I.M.E.* 242 1815

Scott, P.D., Glasser, D. and Nicol, M.J. (1977) Kinetics of dissolution of β-uranium trioxide in acid and carbonate solutions *J Chem Soc, Dalton Trans* 1939-1945

Scott, F.D. and Nicol, M.J. (1976) National Institute of Metallurgy, Report 1858, Randburg, South Africa.

Scott, F.D. and Nicol, M.J. (1976) The kinetics of the leaching of zinc sulphide concentrates in acidic sulphate solutions. Report 1949, Council for Mineral Technology, Randburg, South Africa.

Scott, F.D. and Nicol, M.J. (1977) The kinetics and mechanisms of the non-oxidative dissolution of metal sulphides In J.O'M. Bockris et al (editors) 'Trends in electrochemistry', Plenum, New York, 303.

Scott, F.D. and Nicol, M.J. (1979) The kinetics and mechanism of the non-oxidative dissolution of some iron sulphides in aqueous acidic solutions *J S Afr Inst Min Metall* 79 295

Sillen, L.G. (1965) *'Stability constants of metal-ion complexes'*, *Special publication* 17, The Chem Soc, London.

Simkovich, G. and Wagner, J.B. (1960) The influence of point defects on the kinetics of dissolution of semiconductors *J Electrochem Soc* 110 513

Shafeev, R.S. (1963) The influence of surface properties of sulphide minerals on adsorption of flotation reagents *Trans Inst Min Met* 72 715

Shay, J.L. and Tell, B. (1973) Energy band structure of I-III-VI_2 semiconductors *Surf Sci* 37 748

Shuey, R.T. (1975) *Semiconducting Ore Minerals*, Elsevier, Amsterdam.

Springer, G. (1969) Observations on the electrochemical reactivity of semiconducting minerals *Trans Inst Min Metall* 78 C11

Sullivan, J.D. (1933) *Trans Am Inst Min Met* 106 515

Swank, R.K. (1967) Surface properties of II-VI compounds *Phys Rev* 153 844

Telkes M. (1950) Thermoelectric power and electrical resistivity of minerals *Am Mineral* 35 536

Thomas, G. and Ingraham, T.R. (1967) Kinetics of dissolution of synthetic covellite in aqueous acidic ferric sulphate solutions *Can Metall Quart* 6 153

Tossell, J.A. and Vaughan, D.J. (1981) *Relationships* between valence orbital binding energies and crystal structures in compounds of copper, gold, zinc, cadmium and mercury *Inorg Chem* 20 3333

Trasatti, S. (1986) The absolute electrode potential *Pure and Appl Chem* 58 (7) 955

Tributsch, H. (1977) Solar energy-assisted electrochemical splitting of water *Z Naturforsch* 32a 972

Tributsch, H. and Bennet, J.C. (1977) Electrochemistry and photoelectrochemistry of MoS_2 layer crystals *J Electroanal Chem* 81 97

Turner, D.R. (1956) Anodic behaviour of Ge in aqueous solutions *J Electrochem Soc* 103 252

Tyagai, V.A. and Kolbasov, G.Y. (1971) The contribution of surface states to the charge transport process across CdS-, CdSe-electrolyte interface *Surf Sci* 28 423

Vanden Berghe, R.A.L. *et al* (1974) Electron transfer involving tunnelling from surface states at the dark anodic CdS / indifferent electrolyte interface *Ber Bunsenges Phys Chem* 78 331

Van Sandwijk, A. and Koopmans, K. (1986) An *adsorption* model for the

leaching of sphalerite by iron(III) chloride in hydrochloric acid solutions *Delft Prog Rep* 11 33

Vaughan, D.J. and Craig, J.R. (1978) *Mineral chemistry of metal sulphides* Cambridge University Press, London.

Vaughan, D.J. and Tossell, J.A. (1980) The chemical bond and the properties of sulphide minerals I Zn, Fe, and Cu in tetrahedral and triangular coordination with sulphur *Can Mineral* 18 157

Vegter, N (1987) Plant visit to Vielle-Montange, Personal communication

Veltman, H. *et al* (1977) US Pat 4,004,991 (25 Jan, 1977) (to Sherritt Gordon Mines, Ltd)

Verbaan, B. (1977) Ph.D. Thesis, University of Natal, Durban.

Verbaan, B. (1980) Report no 2038, National Inst. for Metallurgy, Randburg

Verbaan, B. (1981) US Pat 4,274,931 (23 June 1981) (to MINTEK)

Verbaan, B. and Crundwell, F.K. (1986) An electrochemical model for the leaching of a sphalerite concentrate *Hydromet* 16 345

Vermilyea, D.A. (1966) The dissolution of ionic compounds in aqueous solutions *J Electrochem Soc* 113 1067

Vetter, K., (1967) 'Electrochemical Kinetics - theoretical and experimental aspects', Academic Press, New York.

Vijh, A.K. (1973) *Electrochemistry of metals and semiconductors* Marcel Dekker, New York

Wadsworth, M.E. (1972) Advances in the leaching of sulphide minerals *Mineral Sci Engng* 4 (4) 36

Warren, I.H. (1956) *Aust J Appl Sci* 7 346

Williams, R. (1960) Becquerel photovoltaic effect in binary compounds *J Chem Phys* 32 1505

Zavgolis, E.N. and Cooke, S.R.B. (1975) Electrochemical properties of the mineral chalcopyrite *Proc Eleventh Int Mineral Processing Congress*, Cagliari, Universita di Cagliari.

APPENDIX A

MINERALOGICAL ANALYSIS OF SPHALERITE SAMPLES

A.1 Distribution of iron in the (Zn,Fe)S mineral phase

Figures A.1 to A.5 give the distribution of the iron in the (Zn,Fe)S mineral phase for each of the sphalerite samples. The arithmetic mean for each of the these distributions is given in Table 4.4.

Figure A.1 indicates that the Ward's material is very pure, while the other figures indicate the the material is much less pure since the distribution is spread over a wider range.

A.2 X-ray diffraction diagrams for the samples of sphalerite after leaching in ferric sulphate solutions

Figures A.6 to A.10 are the X-ray diagrams for the Black Mountain, Rosh Pinah and Gamsberg sphalerites after leaching in ferric sulphate solutions.

The peaks in each of the diagrams have been identified with the products, namely sphalerite and sulphur, and with the impurities, namely anglesite ($PbSO_4$) and jarosite [$KFe_3(SO_4)_2(OH)_6$]. These measured peaks are given in Tables A.1 to A.3. The peaks for pure sphalerite, jarosite, anglesite and plumbojarosite are given in Table A.4.

From these values, it is possible that the jarosite is a plumbo-jarosite phase, and in addition to the anglesite present in the Black Mountain sphalerite, there may also be plumbojarosite. However, these phases are more difficult to identify from these peaks.

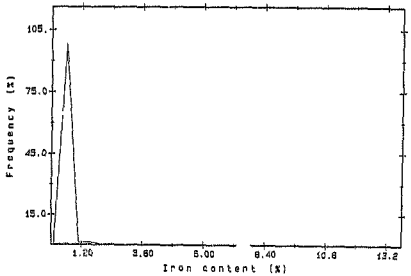

Figure A.1 Iron distribution diagram for Ward's sphalerite

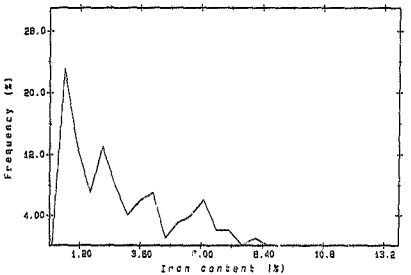

Figure A.2 Iron distribution diagram for Zinnwer sphalerite

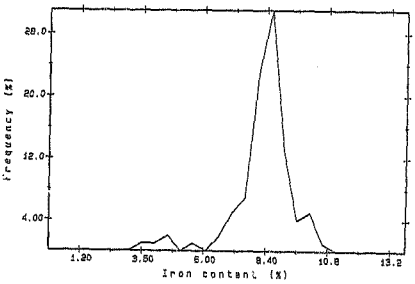

Figure A.3 Iron distribution diagram for Black Mountain sphalerite

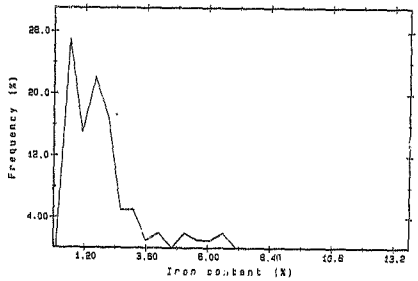

Figure A.4 Iron distribution diagram for Rosh Pinah sphalerite

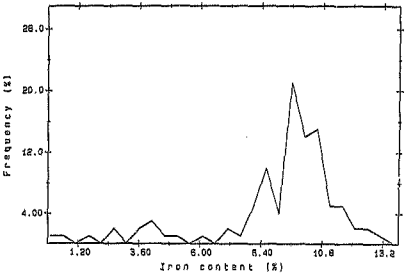

Figure A.3 Iron distribution diagram for Osmaborg sphalerite

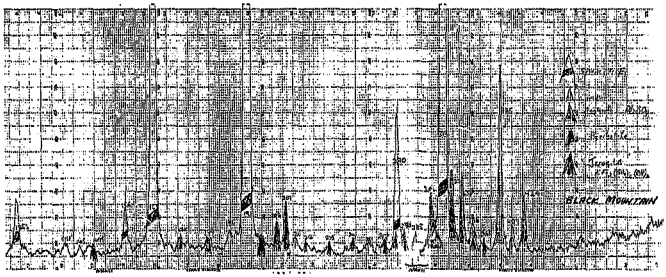

Figure A.6 XRD diagram for Black Mountain sphalerite

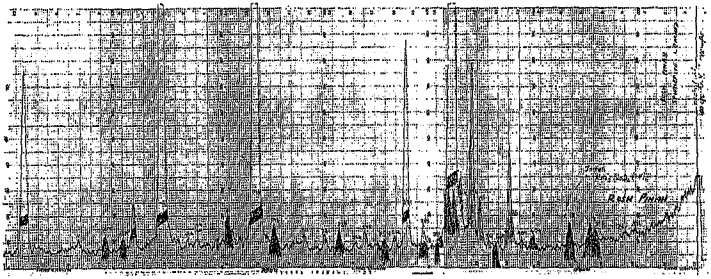

Figure A.) XRD diagram for Kosh Pinah sphalerite

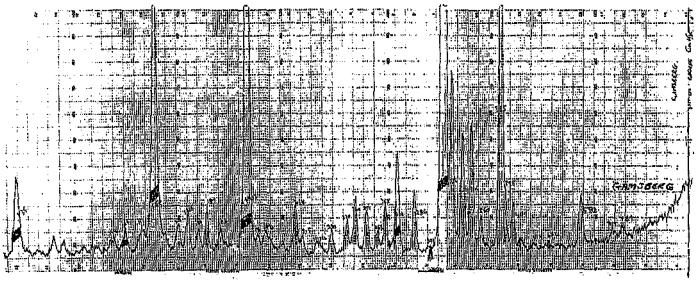

Figure A.8 XRD diagram for Gomsberg sphalerite

Table A.1 X-ray diffraction peaks for Black Mountain sphalerite after leaching in ferric sulphate solutions

Sphalerite	Sulphur	Jarosite	Anglesite
1.353	2.11	-	1.495
1.56	2.51		1.70
1.63	2.85		1.79
1.91	3.22		2.03
2.70	3.33		2.07
	3.46		2.16
	3.85		2.28
	4.04		2.41
			2.62
			2.76
			3.01
			3.22
			3.33
			3.46
			3.60
			4.24

Table A.2 X-ray diffraction peaks for Rosh Pinah sphalerite after leaching in ferric sulphate solutions

Sphalerite	Sulphur	Jarosite	Anglesite
1.353	2.11	1.504	1.70
1.56	2.43	1.540	1.79
1.63	2.62	1.81	2.97
1.91	2.84	1.98	4.29
2.71	3.24	2.27	
3.13	3.36	2.54	
	3.45	2.97	
	3.86	3.69	
		5.10	
		5.74	
		5.98	

Table A.3 X-ray diffraction peaks for Gamsberg sphalerite after leaching in ferric sulphate solutions

Sphalerite	Sulphur	Jarosite	Anglesite
1.35	1.79		
1.65	2.125		
1.63	2.30		
1.923	2.39		
2.70	2.44		
3.13	2.51		
	2.58		
	2.63		
	2.70		
	2.86		
	3.24		
	3.36		
	3.46		
	3.60		
	3.85		
	3.95		
	4.09		
	4.84		
	5.82		
	7.89		

Table A.4 X-ray diffraction peaks for sphalerite, anglesite, jarosite and pumbojarosite

Sphalerite	Anglesite		Jarosite		Plumbojarosite	
3.123	5.38	1.905	5.93	1.480	11.3	1.954
2.705	4.26	1.879	5.72	1.442	6.232	1.829
1.915	3.813	1.793	5.09	1.432	5.933	1.807
1.633	3.622	1.741	3.65	1.428	5.063	
1.561	3.479	1.716	3.55	1.423	4.619	
1.351	3.333	1.656	3.11	1.412	3.834	
1.240	3.220	1.648	3.08	1.399	3.657	
1.103	3.001	1.621	3.02	1.379	3.479	
1.04	2.773	1.611	2.965	1.358	3.114	
0.9557	2.699	1.571	2.861		3.066	
0.9138	2.618	1.542	2.542		2.964	
0.8848	2.406	1.525	2.368		2.868	
0.8244	2.355	1.493	2.302		2.812	
	2.276	1.467	2.287		2.620	
	2.233	1.441	1.977		2.531	
	2.193	1.429	1.937		2.389	
	2.164		1.909		2.370	
	2.133		1.825		2.303	
	2.067		1.776		2.252	
	2.031		1.738		2.145	
	2.028		1.717		2.076	
	1.973		1.690		1.976	

APPENDIX B

EXPERIMENTAL DATA

B.1 Experiments to determine the effect of the solid-state properties on the rate of dissolution

The leaching solution for all these experiments was as follows.

2 M NaCl
0.3 M HCl
0.2 M $FeCl_3$
0.005 M $FeCl_2$

Table B.1 Effect of the iron impurity of the sphalerite on the rate

Run	820	821	823	824	825
Temp °C	65	65	65	65	65
Sample	Ward's	Zincor	Black M	Rosh P	Gamsberg
V mV	577	577	578	577	577
z_o g/l	1.5	1.5	1.5	1.5	1.5
m_S g/l	0.77	0.58	0.266	0.404	0.234
Time	Concencration of zinc in solution, g/l				
0	0.003	0.003	0.002	0.002	0.007
5	0.061	0.130	0.235	0.185	0.300
10	0.081	0.190	0.350	0.280	0.490
15	0.084	0.270	0.450	0.345	0.665
20	0.120	0.320	0.530	0.400	0.770
30	0.170	0.430	0.655	0.500	0.870
45	0.280	0.420	0.825	0.600	0.970
60	0.360	0.600	0.910	0.690	0.990
90	0.390	0.880	0.970	0.830	1.010
120	0.525	0.910	0.960	0.920	1.070

Table B.2 Effect of the iron impurity of the sphalerite on the rate

Run	827	828	830	831	832
Temp °C	80	80	80	80	80
Sample	Ward's	Zinnor	Black M	Rosh P	Gamsberg
V mV	591	592	590	592	592
m_0 g/l	1.5	1.5	1.5	1.5	1.5
Time	Concentration of zinc in solution, g/l				
0	0.016	0.003	0.002	0.004	0.002
5	0.10	0.17	0.33	0.30	0.43
10	0.18	0.28	0.50	0.49	0.66
15	0.23	0.38	0.65	0.51	0.82
20	0.30	0.47	0.75	0.71	0.91
30	0.40	0.65	0.91	0.82	1.03
45	0.55	0.80	1.08	0.97	1.09
60	0.66	0.91	1.05	1.070	1.05
90	0.85	0.97	1.12	1.15	1.10
120	1.04	0.96		1.23	1.12

Table B.3 Effect of the iron impurity of the sphalerite on the rate

Run	833	834	836	837	838
Temp °C	45	45	45	45	45
Sample	Ward's	Zinnor	Black M	Rosh P	Gamsberg
V mV	564	557	559	556	555
m_0 g/l	1.5	1.5	1.5	1.5	1.5
Time	Concentration of zinc in solution, g/l				
0	0.008	0.003	0.002	0.003	0.002
5	0.017	0.062	0.12	0.15	0.28
10	0.023	0.085	0.17	0.17	0.32
15	0.033	0.100	0.25	0.21	0.42
20	0.039	0.100	0.33	0.24	0.50
30	0.052	0.120	0.41	0.28	0.62
45	0.068	0.160	0.48	0.37	0.76
60	0.085	0.200	0.58	0.44	0.78
90	0.135	0.300	0.73	0.52	1.06
120	0.140	0.360	0.97	0.60	1.01

Table 5.4 The effect of UV radiation on the rate of leaching

Run	839	840	842	843	844
Temp °C	65	65	65	65	65
Sample	Ward's	Zincor	Black M	Rosh P	Gamsberg
V mV	577	578	576	577	577
m_o g/l	1.5	1.5	1.5	1.5	1.5
m_f g/l	0.77	0.58	0.266	0.404	0.234
Time	Concentration of zinc in solution, g/l				
0	0.003	0.003	0.002	0.002	0.010
5	0.061	0.175	0.190	0.205	0.330
10	0.120	0.220	0.280	0.270	0.535
15	0.145	0.260	0.380	0.405	0.720
20	0.170	0.320	0.480	0.440	0.815
30	0.230	0.385	0.620	0.550	0.955
45	0.290	0.530	0.780	0.655	1.040
60	0.465	0.650	0.920	0.765	1.080
90	0.570	0.795	1.000	0.930	1.120
120		0.835	1.050	0.995	1.160

Table 5.5 The effect of different oxidants on the rate of leaching of the Ward's sphalerite. Oxidant concentration: 0.2 M
3 g/l Ward's sample

Oxidant	$CuCl_2$	$Co_2(SO_4)_3$	$SnCl_3$
Time	Concentration of zinc in solution, g/l		
0	0 002	0.003	0.002
5	0.041	0.470	0.011
10	0.060	0.840	0.006
15	0.085	1.13	0.004
20	0.108	2.42	0.065
30	0.090	2.61	0.063
45	0.095	3.57	0.065
60	0.099	4.31	0.071

B.2 Experiments to determine the effect of the variation of the ferric and ferrous sulphate concentrations on the dissolution rate

Table B.6 Effect of the ferric and ferrous sulphate concentrations on the rate of leaching of the Gamsberg sphalerite

Run	3	4	5	6	7
Temp °C	78	78	78	78	78
Fe(III) M	0.511	0.511	0.511	0.511	0.511
Fe(II) M	0.001	0.01	0.06	0.11	0.24
H^+ M	0.2	0.2	0.2	0.2	0.2
V mV	624	547	494	472	431
m_0 g/l	2	2	2	2	2
Time	Concentration of zinc in solution, g/l				
0	0.005	0.003	0.002	0.002	0.008
5	0.230	0 140	0.230	0.190	0.170
10	0.345	0.300	0.320	0.270	0.240
15	0.455	0.375	0.380	0.340	0.290
20	0.535	0.470	0.460	0.410	0.350
30	0.675	0.585	0.590	0.520	0.440
45	0.780	0.750	0.730	0.650	0.540
60	0.855	0.820	0.820	0.740	

Table B.7 Effect of the ferric and ferrous sulphate concentrations on the rate of leaching of the Gamsberg sphalerite

Run	8	9	10	11	27
Temp °C	78	78	78	78	78
Fe(III) M	0.126	0.126	0.126	0.126	0.511
Fe(II) M	0.001	0.006	0.05	0.25	0.015
H^+ M	0.22	0.22	0.22	0.22	0.22
V mV	595	527	472	407	527
m_0 g/l	2	2	2	2	2
Time	Concentration of zinc in solution, g/l				
0	0.005	0.005	0.005	0.005	0.005
5	0.22	0.24	0.17	0.12	
10	0.32	0.28	0.24	0.18	
15	0.40	0.36	0.29	0.22	0.33
20					
30	0.59	0.54	0.42	0.30	0.55
45					0.71
60	0.79	0.73	0.55	0.42	0.79
75					0.85
90					0.86
120					0.89

Table B.8 Effect of the ferric and ferrous sulphate concentrations on the rate of leaching of the Gamsberg sphalerite

Run	28	35	36	37	38
Temp °C	78	78	78	78	78
Fe(III) M	0.288	0.544	0.274	0.798	0.282
Fe(II) M	0.016	0.0048	0.0036	0.0076	0.0048
H^+ M	0.22	0.2	0.2	0.2	0.2
V mV	527	575	575	575	564
m_0 g/l	2	2	2	2	2
Time	Concentration of zinc in solution, g/l				
0	0.003	0.005	0.005	0.013	0.005
5		0.19	0.13	0.235	0.20
10		0.29	0.29	0.34	0.30
15	0.35	0.385	0.37	0.445	0.35
20		0.475	0.45	0.535	0.43
30	0.51	0.60	0.57	0.715	0.59
45	0.67	0.755	0.715	0.79	0.825
60	0.76	0.815	0.805	0.90	0.845
75	0.85				
90	0.88	0.863	0.860	0.95	0.91
120	0.94	0.885	0.865	0.965	0.94

Table B.9 Effect of the ferric and ferrous sulphate concentrations on the rate of leaching of the Gamsberg sphalerite

Run	39	40	45	46	47
Temp °C	78	78	78	78	78
Fe(III) M	0.80	0.123	0.613	0.613	0.682
Fe(II) M	0.016	0.0048	0.0036	0.0076	0.0048
H^+ M	0.22	0.2	0.2	0.2	0.2
Zn(II) M			0.051	0.011	
Cu(II) M					0.00519
V mV	527	575	575	575	56[illegible]
m_0 g/l	2	2	2	2	2
Time	Concentration of zinc in solution, g/l				
0	0.005	0.005	0.005	0.013	0.005
5		0.19	0.23	0.235	0.20
10		0.29	0.29	0.34	0.30
15	0.35	0.385	0.37	0.445	0.35
20		0.475	0.45	0.535	0.43
30	0.51	0.60	0.57	0.715	0.59
45	0.67	0.755	0.715	0.75	0.825
60	0.76	0.815	0.805	0.90	0.845
75	0.85				
90	0.88	0.865	0.860	0.95	0.91
120	0.94	0.885	0.885	0.965	0.94

Table B.10 Effect of temperature on the rate of dissolution of Gamsberg sphalerite in ferric sulphate solution

Run	86	87
Temp °C	70	54
Fe(III) M	0.28	0.28
Fe(II) M	0.0048	0.0048
H^+ M	0.2	0.2
V mV	567	548
m_0 g/l	2	2
Time	Concentration of zinc in solution, g/l	
0	0.005	0.005
5	0.16	0.16
10	0.25	0.16
15	0.32	0.18
30	0.49	0.30
60	0.79	0.47
90	0.81	0.64
120		0.71
130	0.90	
150	0.88	0.80
180	0.91	0.84

Table 5.11 Effect of the ferric and ferrous sulphate concentrations on the rate of leaching of the Black Mountain sphalerite

Run	24	25	26
Temp °C	78	78	78
Fe(III) M	0.136	0.136	0.136
Fe(II) M	0.001	0.01	0.05
H^+ M	0.2	0.2	0.2
V mV	395	427	472
m_o g/l	2	2	2
m_f g	1.95	1.95	1.99
Time	Concentration of zinc in solution, g/l		
0	0.005	0.005	0.005
5	0.138	0.119	0.11
10	0.19	0.146	0.156
15		0.169	0.182
30	0.264	0.206	0.229
60	0.317	0.262	0.262

Table 5.12 Effect of the ferric and ferrous sulphate concentrations on the rate of leaching of the Rosh Pinah sphalerite

Run	29	30	31
Temp °C	78	78	78
Fe(III) M	0.511	0.289	0.289
Fe(II) M	0.015	0.01	0.01
H^+ M	0.2	0.2	0.2
V mV	527	527	526
m_o g/l	2	2	2
m_f g	1.96	2.06	
Time	Concentration of zinc in solution, g/l		
0	0.005	0.005	0.20
5		0.10	0.19
10		0.12	0.20
15	0.18	0.13	0.20
30	0.23	0.16	0.20
45	0.26		
60	0.28	0.20	0.21
75	0.29		
90	0.29		
120	0.29		

Run 31 is the residue of run 30 which has been thoughly washed in CS_2 and has then been returned to the solution of run 30. As can been seen there is no further dissolution, suggesting that the layer of sulphur is not the reason for the passivation of the reaction.

Table B.13 Effect of washing the leached residue from Black Mountain in ammonium acetate.

Run	41
Temp °C	78
Fe(III) M	0.134
Fe(II) M	0.015
H^+ M	0.2
V mV	340

Time	Concentration of zinc in solution, g/l
0	0.005
5	0.027
10	
15	0.038
30	0.025
60	0.046

Run 41 is the residue of run 24 that has been washed in ammonium acetate and leached in the above solution.

Table B.14 Effect of ammonium acetate addition on the rate of leaching of the Black Mountain sphalerite.

Run	42
Temp °C	78
Fe(III) M	0.167
Fe(II) M	0.0015
H^+ M	0.3
CH_3COONH_3 g	38
V mV	586
m_o g/l	2

Time	Concentration of zinc in solution, g/l
0	0.005
3	0.13
10	0.18
15	0.20
20	0.21
30	0.24
45	0.26
60	0.30

After 30 mins a precipitate formed in the solution and all the peroxide was added to the solution as the control system tried to maintain the potential.

Computer program for the calculation of the disproportion of Pa(III) and three species in solution


```
      HOMENCLATURE

      d(1)=Ca(+)
      d(2)=Ac(+)
      d(3)=H(+
      d(4)=Th(4++
      d(5)=Pa(V)++
      d(6)=Pa(ZOH)+
      d(7)=Pa(ZOH)2+
      d(8)=Pa(OH)4
      d(9)=HCO3-
      d(10)=Pa(OH)3+
      d(11)=Pa(OH)2++
      d(12)=Pa(OH)3+++
      d(13)=Pa(OH)4++++
      d(14)=Pa(CO3)2+++
      d(15)=Pa(CO3)3

      PROGRAM MAIN

      dimension ta(5),c(15),tot(15),tot1(15),est(6)
      dimension ylo(14,5),yuni(6,5)
      character*1 ans
      dimension result(7,15),x0(15)
      common result/ xo(15),n,k
      common temp
      call ivfile(10,'Name of Datafile (r values)? ')
      do 10 i=1,15
10    read(10,*)(result(j,i),j=1,7)
      write(*,*) ' Number of runs ? '
      read(*,*) n
      call ivfile(11,'Name of Datafile with total init. conc.''s ? ')
      read(11,*)ivl
      do 104 i=1,nruns
      read(11,*)(yuni(j,i),j=1,5)
101   read(10,*)(result(j,i),j=1,7)
      call ivfile(15,'Name of Datafile to store results  ? ')
      call ivfile(16,'Name of Datafile to store 'minor' results  ? ')
      kk=ivl+temp*24.+1
      ta(1)=-1.1276e-4*temp**3.+1.112e-2*temp**2.-1.276e-2*temp**2.
     1+.12 ;ta(2)=-2.998e-4*temp**3.+3.553e-2*temp**2.+2.169e-2*temp**2.

C     CALCULATE EQUILIBRIUM CONSTANTS

      xk(1)=0
      xk(2)=exp(33.32+7629.0/temp)
      xk(3)=0
      xk(4)=exp(-290.12+1291.1/temp+135.6*alog(temp)
      xk(5)=exp(-1.691+2595./temp)
      xk(6)=exp(25.152-7295.4/temp)
      xk(7)=10.**(3.36*exp(-754.0/temp)+3.530)
      xk(8)=exp(15.9696+5797.1/temp)
      xk(9)=exp(25.9395-10515.86/temp)
      xk(10)=exp(13.4351-5965.1587/temp)
      xk(11)=0
      xk(12)=0
      xk(13)=exp(-4.61)
      xk(14)=10.**(-4.65954*1000/(4.571*temp)+1.4)
      xk(15)=0
      xk(16)=0
      xk(17)=0
      xk(18)=0

      nion=8
      if(ivl.eq.11)go to 18
      do 19 i=1,nruns
         ta(3)=yuni(1,i)
         ta(4)=yuni(2,i)
         ta(5)=yuni(3,i)
         ta(6)=yuni(4,i)
         ta(7)=yuni(5,i)
         call equil(ta,0,x,ratio,ask)
         write(19,1004)
         jx=rund(ibs)
         write(19,1001)(x,ta(j),ta(j),ta(j),x,
         write(19,1001)(x,ta(j),ta(j),ta(j),x,
         write(19,1001)(x,ta(j),ta(j),ta(j),x,
         write(19,1001)(x,ta(j),ta(j),ta(j),x,
         write(19,1004)
19    continue
1001  format(1x,13,3e,9(g11.4,1x),in,g11.4)
1004  format(1h,g11.4,/)
      stop
      end

c     subroutine equil(ta,n,x,ratio,ask)

c     PROGRAM TO EVALUATE THE EQUILIBRIUM CONDITIONS OF A SOLUTION
c     GIVEN THE TOTAL SPECIES CONCENTRATION AND THE EQUILIBRIUM
c     CONSTANTS. THE PROGRAM ALSO ACCOUNTS FOR THE ACTIVITY COEFFICIENTS
c     NOT BEING UNITY, AND THE DEBYE-HUCKEL EQUATION IS USED TO
c     CALCULATE THEM.

c     PROGRAM COUPL

      dimension df(n2),ss(135),bb(15),aa(5),fr(5),af(5,5),r(5),gr(5)
      dimension yt(15),gf(),eeq(15),tc(3),df(15),xkarea(30),ssm(15)
      common temp
      common /equcin/ xk(4),n,k
      common /acpcin/ z(15),as(15)

c     ASSUMING TOTAL DISSOCIATION CALCULATE IONIC STRENGTH
c     AND GET INITIAL CONCENTRATION GUESS AT TOTAL DISSOCIATION
c     CONCENTRATIONS.

      ni=nion+3.
      ta(4)=5./8.*ta(1)+ta(2)+.5*ta(3)+ta(5)
         do 40 k=1,5
         ak=ak+ta(k)
         ai=ai+ta(k)*z(k)**2.
40       xi=xi+ta(k)*z(k)**2.*ta(k)
         xi=xi+ak+ta(3)
         ii=0
12    if(ii<1)
c
c     CALCULATE ACTIVITY COEFFIS FROM DEBYE-HUCKEL EQUATION.
c
         do 45 k=1,15
         yt(k)=-.5*z(k)**2.*ai**.5/(1.+ai**.5*(1.+ai*.1*z(k)**2.)
45    yt(k)=10.**yt+.1*z(k)**2.*ai**.5/(1.+.5*ai**.5)
      continue
```

```
      coef11=x(11)*y(1)*y(3)*y(4)**2
      coef21=x(21)*y(1)*y(3)*y(4)/y(6)
      coef31=x(31)*y(1)*y(4)**2/y(7)
      rc_4(4)=x(4)*y(1)*y(4)/y(8)
      coef41=x(41)*y(4)*y(4)
      coef23=x(23)*y(2)*y(3)*y(4)/y(10)
      coef24=x(24)*y(2)*y(4)
CCcoef33=x(33)*y(3)/y(11)
C coef36=x(36)*y(1)*y(3)*y(4)/y(12)
Ccoef111=x(111)*y(1)**2/y(3)*y(4)/y(13)
Ccoef123=x(123)*y(2)*y(4)
Ccoef131=x(131)*y(2)*y(3)/c(13)
      coef41=coef31
      coef16=x(16)
      coef(1)=x(1)
      coef16=coef16
      call outfile(coef,nlocs,eoq,e)
      pause'keep'
      coef(5)=coef(3)*y(4)/c(5)
      coef(5)=coef(5)*y(4)/c(5)
c
c     GENERATE MATRIX AND VECTOR FOR THE SOLUTION OF THE
c     NON-LINEAR EQUATIONS BY A NEWTON-RAPHSON TECHNIQUE.
c     CALCULATE VECTOR G.
c
      call ggf(c,to,g,coef)
      do 55 k=1,3
      ge(k)=g(k)
55    g(k)=-g(k)
c
      CALCULATE Nx1 X 0
c
      a(1,1)=1+coef(1)*c(5)*c(4)**2+coef(2)*c(5)*c(4)+coef(3)
     /          *c(4)**2+coef(4)*c(4)
c     a(1,1)=g(1,1)+coef(9)/c(5)+coef(10)/c(4)**2+coef(11)*c(1)/c(3)**2
      a(1,2)=0
      a(1,3)=coef(1)*c(4)*c(4)**2+coef(2)*c(1)*c(4)
     /          -coef(3)*c(1)/c(5)*2
c     /          -2*coef(10)*c(1)/c(5)**3-4*coef(11)*c(1)**2/c(3)**3
      a(1,4)=2*coef(1)*c(1)*c(4)+coef(2)*c(1)*c(5)+
     /          coef(3)*c(1)*c(4)+coef(4)*c(1)
      a(2,1)=0
      a(2,2)=1
      a(2,3)=coef(5)*c(4)+coef(7)*c(3)*c(4)
c     a(2,3)=coef(5)*c(4)+coef(12)/c(3)**2+2*coef(13)*c(2)/c(3)**3
      a(2,4)=coef(5)*c(3)+ coef(7)*c(5)*c(3)
      a(3,1)=0
      a(3,2)=coef(1)*c(3)*c(4)**2+coef(2)*c(5)*c(4)
      a(3,3)=coef(7)*c(5)*c(4)
      a(3,4)=2*coef(1)*c(2)*c(4)**2+coef(2)*c(1)*c(4)+
     /          coef(5)*c(4)+coef(7)*c(2)*c(4)
     /          +coef(6)*c(3)*c(7)*c(2)*c(4)
      a(4,1)=2*coef(1)*c(3)*c(4)**2+coef(2)*c(5)*c(4)+
     /          coef(3)*c(4)**2+coef(4)*c(4)
      a(4,2)=coef(5)*c(4)+coef(7)*c(3)*c(4)
      a(4,3)=2*coef(1)*c(2)*c(4)**2+coef(2)*c(1)*c(4)+
     /          coef(5)*c(4)+coef(7)*c(2)*c(4)
      a(4,4)=1+2*coef(1)*c(1)*c(4)+coef(2)*c(1)*c(5)+
     /          coef(3)*c(1)*c(4)+coef(4)*c(1)+coef(6)*c(3)*c(7)*c(2)*c(3)*c(5)
      a(4,5)=coef(5)*c(4)
      a(5,1)=0
      a(5,2)=0
      a(5,3)=2.
      a(5,4)=coef(8)*c(5)
      a(5,5)=1+coef(8)*c(4)
c
c     RE-ARRANGING G IN TERMS OF FRACTIONAL DRIFTS.
c
      do 65 k=1,3
         do 55 k=1,5
            g(k+5,k)=a(k+5,k)*g(k+5,k)+a(k+5,k+1)*g(k+5,k+2)+a(k+5,k+3)*g(k+5,k+4)
55       continue
         g(k+5,6)=g(k+5,k+5)
         if(g(k+5).le.0)g(k+5)=1.
65    continue
c
c     MATRIX SCALING
c
      do 75 k=1,5
         g(k+5)=g(k+5)/(a(k+5,k+5)+1.e-5)
         do 70 k=1,5
            a(k+5,k)=a(k+5,k)/(a(k+5,k)+1.e-5)
70       continue
75    continue
c
c     CALCULATE THE INVERSE OF THE MATRIX AND CHECK FOR
c     SINGULARITY USING THE DETERMINANT SUBROUTINE.
c
      call inv1f(a,1,5,5,1,xkmax,ier)
      if(ier.eq.128)go to 170
c
c     CALCULATE THE FRACTIONAL DRIFTS, VECTOR X
c
      do 85 k=1,5
         x(k+5)=a(k+5,6)*g(k+5)
         if(x(k+5).gt.1.)x(k+5)=0.25
         if(x(k+5).lt.-1.)x(k+5)=-0.25
85    continue
c
c     NEXT ITN OF CONCENTRATION CALCULATION
c
      alfanm=1.
      nerror=0
      do 160 k=1,5
         c(k+5)=x(k+5)*(1.+alfanm*c(k+5))
         if(c(k+5).le.0)c(k+5)=1.e-15
         if(abs(alfanm*c(k+5)).gt.0.05)nerror=nerror+1
160   continue
c
c     CALCULATION OF CONCENTRATIONS OF P1 TO C(15)
c
      c(6)=coef(3)*c(1)*c(4)*c(4)
      c(7)=coef(5)*c(1)*c(4)**2
      c(8)=coef(6)*c(1)*c(4)
      c(9)=coef(7)*c(2)*c(5)*c(4)
      c(10)=coef(7)*c(2)*c(3)*c(4)
      c(11)=coef(8)*c(1)*c(2)
      c(12)=coef(9)*c(1)*c(5)
      c(13)=coef(11)*c(1)**2*c(3)**2
```

```
      xions=0.0
      do 155 kp=1,10
         xions=xions+(kp)**2*c(kp)
155   continue
      xions=xions/2.
      if(nerror.gt.0)go to 42
      ac,(i)=c(i)*y(i)
      ass(2)=a(2)*y(2)
      ratio=assig(ass(i)/ass(2))
      a=727.91;39*(temp-298.17)+8.6150e-2*temp*ratio
      go to 175
170   write(6,171)
171   format(5x,' matrix singular ')
      stop
175   a(6)=aeq(2)*a(1)*a(3)*a(4)
      a(7)=aeq(4)*a(1)*a(4)
      a(8)=aeq(5)*a(3)*a(4)
      a(9)=aeq(6)*a(2)*a(4)
      a(10)=aeq(7)*a(2)*a(3)*a(4)
      write(6,176)
176   format(5x,'ionic strength')
      write(6,*)xions
      write(6,177)
177   format(5x,'activity coefficients')
      write(6,*)(y(i: ),i=1,10)
      return
      end


c
c
      subroutine ggl,tot,func,eeq)
      dimension r(15),tot(5),func(5),eeq(14)
      func(1)=r(1)+eeq(1)*r(1)*r(2)*r(4)**2+eeq(2)*r(1)*r(3)*r(4)
      func(2)=func(1)+eeq(3)*r(11)*r(4)**2+eeq(4)*r(11)*r(4)-tot(1)
      func(3)=func(1)+eeq(8)*r(1)/r(3)+eeq(10)*r(1)/r(9)**2
      func(4)=func(1)+2*eeq(1)*r(11)**2/r(3)**2
      func(5)=r(2)+eeq(6)*r(2)*r(4)+eeq(7)*r(2)*r(3)*r(4)-tot(2)
      func(6)=func(2)+eeq(2)*r(2)*r(3)+eeq(10)*r(2)/r(3)**2
      func(7)=r(3)+eeq(1)*r(1)*r(3)*r(4)**2+eeq(3)*r(11)*r(3)*r(4)
      func(8)=func(3)+eeq(5)*r(3)*r(4)+eeq(7)*r(2)*r(3)*r(4)-tot(3)
      func(9)=r(4)+2.*eeq(1)*r(11)*r(3)*r(4)**2+eeq(2)*r(11)*r(3)*r(4)
      func(10)=func(4)+2.*eeq(3)*r(11)*r(4)**2+eeq(4)*r(11)*r(4)
      func(11)=func(4)+eeq(5)*r(3)*r(4)+eeq(6)*r(2)*r(4)
      func(12)=func(5)+eeq(7)*r(2)*r(3)*r(4)+eeq(8)*r(3)*r(4)-tot(4)
      func(13)=r(5)+eeq(9)*r(5)*r(4)-tot(5)
      return
      end


c
c
      subroutine sul(temp,xions,eeq,c)

c
c     PROGRAM TO EVALUATE THE EQUELIBRIUM CONSTANT OF HSO4-=H+ + SO42-
c     IN TERMS OF CONCENTRATION AT A PARTICULAR TEMPERATURE AND IONIC
c     STRENGTH.
c     (FROM PITZER'S CORRELATION)

      real k2,mi,mj,m2
      dimension c(15)
      k2=exp(14.9323)-2925.2/temp
      bhi1=-.9568+45.*k2/temp
      bhi1=-.6574*330.514/temp
      ah=.377+4.66e-4*(temp-273.15)+3.74e-6*(temp-273.15)**2
      z=xions**.5/(1.+1.2*xions**.5)
      f=-ah*(z/(1.+1.2*xions**.5)
      bhi=bhi1*bhi1/xions/2.*(1.-(1+2*xions**.5+xions**.5)*exp(-2*xions**.5))
      bh2=-1.+(1.+2.*xions**.5+2.*xions**.5)*exp(-2*xions**.5))
      bh2=bh2/(xions**2/2.)*bh2
      ch2=ch2/(2.**1.5)
      mh=c(3)
      mi=c(9)
      m2=c(4)
      activity=f+(2*(mi*mh)*bhi+2*(m2*mh)*bh2+
      activy=exp(activity*2*mh*(2*m2+mi)*ch2+6*mi*mh*bh2)
      aeq=h2*activity
      return
      end
```

APPENDIX D

The application of the fluctuating energy-level model to other systems - the influence of the electronic structure of solids on anodic electrochemistry of semiconducting sulphide minerals

Attempts have been made to correlate the rates of dissolution with the solid-state properties of minerals. Pawlek (1969) presented a table that listed the electrical resistivity, the atomic structure and the rate of dissolution of a series of minerals. He admitted that no correlation could be found, and added that little was known of the atomic bonding structure of the minerals. Daiger and Gerlach (1982) proposed that, since the oxidation of the sulphide occurs as a result of the consumption of two holes, fast dissolution rates can be expected when the concentration of holes is high, viz, in p-type semiconducting minerals. Copper sulphides, as well as NiS, FeS and $CuFe_2S_3$ belong to this group, whereas sphalerite and chalcopyrite, which dissolve slowly, are n-type (Daiger and Gerlach, 1982).

Peters (1984) differs from Pawlek (1969) and Daiger and Gerlach (1984), proposing instead that the differences in behaviour between sulphides can be accounted for by changes in the molar volume of the solids when the metal dissolves and solid sulphur forms. For example, pyrrhotite dissolves rapidly, while pyrite has a slow rate of dissolution. Peters proposed that, since the molar volume of pyrite is 12 $cm^3\ mol^{-1}$ of contained sulphur and the molar volume of sulphur is 16 $cm^3\ mol^{-1}$, there will be an increase in volume when the pyrite is oxidized, and the sulphur layer will protect the pyrite from further dissolution. Peters did not consider the differences in the structure and bonding of the minerals in the formulation of his proposal.

Springer (1970) studied the anodic and cathodic polarization curves of n- and p-type pyrite, n-type galena, and n-type chalcopyrite, and found no evidence to suggest a rate-determining involvement of

electronic charge carriers. He concluded that the conduction properties of minerals do not normally play a significant role in the dissolution reactions.

Despite the lack of unanimity in the literature, a deeper understanding of anodic-dissolution reactions can be gained from a consideration of the structure of the solid and the theory of semiconductor electrochemistry (Gerischer, 1970). Most research in semiconductor electrochemistry has been performed with high grade synthetic crystals. Natural ores are often polycrystalline with a high density of impurity levels. On the other hand, it is well known that ores of differing origin may exhibit significant differences in leaching and flotation behaviour, as a result of the differences in the solid-state properties of the minerals. It is therefore of technological importance and academic interest to establish the extent to which leaching and flotation behaviour is governed by the principles of semiconductor electrochemistry.

Metal sulphides display a wide range of structural and electronic properties, shown in Table D.1. Shuey (1975) reviewed the electronic properties of ore minerals, and Vaughan and Craig (1978) presented a volume on the mineral chemistry of sulphides.

This Appendix of the thesis applies the energy-level model of semiconductor electrochemistry summarized in Chapter 3 to the dissolution kinetics of ore minerals. The model takes into account the structure and bonding of the solid as well as its electronic conduction properties. It is used to interpret the anodic electrochemistry of the simple sulphides. It will be shown that dissolution occurs mainly by a hole mechanism if the band gap is greater than 1 eV. In the case of chalcopyrite, which has a band gap of 0.6 eV, it is proposed that both holes and electrons contribute to dissolution. Furthermore, it is proposed that pyrite resists dissolution because its valence band is

Table D.1. Properties of selected base metal sulphides (after Hiskey and Wadsworth, 1981)

Mineral	Formula	Resistivity (Ω m)	Semiconduction type	Open-circuit potential (V)
Pyrite	FeS_2	$0.1 - 3 \times 10^{-2}$	n,p	0.63
Chalcopyrite	$CuFeS_2$	$0.2 - 9 \times 10^{-3}$	n	0.53
Chalcocite	Cu_2S	$10^{-2} - 10^{-5}$	p	0.44
Covellite	CuS	$10^{-4} - 10^{-6}$	metallic p	0.42
Galena	PbS	10^{-5}	n,p	0.28
Sphalerite	ZnS	$10^{5} - 10^{7}$	-	-0.24

of non-bonding character, and holes therefore do not contribute to bond breaking.

D.1 Electrochemistry of cadmium sulphide

The electrochemistry of CdS has been extensively studied with a view to its application in liquid junction solar cells, but has received very little attention from hydrometallurgists.

CdS is an n-type semiconductor with a band gap of 2.4 eV. The valence band is associated with the sulphur anions and the conduction band with the cadmium cations. Single crystals of CdS display classic rectifying properties in which the cathodic current is exponentially dependent on the cathodic potential, while the anodic current is limited by the supply of minority carriers. The anodic current is directly proportional to the intensity of illumination (Gerischer, 1966).

Tyagai and Kolbasov (1971) and Vanden Berghe *et al* (1974) have reported the effects of surface states on CdS and CdSe. An ionic surface state associated with the zero valent sulphur remains on the

surface, available to be reduced. Tyagai and Kolbasov observed that the electron transfer to ferric or ferricyanide ions in solution is not linear in C_{ox} as expected from equation 3.23, but is given by

$$j = k\ C_{ox}^{0.7}\ C_{red}^{0.2}\ \exp[(1-\alpha)\eta F/RT] \qquad D.1$$

where $1-\alpha = 0.7$. This was interpreted as the result of a surface state, the charge of which changed with applied potential and the concentration of reducing agent in solution. This represents a transition between ideal semiconductor behaviour and metal-like behaviour. Vanden Berghe *et al* (1977) examined tunnelling through the surface barrier, and concluded that a surface state energy level was present 0.12 eV below the conduction band (Morrison, 1977).

Gerischer and Meyer (1971) studied the corrosion of CdS crystals by triiodide ions. The reduction of I_3^- has a Tafel slope of 0.6 - 0.8 V decade^{-1}, which is consistent with the surface state results. The corrosion of CdS occurs at a slow rate in neutral solutions, and the addition of I_3^- increases the rate of dissolution, although the I_3^- does not overlap with the valence band. This is further evidence of the surface-state mechanism.

D.2 The electrochemistry and dissolution of galena

Galena is the principal ore mineral of lead, and its dissolution and electrochemical behaviour have been extensively studied. Brodie (1968) studied the anodic behaviour of galena electrodes, and Fadington and Prosser (1969) reported on the dissolution kinetics of natural and synthetic galena in acidic and alkaline solutions. The influence of point defects on the rate of dissolution has often been reported, and extensive research has shown that there is a close correlation between the carrier concentration and the flotation behaviour of galena (Richardson and O'Dell, 1964; Plaskin and Shafeev, 1963; and Holberg and Schneider, 1975).

Galena is a good conductor, displaying both n- and p-type semiconduction. It has the halite structure, the internuclear distance being smaller than the sum of the ionic radii, suggesting some covalency. The band structure associates the bottom of the conduction band with Pb 6p character, and the top of the valence band with S 3p and Pb 6s character (Shuey, 1975). The band gap between the full valence band and the empty conduction band is about 0.37 eV (Shuey, 1975). Pure lead sulphide shows n- or p-type semiconduction, depending on whether sulphur is deficient (n-type) or is in excess (p-type) compared to the stoichiometric PbS. Common impurities in galena are Ag, Bi, Sb, and Cu. Ag is an acceptor (p-type), while Bi and Sb are donors. Cu can act as a substitutional acceptor or an interstitial donor.

Anodic electrochemical experiments (Brodie, 1968) confirm that lead ions go into solution, while the sulphide ions form predominantly elemental sulphur in acidic solutions, sulphate in neutral solutions, and thiosulphate in alkaline solutions (Eadington and Prosser, 1969).

Eadington and Prosser (1969), who investigated the influence of non-stoichiometry on the dissolution kinetics of synthetic lead sulphide, reported that the rate of dissolution after an initial inhibition period is much higher for p-type samples than for n-type samples (Figure D.1), indicating a rate-determining involvement of holes. They proposed that, during the induction period chemisorption of oxygen, associated with a change in surface properties, takes place, and the induction period ends with the nucleation of the first elemental sulphur. The dissolution mechanism proposed is the anodic oxidation of PbS and the cathodic reduction of oxygen in a mixed-potential model. In subsequent work, Eadington (1973) observed that no inhibiton period existed for the dissolution of natural and synthetic samples in nitric acid. Illumination had a greater influence on the dissolution rate of the n-type sample than on the

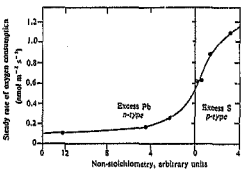

Figure D.1 Effect of non-stoichiometry on the induction period and the steady rate of oxidation (after Eadington and Prosser, 1967)

p-type sample. The influence of point defects was studied by Simkovich and Wagner (1960), and their results support the work of Eadington and Prosser (1969).

Brodie (1968) investigated the anodic electrochemistry of museum grade natural galena. The anodic Tafel slope in acid perchlorate solution was 0.057 V decade^{-1} - which is close to the 0.059 V decade^{-1} expected for a semiconductor electrode - for one of his samples, and 0.076 V decade^{-1} - which is consistent with the presence of surface states - for the other. Brodie reported that at 0 pH the production of sulphur occurs up to a potential of 0.9 V, above which the production of sulphate is detected. The formation of a $PbSO_4$ film passivates the electrode at these potentials.

Richardson and O'Dell (1984) studied the semiconducting characteristics of pure natural galena and synthetic lead sulphide, using

electrochemical, interfacial-capacitance and surface-photovoltage (SPV) measurements to characterise the electrodes. Variation in capacitance and SPV occurs over a potential range greater than the band gap, indicating that changes in the Helmholtz potential cannot be neglected. The anodic Tafel slopes ranged from 0.06 to 0.08 V decade^{-1}, which is consistent with the surface-state semiconductor model. Further changes in the electrode potential in the anodic direction presumably occur across the Helmholtz layer, and metal-like Tafel behaviour is expected.

Paul *et al* (1978), using cyclic voltammetry, examined the anodic behaviour of natural crystals and reported that the electrode passivates at potential greater than 0.6 V vs SCE as a result of the formation of a basic lead sulphate on the galena surface. The Tafel slopes, which were dependent on the the potential and the concentration of lead in solution, range between 0.045 and 0.12 V decade^{-1}. Paul *et al* (1978) concluded that these results were not consistent with a two-electron transfer mechanism, and proposed that dissolution occurs in two single-electron transfer steps in which an 'S^{-}' intermediate was formed. On the basis of this mechanism, they derived equations to describe their results.

Although this mechanism is not incompatible with their results (Paul *et al*, 1978), it is incompatible with the the mechanism of Richardson and O'Dell (1984), who proposed that the change in Tafel slope at high potentials is a result of Fermi-level pinning, and that a metal-like Tafel slope (0.12 V decade^{-1}) is expected. A slope of 0.084 V decade^{-1} is the result of a significant potential drop over the Helmholtz layer increasing the Tafel slope from the expected 0.059 V decade^{-1}. Adsorption of potential-determining species on the surface would result in a linear dependance of $dV_p/d\log(Pb^{2+})$ with a slope of -0.03 V decade^{-1}, which is observed from Paul's data at low current density. Studies of the structure of the double layer of galena as a function of lead concentration using the methods of Buddy (1964), for example, might clarify this aspect. The adsorption of copper ions

which is important in flotation, should also be investigated using semiconductor techniques.

Paul *et al* (1978) reported that illumination did increase the rate of anodic dissolution by a factor of 3 to 7 if the electrode was held at a potential of between 0.2 and 0.35 V vs SCE, which corresponds to a small peak before the main anodic peak for the bulk oxidation of the electrode. Since no large photo-effect was observed on the main anodic peak, they concluded that semiconducting properties were not an important factor in dissolution kinetics. Their results, interpreted in terms of the semiconductor model, suggest that, at potentials more anodic than the small peak at 0.3 V vs SCE, the Fermi level is pinned at the valence-band edge, and if this is the case the SPV would be saturated, and no photo-effect would be observed (Richardson and O'Dell, 1984).

In the presence of oxygen, the anodic Tafel slopes range between 0.18 and 0.22 V decade^{-1} (Richardson and O'Dell, 1984). Richardson and O'Dell attributed this to the formation of a PbO film on the surface, such that the applied potential was distributed between the space-charge layer, the PbO film, and the Helmholtz layer.

2.3 *The electrochemistry and dissolution of pyrite*

Hiskey and Schlitt (1981) recently reviewed the aqueous oxidation of pyrite. Warren (1956) reported the first detailed kinetic study, and observed an activation energy of 83.7 kJ mol^{-1} for the oxygen pressure leaching of pyrite between 130 and 210°C. The rate of reaction was proportional to the square root of the oxygen partial pressure, which is consistent with the mixed potential model. The activation energy was reported to range between 58.6 and 51.1 kJ mol^{-1} for pressure leaching below 130°C.

Anodic dissolution of pyrite at 1.05 V is thought to proceed according

to the following stoichiometry (Majima, 1969):

$$FeS_2 + 8H_2O \rightarrow Fe^{3+} + 2SO_4^{2-} + 16H^+ + 15e^- \qquad D.2$$

with sulphate as the principal sulphur product. Dutrizac and MacDonald (1974) reported that sulphur and sulphate were produced concurrently by separate but related processes. Nevertheless, the oxidation of sulphur to sulphate, although thermodynamically possible, must be extremely slow. Sulphur is a stable product in the oxidative dissolution mechanism (Dutrizac and MacDonald, 1974).

An important finding of Bailey and Peters (1976) was that the sulphate formed from pyritic sulphur contains oxygen acquired from water instead of from oxygen gas. Evidence in support of this hypothesis was obtained from ^{18}O tracer experiments. In addition, detailed stoichiometric determinations showed that the sulphate yield varied between 60 and 90%, and increased with increasing oxidation potential.

Biegler and Swift (1979) proposed a mechanism involving the electrochemical transfer of the oxygen in the water molecule to the sulphur atoms in the pyrite lattice. The mechanism they proposed is

$$FeS_2 + H_2O \rightleftharpoons FeS_2(OH)_{ads} + H^+ + e^- \qquad D.3$$

$$FeS_2(OH)_{ads} \rightarrow FeS_2(O)_{ads} + H^+ + e^- \qquad D.4$$

where the second step is rate-limiting. They used the Temkin isotherm, and derived an equation that predicted a Tafel slope of 0.059 V decade^{-1} and a dependence of -0.03 V per pH unit for transfer coefficients of 0.5 for both reactions. Biegler and Swift (1979) measured a Tafel slope of 0.095 V and Meyer (1979) reported a dependence of -0.03 V per pH unit.

Pyrite is generally regarded as displaying noble electrochemistry. It has a high open-circuit potential and is galvanically protected from

corrosion when in contact with other [illegible]erals. Parker *et al (1980)* presented current-voltage curves that [illegible] very similar to those of platinum.

Structure of FeS_2

Pyrite may have both n- and p-type conductivity, and p-type having the higher resistivity ($\approx 1 \times 10^{-3}$ Ω·m for n-type and $\approx 3 \times 10^{-2}$ Ω·m for p-type) (Shuey, 1975). Pyrite has a cubic structure, represented as $Fe^{2+}(S_2)^{2-}$ by the ionic model. The lower part of the conduction band is derived from the anti-bonding e_g^* doublet of 3d orbitals on Fe, while the upper part is derived from the 4s orbital. The valence band is derived from the t_{2g} triplet of 3d orbitals on Fe, and, most importantly, remains *non-bonding* (Shuey, 1975; Vaughan and Craig, 1978; and Goodenough, 1972). The energy separation between the non-bonding t_{2g} and the anti-bonding e_g^* orbitals is, therefore, the band gap. Bither *et al* (1968) measured the optical reflectivity of pyrite, and inferred a band gap of 0.9 ±0.1 eV. Since the sulphur atoms are in octahedral co-ordination about the iron, the overlap between orbitals is slight, and the valence band is narrow, about 1 eV. The band derived from the sulphur 3p levels is about 7 eV wide, and is just below the t_{2g} valence band. The 'one-electron' energy band diagram for pyrite is shown in Figure D.2.

The influence of the structure of pyrite on the dissolution kinetics

An important difference between transition metal disulphides, such as pyrite and molybdenite, and other polar semiconductors, such as CdS, ZnO, and GaP, is that the valence band is narrow and of non-bonding character. Electron transfer with this band (hole injection) will therefore have no effect on the structure or bonding of the solid, and corrosion will not occur. This feature was exploited by Tributsch and

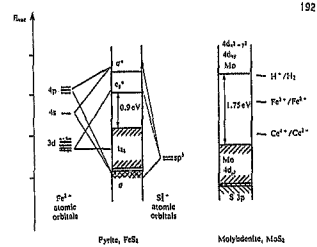

Figure 8.2 The band diagram for pyrite and molybdenite. The pyrite diagram shows a simplified molecular orbital diagram indicating the origin of the non-bonding valence band, the t_{2g} band. The crystal-field splitting of the Mo 4d orbitals in MoS_2 is also shown. The $4d_{z^2}$ *band of* MoS_2 *is a non-bonding valence band.*

co-workers (Tributsch, 1977; Tributsch and Bennet, 1977; Jaegermann and Tributsch, 1983; Ennaoui *et al*, 1986) in their search for a suitable material for the conversion of solar energy. Holes in the t_{2g} band of pyrite and the d_{z^2} band of molybdenite are capable of oxidizing water, and subsequently of producing oxygen as a fuel (*splitting of water*). *Tributsch* (1977) *reported* that the production sulphate was the predominant long term photo-anodic product of MoS_2, according to

$$MoS_2 + 8H_2O + 18h^+ \xrightarrow{18h\nu} Mo(VI) + 2SO_4^{2-} + 16H^+ \qquad D.3$$

where hν refers to the energy of the incident photon. He also proposed a mechanism for the oxygen-liberation reaction, and a scheme for the choice of suitable *transition metal disulphides for* photo-anodic devices (Tributsch, 1977). There seems little doubt that the non-bonding character of the valence band is the reason for the

slow dissolution behaviour and the reversible current-voltage behaviour of both pyrite and molybdenite.

The formation of a hypothetical sulphur layer that is capable of preventing further oxidation is not consistent with the observed Tafel slopes, and Fuerstenau's (1983) proposal that dense sulphur layers are the reason for the slow rates of oxidation of pyrite must be rejected in favour of an explanation based on the band structure of pyrite.

Recently Tributsch and co-workers (Jaegermann and Tributsch, 1983) examined the photo-electrochemistry of natural and synthetic pyrites. The electrochemical behaviour of the natural samples was quasi-metallic, and a Schottky barrier was not observed, indicating the high level of doping of the natural crystal. Anodic photo-effects were observed for all samples, however Jaegermann and Tributsch (1983) concluded that surface states within the band gap caused the applied potential to appear mainly across the Helmholtz layer (Fermi-level pinning), and subsequently concentrated their attention on RuS_2, which also has a similar band structure to pyrite, but produces photo-anodic oxygen, in contradistinction to pyrite corrodes to sulphate and Fe(III).

A possible mechanism for the oxidation of FeS_2 is shown in Figure D.3. Holes are initially injected into the t_{2g} valence band by the oxidising agent. These holes do not result in corrosion but are able to split water according to the reaction

$$H_2O + h^+ \rightarrow H^+ + {}^{\cdot}OH \qquad D.6$$

where $^{\cdot}OH$ is an intermediate hydroxide radical. The energy level of the $^{\cdot}OH/OH^-$ couple has been estimated to be 2.7 V vs SCE by Memming (1969) and is shown in Figure D.2. The $^{\cdot}OH$ radical is a strong oxidizing agent and reacts directly with the S valence band to form sulphate. Oxygen from the water molecule becomes incorporated directly in the sulphate ion. The $^{\cdot}OH$ radical can oxidize the S valence

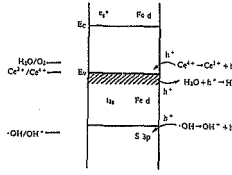

Figure D.3 A simplified scheme for the dissolution of pyrite by an oxidant, neglecting the effects of surface states.

Table D.2 Leaching of MoS_2 in various leaching systems (after Krishnaswy and Fuerstenau, 1982)

Redox couple	V^0_{redox} (V vs SCE)	Dissolution rate
Fe^{3+}	0.77	no reaction
MnO_2	0.8 to 1.0	slow reaction
HNO_3	0.95 to 1.0	slow reaction
MnO_4^-	1.2	moderate reaction
Anid chlorate	1.2	moderate reaction
Hypochlorite	1.4	fast reaction

band directly to produce sulphur. The iron enters the solution as Fe^{3+} and therefore consumes an extra hole.

Tributsch (1977) presented a similar scheme in which OH^- is chemisorbed by the oxidized metal atom. The rate-determining steps in this model are the same as those considered by Biegler and Swift (1979). The measured Tafel slope is 0.095 V decade^{-1} and the predicted slope is 0.059 V decade^{-1} for a variation in the Helmholtz potential, indicating that the applied potential appears across the space-charge layer and the Helmholtz layer. A Tafel slope of 0.095 V decade^{-1} is typical of the transition between a semiconductor Tafel slope of 0.059 V decade^{-1} and a metal-like Tafel slope of 0.118 V decade^{-1}. Similar behaviour for germanium was shown by Boddy (1963) to be a result of the significant change in the potential drop across the Helmholtz layer in addition to the potential drop across the space charge layer. Specific adsorption at the inner Helmholtz plane by chloride ions, or an increase in dislocation defects, would increase the Tafel slope to 0.118 V.

Biegler and Swift (1979 a) suggested that the sulphur and sulphate pathways have very similar activation energies or the same rate-limiting step. This is not inconsistent with the above mechanism if the rate-limiting step is either the injection of holes into the t_{2g} valence band or the splitting of water. Biegler (1975) reported that there was no detectable correlation between the electrochemical reduction of oxygen at a pyrite electrode and the semiconducting properties of various pyrite samples. This suggests that the splitting of water is a feasible rate-determining step.

Although the open-circuit potential of pyrite is 0.62 V, significant corrosion does not occur until the redox potential is about 1.0 V. Apparently, energy levels below 1.0 V (Figure D.2) do not overlap sufficiently with the t_{2g} band to inject holes. Thus, the greater the electrode potential, the greater the rate of electron transfer, and the greater the rate of dissolution.

The dissolution rate of molybdenite is slow with oxidizing agents having V^{o}_{redox} values less than 1.0 V (Krishnasway et al, 1982). Table D.2 summarizes the leaching rate in various leaching systems. Krishnasway et al (1982) studied the electrochemistry of this mineral and interpreted the results in terms of n-type conductivity.

The dissolution rate of arsenopyrite is also expected to be slow since it too has the pyrite structure. Indeed, arsenopyrite does fall into the category of minerals that are 'difficult to dissolve'.

D.4 The electrochemistry and dissolution of chalcopyrite

The anodic dissolution of chalcopyrite is thought to occur according to (Biegler and Swift, 1979 b):

$$CuFeS_2 \rightarrow Cu^{2+} + Fe^{3+} + 2S + 5e^- \qquad D.7$$

and

$$CuFeS_2 + 8H_2O \rightarrow Cu^{2+} + Fe^{3+} + 2SO_4^{2-} + 16H^+ + 17e^- \qquad D.8$$

Biegler and Swift (1979 b) found that 86% of the sulphide sulphur reports as elemental sulphur, and 14% as sulphate. Ferric chloride leaching, which follows linear kinetics, is 4 to 5 times more rapid at 80 - 90°C than ferric sulphate leaching, which follows parabolic kinetics. Chloride solutions yield sulphur almost exclusively, whereas sulphate solutions produce between 14 and 25% sulphate.

Dutrizac (1981) showed that, in chloride solutions, dissolution followed linear kinetics, and that the rate was proportional to $[Fe^{3+}]^{0.34}$. The rate in sulphate solutions was proportional to $[Fe^{3+}]^{0.12}$, and followed parabolic kinetics. Jones and Peters (1976) showed that, in sulphate solutions, corrosive attack was highly selective, in as much as it only occurred in fissures or at grain

boundaries; whereas, in chloride solutions, attack occured over the entire surface. The addition of ferrous chloride had no effect on the rate of leaching, yet the addition of cupric chloride increased the rate. This was attributed to Cu^{2+} being the primary oxidant.

Many researchers have proposed that the oxidation products are resistive. Sulphur (Munoz *et al*, 1979), p- or n-type semiconductors such as p-type CuS, and metal-deficienc polysulphides (Biegler and Swift, 1979 b; Linge, 1976; Parker *et al*, 1980) have all been proposed as hindering the transfer of electrons or ions at the solution interface.

Structure of $CuFeS_2$

Chalcopyrite is a good conductor with a resistivity of about 10^{-3} Ω·m (Shuey, 1975). It is an n-type semiconductor, due to metal excess, with a band gap of about 0.6 eV. The ionic bonding mod l of chalcopyrite is represented as $Cu^{+}Fe^{3+}(S^{2-})_2$. Apparently, there is not extensive covalence among the anions, but there is extensive covalence between the cations and anions (Shuey, 1975). Unfortunately, precise computation of the energy bands in chalcopyrite is difficult because of its antiferromagnetism. However, studies of other I-III-VI compounds, in particular Fe-doped $CuGaS_2$, suggest that the lower part of the conduction band of chalcopyrite is Fe 3d in character, while the upper part of the valence band is Cu 3d and S 3p in character (Shay and Tell, 1974; Jaffe and Zunger, 1983). The relevant 'one-electron' band diagram is shown in Figure D.4.

Application of the energy-level model to the corrosion of $CuFeS_2$

Parker *et al* (1981) conducted extensive studies of the electrochemistry of chalcopyrite in chloride solutions in the temperature range 70 to 90 °C and the potential range 0.2 to 0.6 V (SCE), which is appropriate for chalcopyrite leaching. They reported that the rates

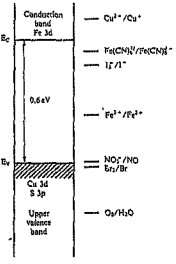

Figure D.4 The energy level diagram for $CuFeS_2$, indicating the Cu 3d contribution to the valence band, and the Fe 3d contribution to the conduction band.

of reduction of oxidants were in the order

$$Br_2,\ CuCl_2,\ I_3^- > Fe(CN)_6^{3-} > FeCl_3 > Fe_2(SO_4)_3,\ Cl_2$$

The location of the bands at the flatband potential and the redox potentials of these oxidants is shown in Figure D.4. In order for electron capture or hole injection to occur, the energy level of the oxidant must overlap the conduction-band edge or the valence-band edge, respectively. It is apparent from the diagram that the rate of reduction of $CuCl_2$ and I_3^- is high because the energy levels of those ions overlap the conduction-band edge, and the rate of reduction of Br_2 is high because the bromine energy level overlaps the valence-band edge. In contrast, the iron chloride and iron sulphate energy levels are well within the band gap, and the rate of reduction is low. $Fe(CN)_6^{3-}$ is reported by Parker *et al* (1981) as having a lower rate of

reduction than I_3^-, which has a higher E^o_{redox}, but this is because they compared these rates at different temperatures. The rate of reduction of $Fe(CN)_6^{3-}$ was determined at 25°C, while the others were all determined at 80°C. The level of Cl_2 is well below the valence-band edge.

Parker et al (1981) also reported anodic saturation currents, which are typical for n-type semiconductors where the supply of holes is migration-limited, for the oxidation of Fe^{2+} in solution. Similarly, Beckstead *et al* (1976) presented results showing that the rate of dissolution increased with Fe^{3+} and then reached a steady value, indicative of *saturation currents*. Saturation currents were not found for I^- or $CuCl_2^-$ by Parker *et al* (1981), however, since the energy levels of these ions overlap the conduction band edge. *From these arguments*, it may be concluded that the interaction of
I_3^-/I^-, $CuCl_2/CuCl_2^-$ and $Fe(CN)_6^{3-}/Fe(CN)_6^{4-}$ are
conduction band processes, while Fe^{3+}/Fe^{2+} and Br_2/Br^- are
valence band processes.

Zovgolis and Cooke (1975) presented results suggesting an anodic limiting-current due to migration of holes (minorities) in the n-type chalcopyrite. They illuminated the rear of the sample and observed that the current density is proportional to the light intensity. Subsequently, they have been severely criticized for illuminating the rear of their sample, and for the fact that the photo-effect occurred only at high (>3 V) anodic potentials (Biegler, 1975).

Mechanism of dissolution of chalcopyrite

An interesting observation of Parker *et al* (1981) and others (Jones and Peters, 1976) is that the addition of $CuCl_2$ to a $FeCl_3$ solution results in enhanced current densities at a chalcopyrite electrode.

Table D.3 presents a selection of data from Parker *et al* (1981), which indicates that the anodic dissolution of chalcopyrite occurs with a contribution of holes in the valence band and electrons in the con-

Table D.3 Comparison of the corrosion currents of chalcopyrite. (after Parker *et al*, 1981)

Ox	Red	V_{corr} (V va SCE)	j_{corr} ($\mu A\ cm^{-2}$)	Source
Fe^{3+}	Fe^{2+}	0.39	5500	Ward's
Fe^{3+}/Cu^{2+}	Fe^{2+}	0.48	11000	Ward's
Cu^{2+}	Cu^{+}	0.28	250	Ward's

duction band. This is the case for many semiconductors, such as Ge, with a band gap of less than 1 eV (Gerischer and Mindt, 1966). Since the dissolution current for the contribution of holes from oxidant Fe^{3+} is greater than for the contribution of electrons to Cu^{2+} in solution, it is assumed that the initial step in the dissolution of chalcopyrite is the consumption of a hole. Chalcopyritic Fe^{3+} is associated with the conduction band and chalcopyritic Cu^{+} with the valance band; the electropositive Fe^{3+} will therefore be released into solution, and the Cu^{+} will remain after the initial step. The initial hole transfer is followed by electron transfer, according to

$$CuFeS_2 + 3h^+ \rightarrow Fe^{3+} + \cdot CuS_2 \qquad D.9$$

followed by hole transfer

$$\cdot CuS_2 + 2h^+ \rightarrow Cu^{2+} + 2S \qquad D.10$$

or electron transfer

$$\cdot CuS_2 \rightarrow Cu^{2+} + 2S + 2e^- \qquad D.11$$

The first step illustrates the breaking of the Fe-S bond and the

second the breaking of the Cu-S bond. $^{\cdot}CuS_2$ is an unstable radical intermediate. This mechanism implies that copper remains in the lattice because it is associated with the valence band, which is consistent with the observation that the Fe/Cu ratio in solution is greater than 1 in the initial stages of leaching.

The radical intermediate, $^{\cdot}CuS_2$, may decompose to form a stable CuS intermediate according to

$$^{\cdot}CuS_2 \rightarrow CuS + S \qquad D.12$$

Biegler and Swift (1979 b) presented cyclic voltammograms for pure natural chalcopyrite. A large anodic response occurs at potentials greater than 1.0 V. Prior to this response, a smaller 'prewave' response occurs at 0.8 V, which they interpreted as the formation of a copper sulphide film.

The formation of surface films on $CuFeS_2$

The application of a positive potential pulse to the chalcopyrite electrode produces an anodic current response due to oxidation of the electrode. This current subsequently decays with time to a steady state value. Reactivation occurs if the electrode is kept on open circuit and, when the potential is re-applied, large currents flow that again decay with time. Parker *et al* (1981) interpreted this as the formation of a metal-deficient polysulphide film that slows the transport of Cu^{+} and Fe^{2+} ions to the solution. This film is supposed to break down thermally (reactivation of the electrode) to produce sulphur.

Munoz *et al* (1979) concluded that the kinetics in sulphate solutions were controlled by diffusion through a sulphur product-layer. Thus, they attributed the high activation energy to the rate-determining transport of electrons through the sulphur product layer, and used Wagner's theory to describe the kinetics. However, the sulphur layer

is porous and is expected to have a high concentration of impurities. Parker *et al* (1980) removed the sulphur with CS_2 and failed to observe any effect on the rate. Therefore it is not clear that the sulphur forms a protective layer.

McMillan *et al* (1982) reported anodic currents that decayed with time. A series of potential pulses in the range 0.2 -0.6 V vs SCE revealed a blue product layer, suggesting a copper-rich sulphide phase. McMillan *et al* (1982) interpreted their results as showing the formation of a protective layer in which the diffusion of ions was rate-limiting. McMillan *et al* (1982) used natural crystals, and compared the electrochemistry of n- and p-type samples. They then observed that semiconduction type had no influence on the electrode behaviour. However, their p-type specimen had significant pyrite inclusions, rendering their conclusions doubtful because of the possibility of galvanic interactions.

The growth of a film should lead to Tafel slopes greater than 0.118 V decade^{-1} (Vijh, 1973). McMillan *et al* (1982) reported slopes of 0.2 V per decade due to the formation of a film of CuS or intermediate copper sulphide; indeed, a blue surface film has been frequently observed (Parker *et al*, 1981; Jones and Peters, 1976; McMillan *et al*, 1982), suggesting covellite. If such a film formed on the surface of the electrode, the current would decrease until a stable copper sulphide formed. Moreover, reactivation would occur on open circuit as the original chalcocite-covellite intermediate formed, since both the solid-solid and the solid-solution boundary are reversible (Kook and MacIntyre, 1976).

Biegler and Horne (1984) analysed the anodic 'prewave' and presented evidence for the formation of a CuS film about 3 nm thick. The ratio of iron to copper during leaching, the dissolution of copper during the prewave, and an analysis of the charge passed in reducing the prewave product suggest that chalcopyrite initially produces a CuS film, sulphur, Cu^{2+} and Fe^{2+}.

The copper sulphide film, whatever layer is formed, does not inhibit the rate of leaching in chloride solutions after the layer thickness has reached a steady state, since linear kinetics and a strong dependence on ferric chloride concentration are observed (the one-half dependence on Fe^{3+} suggests metal-like corrosion control due to Fermi-level pinning). In sulphate solutions, however, a layer apparently does inhibit leaching since 'parabolic' kinetics are observed. This difference in behaviour might be due to the ability of chloride ions to be specifically adsorbed at the surface, whereas sulphate ions are not. This would result in surface states within the film band gap that would aid the passage of current, and hence would catalyse the electrochemical dissolution of the film.

The production of sulphate as the final chalcopyritic sulphur product is envisaged as occurring by the same mechanism as that discussed for pyrite. Holes that have been injected into the Cu 3d part of the valence band are capable of oxidizing water, and presumably the $^{\cdot}OH$ radicals directly oxidize the valence-band sulphur to sulphate. The oxidation of elemental sulphur is very slow, and is not considered to contribute to the production of sulphate.

D.5 *The dissolution and electrochemistry of copper sulphides*

Chalcocite

Sullivan (1933) studied the dissolution of chalcocite ores containing 5 to 10 % Fe at temperatures in the range 23 to 95°C. Cu_2S dissolves according to the reaction

$$Cu_2S + 2Fe^{3+} \rightarrow Cu^{2+} + 2Fe^{3+} + CuS \qquad D.13$$

$$CuS + 2Fe^{3+} \rightarrow Cu^{2+} + 2Fe^{3+} + S \qquad D.14$$

where the CuS intermediate is not the mineral covellite. Sullivan noted that the rate is independent of pH.

Marcantonio (1976) identified two stages in the ferric sulphate leaching of natural chalcocite in which the product sequence $Cu_2S \rightarrow Cu_{1.8}S \rightarrow Cu_{1.2}S \rightarrow CuS$ occurred. The first stage included the rapid formation of $Cu_{1.8}S$ and the slower formation of blue-remaining covellite, $Cu_{1.2}S$. The second stage is the dissolution of $Cu_{1.2}S$ to form Cu^{2+} in solution and elemental sulphur. The kinetics of the first stage was first order in Fe^{3+} concentration and the activation energy was low (11.5 kJ mol^{-1}); the leaching results were modelled as solution diffusion control in conjuction with spherical shrinking core geometry. The second-stage reaction was slower than the first stage, and the kinetics were half order in Fe^{3+} with a high activation energy (75.5 kJ mol^{-1}); the leaching results for this latter stage were modelled as an electrochemical reaction with cylindrical particle geometry.

Copper sulphide minerals have a solid solution range Cu_2S - CuS, the thermodynamics of which are not clearly understood (Potter, 1977). Chalcocite is consistently p-type, and has a band gap of about 1.8 eV. An indirect absorption edge at 1.1 eV for light perpendicular to the c-axis and at 1.4 eV for light parallel to the c-axis, have been attributed to interband transitions. The conduction band is derived from the Cu 4s orbital, and the top of the valence band from the S 3p level (Tossel and Vaughan, 1981). An empirical energy level diagram constructed from sulphur X-ray emission spectra of Cu_2S is in agreement with the quantum mechanical calculations of the triangular coordinated CuS_3^{5-} cluster. An ionic model for chalcocite would be $(Cu^+)_2S^{2-}$ and, for a copper-deficient chalcocite, $Cu_{2-x}S$, it would be $(Cu^+)_{2-2x}(Cu^{2+})_xS^{2-}$. In the band model, a hole introduced for each missing Cu^+ (acceptor defect) is delocalized, with a mobility of 2 - 10 $cm^2\ V^{-1}\ s^{-1}$. Chalcocite exhibits high ionic mobility in the range 5 - 10 $cm^2\ V^{-1}\ s^{-1}$, due to the high mobility of Cu^+ ions.

Koch and MacIntyre (1976) prepared thin film electrodes of synthetic

Cu_2S by vacuum evaporation, and measured the changes in the reflectance and absorbance of the electrode with anodic dissolution (removal of copper ions). They observed that, when the anodic current was interrupted, the original spectrum returned. In addition, CuS produced by anodic treatment could be converted to the original material by reversal of the current, evidence of the reversibility of both the solid-state and solid-solution reactions. Figure D.5 plots the open-circuit potentials of the electrode as a function of copper removal. The plateaus correspond to two-phase regions, and the sharp rises to compositional changes. The phases identified are:
Cu_2S; $Cu_{1.92}S$ to $Cu_{1.91}S$; $Cu_{1.86}S$ to $Cu_{1.8}S$; $Cu_{1.68}S$ to $Cu_{1.65}S$; $Cu_{1.4}S$ to $Cu_{1.36}S$; CuS

The wavelength of the maximum absorbance decreased from 2300 to 1200 nm for the $Cu_{1.93}$-$_{1.91}S$ to 670 nm for CuS. Wavelengths less than 1250

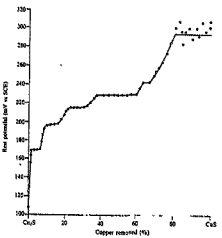

Figure D.5 Rest potentials of a thin film chalcocite electrode as a function of the copper content in the range Cu_2S - CuS (after Koch and McIntyre, 1972)

nm were interpreted as band to band transitions. The shift to lower wavelengths reflected the progressively lower Fermi level in the valence band as the copper content decreased. The extraction of copper ions from Cu_2S was accompanied by the removal of electrons from the top of the valence band. As a result, the adsorption band shifted to higher energies since the difference in energy between the highest filled levels of the valence band and the conduction band increased (Muller, 1972).

Hillrichs and co-workers (Hillrichs and Bertram, 1983; Hillrichs *et al.*,1982) investigated the electrochemistry of synthetic Cu_2S using cyclic voltammetry. They reported a sharp anodic peak at 0.4 V vs 3.5 M calomel electrode (CE) in which the diffusion of copper in the solid was claimed to be rate-determining. This peak reached a maximum due to the formation of CuS which apparently limited further the diffusion of copper ions. Results at potentials greater than 1 V vs 3.5 M CE are interpreted in terms of CuO formation and dissolution. Figure D.6 illustrates their interpretation of the cyclic voltammogram of Cu_2S and CuS.

Biegler and Swift (1977) used natural and synthetic chalcocite and synthetic digenite anodes. In their galvanostatic experiments the potential rose steeply after a certain period, which led the authors to concur with Ettienne and Peters (1972) that the diffusion of copper was impeded by the precipitation of a copper salt in the pores of the solid. Price (1981) later re-analysed the published data and proposed a model that combined solid-state diffusion and electrochemical reaction in the first stage of reaction (product CuS).

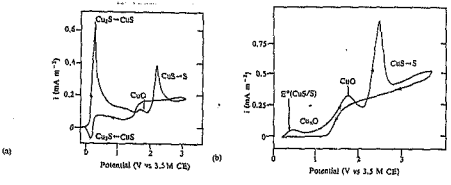

Figure 3.6 Cyclic voltammogram of (a) Cu_2S and (b) CuS in 1M H_2SO_4 (after Hillirche *et al*, 1981)

Covellite

Thomas and Ingraham (1967) leached rotating discs of synthetic CuS in 0.1 M H_2SO_4 and 0.25 M $Fe_2(SO_4)_3$. The rate of reaction was determined from the concentration of the copper ions in solution. They report a transition from interfacial control at 25°C to solution diffusion control at 80°C. Dutrizac and MacDonald (1974 b) reported that the rates of dissolution of natural and synthetic CuS were slow, but increased during the initial stages of dissolution owing to pit formation. The reaction

$$CuS + 2Fe^{3+} \rightarrow Cu^{2+} + 2Fe^{2+} + S \qquad D.15$$

was observed to be directly dependent on Fe^{3+} concentration below 0.005 M, but independent of Fe^{3+} concentration above 0.005 M. The rate-controlling step was found to be a reaction at the surface. The

sulphur product did not form a protective layer.

The crystal structure of covellite is more complex than that of sphalerite galena, pyrite or chalcopyrite (Shuey, 1975). The copper occurs in both triangular and approximately tetrahedral co-ordination, and two thirds of the sulphur atoms are S_2^{2-} anions Vaughan and Tossel, 1980). The proposed ionic model for covellite is $Cu^{2+}_{II}(Cu^{+}_{III})_2S^{2-}S_2^{2-}$ in which Cu^{2+} is in a triangular site, and Cu^{+} is in a tetrahedral site. The calculated electronic structure for CuS indicates that the top of the partially-filled valence band is predominantly Cu 3d in character, and the conduction band is Cu 4s in character. CuS is a p-type metallic conductor because the valence band is partially filled. The energy difference between the Fermi energy and the bottom of the conduction band is about 2 eV.

The passivation behaviour of covellite was investigated by Hillrichs and Bertram (1983) using cyclic voltamametry. They reported a dependence of 0.4 V per pH unit, and showed that the open-circuit potentials were compatible with the formation of a layer of copper oxide or copper hydroxide. Dissolution occurred only at relatively high potentials (>1.3 V vs 3.5 M CE) owing to the formation and dissolution of the CuO film. This may also have been due to the fact that the upper valence band is mainly a crystal field band, similar to the valence band of pyrite. Peters (1983, 1977) and Ghali *et al* (1982) proposed that the sulphur product-layer hinders the rate of reaction.

D.6 Summary

The electrochemistry of galena, pyrite, chalcopyrite, chalcocite and covellite has been reviewed in this section. It has been established that the electronic structure of these minerals sulphides plays an important role in each mineral's electrochemical behaviour. Possible mechanisms that are consistent with the experimental results and the theory presented in Chapter 3 are given.

In the case of pyrite, crystal field splitting results in a valence band that is of non-bonding character, and holes in this band can not result in bond breaking. Thus, pyrite resists dissolution. This proposal is in contrast to the work of Peters (1984) who proposed that a dense sulphur layer in the cause the slow dissolution. The proposal must be rejected in favour of an explanation based on the electronic structure of pyrite.

The kinetics of the dissolution of chalcopyrite is complicated by the formation of a surface film, probably copper sulphide. It is argued in this section that the Cu^{2+}/Cu^{+}, $Fe(CN)_6^{3-}/Fe(CN)_6^{4-}$ and I_3^-/I^- couples are conduction band processes, while the Fe^{3+}/Fe^{2+} and Br_2/Br^- couples are valence band processes. Since the addition of $CuCl_2$ to a $FeCl_3$ leaching solution enhances the rate of dissolution, it is proposed that the dissolution mechanism involves both electrons and holes. This mechanism is similar to that proposed for the dissolution of Ge.

Author Crundwell Frank Kenneth
Name of thesis The role of charge-transfer mechanisms in the oxidative and non-oxidative dissolution of Sphalerite. 1988

PUBLISHER:
University of the Witwatersrand, Johannesburg
©2013

LEGAL NOTICES:

Copyright Notice: All materials on the University of the Witwatersrand, Johannesburg Library website are protected by South African copyright law and may not be distributed, transmitted, displayed, or otherwise published in any format, without the prior written permission of the copyright owner.

Disclaimer and Terms of Use: Provided that you maintain all copyright and other notices contained therein, you may download material (one machine readable copy and one print copy per page) for your personal and/or educational non-commercial use only.

The University of the Witwatersrand, Johannesburg, is not responsible for any errors or omissions and excludes any and all liability for any errors in or omissions from the information on the Library website.